

# Design of a business jet

Group: G2

Cristian Asensio García  
Juan Garrido Moreno  
Yi Qiang Ji Zhang  
Alexis Leon Delgado  
Alba Molina Cuadrado  
David Morante Torra  
Teresa Peña Mercadé  
Ferran Rubio Vallhonrat  
Iván Sermanoukian Molina  
Santiago Villarroya Calavia

Professor:  
Martí Coma Company

Aircraft Design

Bachelor's degree in Aerospace Technology Engineering  
Escola Superior d'Enginyeries Industrial, Aeroespacial i  
Audiovisual de Terrassa  
Universitat Politècnica de Catalunya

October 2020



# Contents

<b>Contents</b>	i
<b>List of Figures</b>	vii
<b>List of Tables</b>	xii
<b>Abstract</b>	xiii
<b>Objective</b>	xv
<b>Scope</b>	xvii
<b>Nomenclature</b>	xviii
<b>1 State of the art</b>	1
1.1 Review of the market . . . . .	1
1.2 Conclusions . . . . .	3
<b>2 Conceptual design</b>	7
2.1 Fuselage preliminary design . . . . .	7
2.1.1 Drag and optimization of the external shape . . . . .	8
2.1.2 A design procedure for fuselages with cylindrical mid section	10
2.1.3 The fuselage of general aviation aircraft . . . . .	11
2.1.3.1 Importance of comfort and payload density . . . . .	11
2.1.3.2 Cabin design . . . . .	13
2.1.4 Flight deck design . . . . .	14
2.1.4.1 Location of the pilot's seat and the flight controls	14
2.1.4.2 Visibility from the cockpit . . . . .	15
2.1.4.3 Flight deck dimensions and layout . . . . .	15
2.1.4.4 Emergency exits for crew members . . . . .	16

---

<b>2.2</b>	<b>Wing configuration . . . . .</b>	<b>17</b>
2.2.1	Vertical position of the wing . . . . .	17
2.2.2	Wing plan shape . . . . .	18
2.2.3	Aspect ratio . . . . .	19
2.2.4	Taper ratio . . . . .	21
2.2.5	Wing Sweep . . . . .	22
2.2.6	Wing twist . . . . .	23
2.2.7	Dihedral . . . . .	24
2.2.8	Winglets . . . . .	25
<b>2.3</b>	<b>Power plant . . . . .</b>	<b>26</b>
2.3.1	Type of propellers . . . . .	27
2.3.1.1	Internal combustion engines . . . . .	27
2.3.1.2	Turbine Engines . . . . .	28
2.3.1.3	Turboprop Engines . . . . .	31
2.3.2	Position of the engines . . . . .	32
2.3.2.1	Wing-mounted podded engines . . . . .	33
2.3.2.2	Fuselage-mounted podded engines . . . . .	34
2.3.2.3	Private jet engines . . . . .	35
2.3.3	Number of engines . . . . .	35
<b>2.4</b>	<b>Tail configuration . . . . .</b>	<b>36</b>
2.4.1	Common configurations . . . . .	37
2.4.1.1	Conventional tail . . . . .	37
2.4.1.2	T-Tail . . . . .	38
2.4.1.3	Cruciform tail . . . . .	39
2.4.2	Other configurations . . . . .	40
2.4.3	Tail configuration choice . . . . .	40
<b>2.5</b>	<b>Landing gear configuration . . . . .</b>	<b>42</b>
2.5.1	Classic or tailwheel . . . . .	42
2.5.2	Nosewheel or tricycle . . . . .	43
2.5.3	Tandem . . . . .	44
2.5.4	Other unconventional configurations . . . . .	46
2.5.5	Comparison and choice of landing gear configuration . . . . .	46
<b>3</b>	<b>Weights and performance . . . . .</b>	<b>49</b>
3.1	First estimation . . . . .	49

3.1.1	Weights and fuselage dimensions . . . . .	49
3.1.2	Power plant selection . . . . .	51
3.2	Weight determination . . . . .	54
3.2.1	Take off weight ( <i>TOW</i> ) . . . . .	54
3.2.2	Maximum take off Weight ( <i>MTOW</i> ) . . . . .	54
3.2.3	Operative Empty Weight ( <i>OEW</i> ) . . . . .	55
3.2.3.1	Torenbeek criterion . . . . .	55
3.2.3.2	Similarities criterion . . . . .	56
3.2.4	Payload . . . . .	57
3.2.5	Fuel Weight . . . . .	58
3.2.5.1	Cruise resolution . . . . .	62
3.2.5.2	Loiter resolution . . . . .	63
3.2.5.3	General weight ratio . . . . .	65
3.2.6	Final weight computation . . . . .	65
3.2.6.1	Roskam's method . . . . .	65
3.2.6.2	Single height methodology (SHA) . . . . .	67
3.2.6.3	Multiple height methodology (MHA) . . . . .	70
3.3	Centering . . . . .	71
3.3.1	Impact of power plant on the position of the CG . . . . .	73
3.3.2	Impact of passenger on the position of the CG . . . . .	73
3.3.2.1	Rows order . . . . .	74
3.3.2.2	Columns order . . . . .	74
3.3.3	Impact of Baggage compartment on the position of the CG	75
3.3.4	Impact of fuel weight on the position of the CG . . . . .	75
3.3.5	Resulting load and balance diagram . . . . .	77
<b>4</b>	<b>Design point selection</b>	<b>79</b>
4.1	Take-off . . . . .	79
4.2	Second segment . . . . .	81
4.3	Cruise . . . . .	84
4.4	Landing . . . . .	88
4.5	Final selection (1st iteration) . . . . .	91
4.5.1	Thrust at take-off required . . . . .	92
4.5.1.1	Engine selection . . . . .	93
4.5.2	Wing surface required . . . . .	95

4.6	Second iteration and sizing results summary . . . . .	95
<b>5</b>	<b>Weight-Range Diagrams</b>	<b>97</b>
5.1	Weight to Range Diagram . . . . .	97
5.1.1	TOW ascending section . . . . .	98
5.1.2	<i>MTOW</i> constant section . . . . .	99
5.1.3	TOW descending section . . . . .	99
5.2	Payload to Range Diagram . . . . .	102
<b>A</b>	<b>Baggage compartment volume</b>	<b>105</b>
<b>B</b>	<b>Torenbeek criteria weight increment computation</b>	<b>107</b>
<b>C</b>	<b>Breguet's equation derivation</b>	<b>109</b>
C.1	Breguet's equation for range . . . . .	109
C.1.1	Analytical resolution . . . . .	110
C.1.2	Numerical resolution . . . . .	111
C.2	Breguet's equation for endurance . . . . .	112
C.2.1	Analytical resolution . . . . .	113
C.2.2	Numerical resolution . . . . .	113
<b>D</b>	<b>Numerical analysis</b>	<b>115</b>
D.1	Euler approximation . . . . .	115
D.2	Runge Kutta method . . . . .	116
<b>E</b>	<b>Regression code</b>	<b>119</b>
<b>F</b>	<b>ISA atmosphere MATLAB code</b>	<b>125</b>
<b>G</b>	<b>Weight-computing MATLAB code (Runge-Kutta)</b>	<b>129</b>
G.1	Main code . . . . .	129
G.1.1	Range-solving function . . . . .	139
G.1.2	Autonomy-solving function . . . . .	142
<b>H</b>	<b>Weight-computing MATLAB code (Euler)</b>	<b>145</b>
H.1	Main code . . . . .	145
H.1.1	Range-solving function . . . . .	155
H.1.2	Autonomy-solving function . . . . .	158

<b>I Parabolic polar</b>	<b>161</b>
I.0.1 Parabolic Polar graph's representation . . . . .	164
<b>J Parabolic polar MATLAB code</b>	<b>167</b>
<b>K Design point MATLAB code</b>	<b>169</b>
<b>L Weight to Range Diagrams MATLAB code</b>	<b>173</b>
L.1 Main code . . . . .	173
<b>Bibliography</b>	<b>189</b>



# List of Figures

1.1	Gulfstream G650. Credit: Gulfstream . . . . .	2
1.2	Cessna Citation Latitude. Credit: Textron Aviation . . .	3
1.3	Bombardier Global 8000. Credit: Bombardier . . . . .	4
2.1	Drag coefficient as function of the slenderness. . . . .	9
2.2	Dassault Falcon 8X Circular Cross Section . . . . .	13
2.3	Air Force Reserve crewmembers board a C5-M Super Galaxy. Credit: Lisa Krantz/San Antonio Express-News . . . . .	17
2.4	Numerical calculations of the induced drag factor for linearly tapered and elliptic wings. Source: [1] . . . . .	21
2.5	Decomposition of the velocity round the wing due to the wing sweep. Source: [2] . . . . .	23
2.6	Additional dihedral effect produced by the interference of the Wing-Fuselage configuration. Source: [3] . . . . .	25
2.7	Different winglet shapes. . . . .	26
2.8	Ideal Otto Cycle. Source [4]. . . . .	28
2.9	Radial engine. Source [4]. . . . .	28
2.10	Cutaway view of turbojet engine. Source [4] . . . . .	29
2.11	Cutaway view of turbofan engine . . . . .	31
2.12	Cutaway view of turboprop engine . . . . .	31
2.13	Cutaway view of the afterburning turbojet . . . . .	32
2.14	Installation of high-by-pass-ratio engines on the wing and in the rear fuselage. Source: [5] . . . . .	33
2.15	Location effects on interference drag of a wing-mounted nacelle. Source: [5] . . . . .	34
2.16	Example of the shape of engine nacelles mounted to the rear sides of the fuselage. Source: [5]. . . . .	35

2.17	Available configurations for aft-mounted engines. Source [6]. . . . .	36
2.18	Aircraft with a conventional tail. Source: [7] . . . . .	38
2.19	Aircraft with T-tail configuration. Source: [7] . . . . .	39
2.20	Aircraft with a cruciform tail. Source: [7] . . . . .	40
2.21	Classic or tailwheel configuration. . . . .	43
2.22	Aircraft with nosewheel undercarriage. . . . .	44
2.23	Aircraft with simple-tandem undercarriage. . . . .	45
2.24	Aircraft with double-tandem undercarriage. . . . .	46
3.1	Mission Profile . . . . .	59
3.2	Suggested fuel-fractions for several mission phases. Source: [8] . . . . .	62
3.3	Suggested values for $L/D$ , $c_j$ , $\eta_p$ and for $c_p$ for several mission phases. Source: [8] . . . . .	64
3.4	Roskam's algorithm for computing the design weights. . . . .	66
3.5	Convergence of the operating empty weight <i>OEM</i> using Torenbeek criterion. . . . .	67
3.6	Convergence of the operating empty weight <i>OEM</i> using similarities criterion. . . . .	69
3.7	Evolution of the aerodynamic efficiency along the cruise stage. . . . .	70
3.8	CG Weight Versus CG Position Chart . . . . .	72
3.9	Power plant effect on load and balance diagram. Source: [5]	73
3.10	Passenger effect on load and balance diagram. . . . .	74
3.11	Baggage compartment effect on load and balance diagram	75
3.12	Fuel effect on load and balance diagram . . . . .	77
3.13	Resulting load and balance diagram . . . . .	78
4.1	Graph regarding the take-off limitation. . . . .	81
4.2	Graph regarding the second segment limitation . . . . .	84
4.3	Graph regarding the cruise limitation . . . . .	88
4.4	Definition of FAR 25 landing distances. Source: [8] . . . . .	89
4.5	Graph regarding the landing limitation . . . . .	91
4.6	Design point selection (1st iteration) . . . . .	92
4.7	CF34-8C5B1 Engine. Source: [9] . . . . .	94

4.8	CF34-8C5 Engine comparison. Source: [9] . . . . .	94
4.9	Design point selection (2nd iteration) . . . . .	96
5.1	Weight to range diagram 1 . . . . .	101
5.2	Weight to range diagram 2 . . . . .	102
5.3	Payload to range 1 . . . . .	104
5.4	Payload to range 2 . . . . .	104
A.1	Linear regression of the baggage compartment volume . .	105
B.1	Linear regression of the $\Delta W_E$ value. . . . .	108
I.1	Correlation between $S_{wet}$ and Maximum Take-off Weight $W_{TO}$ . . . . .	162
I.2	Drag polar for different aircraft configurations. . . . .	164



# List of Tables

1.1	Similar aircraft data table. The models highlighted in green are the finally selected as most similar aircraft. (Part 1/2). . . . .	5
1.2	Similar aircraft data table. The models highlighted in green are the finally selected as most similar aircraft. (Part 2/2). . . . .	6
2.1	Characteristic flight deck distances. . . . .	16
2.2	Tail configurations performance comparison . . . . .	41
2.3	Landing gear configurations comparison . . . . .	47
3.1	Main fuselage and weight specifications of similar aircraft. . . . .	49
3.2	Wing specifications of similar aircraft. . . . .	50
3.3	Expected set of characteristic parameters. . . . .	50
3.4	Operative engine specifications at sea level for similar aircraft. . . . .	51
3.5	Engine specifications for similar aircraft. . . . .	52
3.6	Reference set of characteristic propulsive parameters at sea level. . . . .	52
3.7	Reference set of characteristic propulsive parameters. . . . .	53
3.8	$\alpha$ parameter for the different similar airplanes. . . . .	56
3.9	Performance characteristics at cruise stage (analytically computed). . . . .	63
3.10	Performance characteristics at loiter stage. . . . .	64
3.11	Exact values of the <i>MTOW</i> and <i>OEW</i> for a SHA analysis. . . . .	68
3.12	Exact values of the <i>MTOW</i> and <i>OEW</i> for a MHA analysis. . . . .	71
3.13	CG limits data from similar aircraft (1). Sources: [10][11][12][13] . . . . .	71
3.14	CG limits data from similar aircraft (2). Sources: [10][11][12][13] . . . . .	72
4.1	Ascend requirements set by FAR 25.111 and FAR 25.121 . . . . .	81
4.2	Summary of the design point parameters . . . . .	96
5.1	Starting weight values for the Weight to Range diagram . . . . .	98
5.2	Inter medium weight values for the Weight to Range diagram . . . . .	99

5.3	Last weight values for the Weight to Range diagram . . . . .	101
I.1	$C_{D0}$ for different aircraft configurations. . . . .	163
I.2	Drag polars for different aircraft configurations. . . . .	164

# **Abstract**

This project develops the university-level design of a highly competitive private jet aircraft based on the knowledge presented in the “Aircraft Design” subject. The design process that is covered by the project is a conceptual approach, complemented by a wide-range review of the market that provides a general insight of the most successful jet aircraft competitors, currently operating long-haul flights. Furthermore, both a preliminary design and a more in-depth analysis of the aerodynamics and performance of the aircraft have been developed, including numerical simulations. It concludes with a discussion of the results and recommendations to design a more competitive aircraft.



# Objective

## Aim of the study

The study aims to develop a preliminary design of a fixed-wing aerodyne able to carry a reduced number of people in intercontinental flights at the maximum possible Mach number.

## Requirements

This section is aimed to provide strict and measurable statements that will guide and limit the study, to minimise weak spots and vague actions that could lead to misunderstandings:

- The nominal number of passengers will be 10.
- The nominal range of the aircraft, carrying the maximum payload must be of, at least, 4500 NM to allow ample and proper intercontinental flights.
- The cruising speed must be of Mach 0.80 and the maximum of 0.9.
- The number of crew will be 2 pilots plus a flight attendant.
- The payload value with maximum fuel weight must be higher than 1700 lb.



# Scope

With the aim of designing a private jet, able to compete in the current market and excel in maximum speed, at a university-level, some of the most important parts of a complete design will be included.

An analysis of the different competitors will be done. Then, the preliminary configuration of the aircraft will be determined in different sections including fuselage, wing, power-plant, tail and landing system.

A wide study, including iterative processes and analytical equations, will be done in order to estimate the different sub-weights of the aircraft that compose the final weight of the aircraft. Furthermore, the impact of the payload and other factors on the center of gravity will be taken into account.

After that, the payload-range diagram will be elaborated and this will lead to the determination of the design point for take-off, cruise and landing.

Last but not least, a thorough analysis of the Breguet equation will be done via analytical and different numerical resolutions.



# Chapter 1

## State of the art

### 1.1 Review of the market

To begin with the project, an analysis of the different competitors has been made. Several aircraft models representing each enterprise have been selected to deepen in their characteristics and develop a reference criteria to set the requirements that represent the market necessity. The values for the different characteristics can be appreciated in Tables 1.1 and 1.2. It is worth mentioning that the aircraft filled in green are the ones finally selected due to their high similarity to the specifications of the business jet to be design in this project.

Embraer currently produces the Phenom 100 EV, the Praetor 600 and the Lineage 1000e, three very different jet models from each other, allowing to offer products that widely cover the demand. The Phenom 100 EV, which is the smallest of the family, has the smallest range and the lowest max speed in the current private jet industry. On the other side, the Praetor 600 and the Lineage 1000e have a very similar performance as they have almost the max speed and range. The biggest between this two models is the capacity, since the Lineage 1000e can fit up 19 passengers, 7 more than the Praetor 600.

The next company to be analyzed is Dassault Aviation. This French manufacturer is known for producing military and business jets, from which shall be highlighted the Rafale from the first group and the Falcon family from the second. This last family of airplanes is the one which has been studied, in particular the Falcon 8X

and the Falcon 2000LX. The Falcon 8X is the model with greater characteristics, meaning that it has more passenger capacity and more nominal and maximum ranges, but both admit nearly the same quantity of maximum payload. This jet also has a higher cost per hour due to its characteristic feature, it has three engines instead of two as the great majority of business jets.

Currently, Cessna has on the market 4 different models. Unlike the Embraer, these have quite similar performance between them. Compared to the entire offer, the Cessna models have a medium-low range. The Longitude and Sovereign+ both have a maximum capacity of 12 passengers, and the Citation X+ and Latitude models have a maximum capacity of 8. The differential feature among models is the max speed, where the Citation X+ stands out with the highest velocity between all the different companies' models.

Bombardier Aviation is a branch of the Canadian enterprise Bombardier Inc. Its main families in production are the Learjet, the Challenger and the Global. The Global models 5500 and 8000 have the nearly same capacity and have quite similar velocities. Their difference comes when analyzing their range and their maximum payload, being the 8000 and 5500 the ones with greater values in each field respectively. A third model from the same brand has also been chosen. It is the Learjet 75 Liberty. This model has lower values in each of the characteristics, representing the short-range market sector.



FIGURE 1.1: Gulfstream G650. Credit: Gulfstream

Gulfstream stands out compared to other companies for having the models with the greatest range. On the one hand, the G700, the G650ER and the G650 all have a range with 8 passengers and 4 crew members above the 7000 NM. Besides, these three models also have the same max speed and capacity, for up to 19

passengers. On the other hand, the G280 has the slowest max speed, the smallest capacity and more or less half of the range compared to the other Gulfstream models.

Two Hawker-Beechcraft airplanes have been analyzed despite not being in production since 2013. The Hawker 4000 has greater values in all the characteristics than the Hawker 750 but they are still below the average of the rest of analyzed models. The Hawker 750 is a perfect example of a short-range airplane as it has a range below 2000 NM and a Mach number of just 0.8.

## 1.2 Conclusions

Once each of the business jet manufacturing companies has been analyzed, it is possible to draw a general conclusion about the market situation. To this end, the main characteristics we have taken into account have been range, capacity and max speed, proportional to cruise speed.

On the one side, it is important to take into account the maximum values in each of the three aspects mentioned. The fastest model is the Cessna Citation X+ with a max speed Mach of 0.935, while the slowest is the Embraer Phenom 100 EV with a Mach of 0.7. In terms of range, the aircraft with the highest performance is the Bombardier Global 8000 with a total of 7900 NM with 8 passengers and 4 crew. In contrast, the Phenom 100 EV with a range of 1178 NM with 4 passengers is the worst placed as regards that characteristic. By and by, the jet with the smallest capacity is again the Phenom 100 EV with a limit of 8 people including crew. Opposing that, the Lineage 1000e, the G700, the G650ER and the G650 models all have a maximum capacity of 19 people.



FIGURE 1.2: Cessna Citation Latitude. Credit: Textron Aviation

However, on the other side, it is more important to define the general situation of the private jet market. Clearly, three types of models can be differentiated. The first group is characterized by having a range of less than 2000 NM, a maximum capacity of approximately 8 passengers and a relatively low max speed. Within this group are models such as the Embraer Phenom 100 EV and the Bombardier Learjet 75 Liberty. In the second group, there are the models like the Embraer Praetor 600 and the Gulfstream G280 with a capacity between 8 and 12 passengers and with a range around 4000 NM. Finally, in the third group we can find the biggest airplanes. These models can carry up to 19 passengers and their range reaches around the 7000 NM. They are also generally the ones with the highest max speeds as they do not go below 0.9 Mach, such as the Bombardier Global 8000 and the Gulfstream 6700.

Finally, from the same analysis of the conclusions, it is easy to see what the current situation of the private jet market is and what is the product the companies are not supplying. From this perspective, at present there is no jet with a small capacity and at the same time a large range. In this way and to fill this gap in the market, is the performance what we have been tried to achieve with this study and design. Speed has also been optimized as well, since it is one of the factors that is given more importance when traveling long distances.



FIGURE 1.3: Bombardier Global 8000. Credit: Bombardier

Brand	Model	Normal range [NM]	Payload W/ full fuel [lb]	Max payload [lb]	Max Mach	Max Passengers
Embraer	Phenom 100 EV	1178 (4 pax)	-	1775	0.7	6/7 pax + 1/2 crew
	Praetor 600	4018 (4 pax)	2194	4001	0.83	8-12 pax + 2 crew
	Lineage 1000e	4440 (8 pax)	-	9625	0.82	13 (typ) - 19 pax
Dassault	Falcon 8X	6290	2200	4900	0.90	12 pax + 2 crew
	Falcon 2000LX	3970	1590	4950	0.86	8 pax + 2 crew
Cessna	Longitude	3500 (4 pax)	1600	-	0.84	12 pax + 2 crew
	Citation X+	3229	1505	2514	0.94	8 pax + 2 crew
	Latitude	2700 (4 pax)	1000	2774	0.80	9 pax + 2 crew
	Sovereign+	-	1400	2765	0.80	12 pax + 2 crew
Bombardier	Learjet 75 Liberty	2080 (4 pax)	-	2902	0.81	9 pax
	Global 5500	5900 (8 pax)	-	7139	0.90	16 pax
	Global 8000	7900 (8 pax)	-	5700	0.93	17 pax
Gulfstream	G700	7500 (8 pax)	2235	6385	0.90	19 pax
	G650ER	7000 (8 pax)	1800	6500	0.90	19 pax
	G650	7000 (8 pax)	1800	6500	0.90	19 pax
	G280	3600 (4 pax)	1000	4050	0.84	10 pax
Hawker	750	1968	2200	-	0.80	8 pax + 2 crew
Beechcraft	4000	-	1200-1400	2300	0.80	12 pax + 2 crew

TABLE 1.1: Similar aircraft data table. The models highlighted in green are the finally selected as most similar aircraft. (Part 1/2).

Brand	Model	Take-off field length [ft]	Landing distance [ft]	Thrust per motor [lbf]	Number of engines	Cost per hour [\$/h]
Embraer	Phenom 100 EV	3190	2430	1730	2	-
	Praetor 600	4436	2615	7528	2	-
	Lineage 1000e	6076	2450	18500	2	6345.19\$ (450h)
Dassault	Falcon 8X	6000	2150	6722	3	3803,75
	Falcon 2000LX	5878	4484	7000	2	3.089,71\$
Cessna	Longitude	4840	3170	7665	2	3912.07\$ (450h)
	Citation X+	5280	3330	-	2	4.041,33\$
	Latitude	3580	2480	5907	2	3492.09\$ (450h)
	Sovereign+	3530	2600	5907	2	3443.22\$ (450h)
Bombardier	Learjet 75 Liberty	4440	2296	3850	2	-
	Global 5500	5490	2207	15125	2	-
	Global 8000	5880	2450	16500	2	-
Gulfstream	G700	6250	-	18250	2	-
	G650ER	6299	2680	16900	2	-
	G650	5858	-	16900	2	5.373,54
	G280	4750	2270	7264	2	-
Hawker	750	4696	2245	4.750	2	
Beechcraft	4000	5068	2475	6900	2	2667-3980 \$

TABLE 1.2: Similar aircraft data table. The models highlighted in green are the finally selected as most similar aircraft. (Part 2/2).

# **Chapter 2**

## **Conceptual design**

The objective of this chapter is to thoroughly define all the aspects that must be taken into account as regards the design of the general configuration of the aircraft. No definitive result will be obtained at the end of it: only qualitative decisions and reference values are going to be fruit of the following developed contents.

### **2.1 Fuselage preliminary design**

The fuselage consists of the space where the payload is carried. Such is the importance of this part that the preliminary general layout of the aircraft goes hand in hand with the fuselage. In order to best meet its usefulness, these are the most important characteristics to consider:

- As stated before, the fuselage is the space carrying the payload to a certain destination at a specified speed, so it must offer protection from climatic factors and external noise. It also must permit rapid loading and unloading operations.
- The front part of the fuselage is the most suitable location to place the cockpit.
- The fuselage may be utilized as the key part of the structure, where the other main parts are joined.

- As it represents the largest space in the plane, many systems like the engines or the retractable undercarriage are housed there.

However, with the characteristics enumerated above, there is not enough to make a first design of the fuselage. There are some additional structural, economic and aerodynamic aspects, listed below, that severely affect the whole plane configuration.

- The drag of the fuselage must be minimized as it represents around the 20 to 40 % of the zero-lift drag. For each 10% increase in diameter, the total aerodynamic drag is increased by 1.5 to 3 %. The fuselage drag is mainly determined by shape and the size of the wet area.
- The structure has to be rigid, light, possess a fixed useful life and be strong enough to resist the loads. It also must be easy to maintain and inspect. To avoid fatigue failure the skin of the pressure cabin is subjected to a low stress level, around 30 % of the limit. In this matter, the best option for the pressure cabin is the circular section.
- As far as the fuselage is concerned, the smaller and more compact it is designed, the more the operating costs are reduced. However, the extreme at which the customer rejects the aircraft as a lack of comfort and size must not be exceeded.
- The fuselage modifies the aerodynamic of the plane, being affected the tail configuration. The volume of the fuselage is proportional to the destabilizing effect in pitch and yaw moments, effect offsetted by the empennage itself.

### 2.1.1 Drag and optimization of the external shape

First of all, it should be noted that unlike almost all the elements of a transport plane, the fuselage is hardly optimized. However, how large the drag will be is largely determined by the responses to the following answers:

- Should be the goal to get the perfect streamline shape with minimum drag, or is a cylindrical mid-section to be preferred?

- Should a long, slender shape be adopted or would a short, squat fuselage be better?

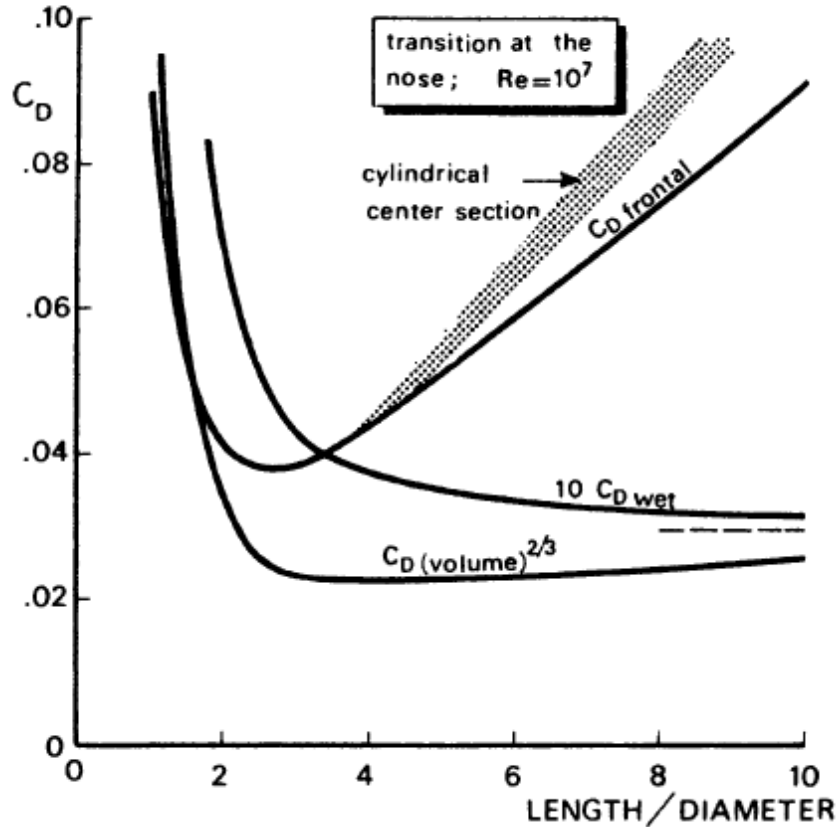


FIGURE 2.1: Drag coefficient as function of the slenderness.

As can be seen in the Figure 2.1 the variation of the aerodynamic drag coefficient is represented as a function of the slenderness for a streamline body and for a cylindrical center section body. If we analyze the dimensionless curve through the front surface we can see that in the case of the optimized body, the coefficient of aerodynamic drag decreases drastically as the slenderness increases to 3.5, where it reaches a minimum. Then the  $C_D$  increases again but with a lower slope than in the previous stage.

If we now compare with the values for the body with a circular section, we can see values very similar to the body streamline body. The curve is almost the same only that from the minimum, around a 3.5 slenderness it separates, giving slightly higher values for the circular case. This minimal difference makes circular section

very common in transport aircraft, since from a structural and spatial point of view it has many advantages.

- Simplified structural design and manufacture.
- With an efficient layout it is possible to almost completely eliminate waste of unused space.
- Improved flexibility of the seating distribution.
- Further development is facilitated by increasing the length of the fuselage.

### **2.1.2 A design procedure for fuselages with cylindrical mid section**

According to Fuselage configuration studies by J.Morris and D.M Ashford summarized in [5], these are the steps to follow for the design of the fuselage of a transport plane with cylindrical mid-section. In the current case of study, a plane with few passengers, this method is applied by considering that the passenger cabin is almost cylindrical.

1. Selection of the number of side by side seats in the cross-section. The diameter fitting this number of seats will likely determine the central part of the fuselage. Part of the other fuselage dimensions will most likely be dependent to the previous chosen diameter.
2. Design the cross-section having into the important parameters as seat dimensions, seat pitch and safety provisions.
3. The external shape can be determined by assuming the minimum wall thickness.
4. Now, it will be possible to add to the planview the non-cylindrical parts, the fuselage nose and the tail. These two parts should be as short as possible.
5. For the size of the prismatic portion, it is taken into account the fuselage nose and tail by subtracting from the total payload the two capacities.

6. From the frontal and lateral planes the following aspects are decided:
  - The main dimensions of the cockpit.
  - The dimensions and location of doors, windows and emergency exits.
  - The tail of the fuselage.
  - The location of the wing centre-section, the attachment of the engines and the landing gear, the pressurization and the air-conditioning system and the electronic systems.
  - The presence of adequate space below the cabin floor for cargo. If this is not possible, a modification of the cross-section could be the solution.
7. If the designed distribution does not fit with the needs, the process must be repeated again since the beginning. It will be necessary to consider other planning schemes.

The following steps will lead us to a provisional design, because a lot of information such as the fitting site between the wing and the fuselage is still unknown. Another crucial point that will surely require making certain changes is the position of the center of gravity. In this way, except for the influence of the fuselage shape on weight and aerodynamic resistance, almost all of this part is made by means of drawings and sketches.

### 2.1.3 The fuselage of general aviation aircraft

#### 2.1.3.1 Importance of comfort and payload density

As analysed by Torenbeek [5], the fuselage ought to be able to fulfill a number of minimum requirements in terms of comfort and well-being:

- **The design and arrangement of the seats**

This property is of maximum relevance in both commercial airliners and private jets. General aviation tends to distinguish passengers with the space they are granted throughout the flight so that First Class Clients seats take

up several Tourist's class seats. In our case, comfort is of utmost importance for the clients and not only the seats will not take up most of the interior space but other amenities such as furniture and seats should be present.

- **The general aesthetic impression**

The suggestion of spaciousness within the limited dimensions of the cabin is crucial on board of the aircraft. The layout of the interior should not induce claustrophobia and is recommended to be pleasant to the eye.

- **Room availability and climate control**

There should be enough space for the traveller to move about the cabin without much effort in a comfortable atmosphere where the temperature, moisture and a provision of an adjustable supply of air could be controlled at any time throughout the voyage. Furthermore, the rates of pressure variation are intended to be kept within acceptable limits during climb and descent manoeuvres.

- **Noise and presence of resonances**

The excessive noise and the presence of resonances can be unpleasant for the passengers. In recent years, advances have been made both in the types of passive materials used for aircraft thermal and acoustic insulation and in highly complex, electronic noise cancellation systems currently under investigation and some minor use by most aircraft manufacturers. The effectiveness of these measures is analysed with the speech interference level (SIL). The SIL is an acoustical parameter calculated from sound pressure levels measures in octave bands which is used to characterise a noise signal in the frequency range where the human ear has its highest sensitivity [14].

With this method certain locations that represent the position of a passenger's ears whilst seated to determine possible noise entry paths and subsequent insulation and isolation needs.

- **Accelerations**

Comfort is largely influenced by wing design and the flexibility of the fuselage structure. The variations of speed should not be noticed by the passengers unless external factors complicate the manoeuvres.

- **Private amenities**

Lavatories and washrooms are amenities which cannot degrade the overall analysis of the aircraft. Although the majority of commercial aircraft reserve small cubicles, private aviation requires large areas not too different from ground amenities. Normally, extra facilities such as a modern shower or stylish sink can make a considerable difference.

- **Stewardess services**

In-flight meals, including meal service and snacks, as well as entertainment (if requested) ought to be available at any time.

#### 2.1.3.2 Cabin design

The first step is to design the cross section of the fuselage, which is influenced by the number of seats, the dimensions of the aisle(s) and other amenities to be placed abreast.

In the case of pressure cabins the cross-section will generally be a circle but it may be built up from segments with different radii.

If no baggage can be carried under the cabin floor, the fuselage belly contour may be flattened.

In either aircraft where the pressure cabin is limited to the cockpit or in an unpressurised fuselage, a rounded rectangular, elliptical or oval cross-section is a common choice.

A first approximation assumes that the wall thickness is a 2% of the fuselage width plus 1 inch, normally a value around 25 mm.

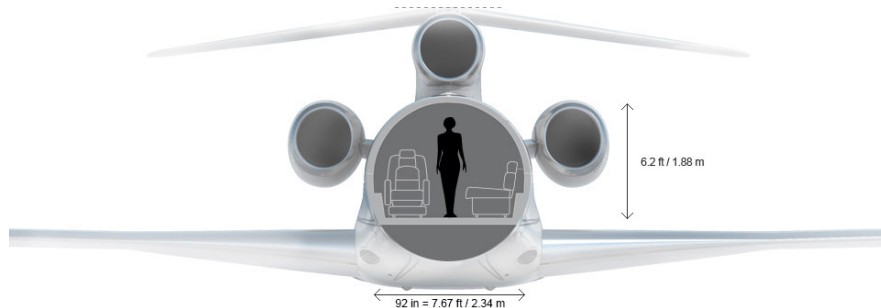


FIGURE 2.2: Dassault Falcon 8X Circular Cross Section

Remarkably enough statistics show that aircraft size effect on the wall thickness does hardly exist although wide variation might exist.

According to FAR 23 and the European homonym regulation, emergency exists must be located to allow escape in any probable crash attitude. The airplane must have at least one emergency exit on the opposite side of the cabin from the main door as specified in section 23.783.

In case the pilot compartment is separated from the cabin by a door that is likely to block the pilot's escape route in a minor crash, there must be an exit in the pilot's compartment.

The slenderness of the fuselage can be obtained as follows:

$$\text{Slenderness} = \frac{l_f}{a_f}$$

where  $l_f$  is the longitude of the fuselage and  $a_f$  corresponds to the diameter of the cross section.

## 2.1.4 Flight deck design

### 2.1.4.1 Location of the pilot's seat and the flight controls

The difficulty of this process is not only in the positioning of the airplane controls, but also in the relative position of the pilot respect to the window. This is complicated since the height of the pilots is changing. To design the entire system the reference eye point is used, and from there the different distances and positions will be defined:

1. The reference eye point must be located not less than 12.7 cm of the rearmost extremity when the control is in its most rearward position.
2. The reference eye point must be located between two vertical longitudinal planes which are 2.54 cm to either side of the seat centerline.
3. Any person from 1.63 m to 1.91 m tall, sitting in the seat must be able to adjust the seat with the seat back in the upright position, so as to locate the midpoint between his eyes at the reference eye position. With the seat

belts fastened, he/she must also be able to operate the aircraft controls with lap strap and shoulder harness fastened.

To achieve this, most seats are horizontally and vertically adjustable and the backrest can be reclined backwards. Lateral movement is also allowed on some seats to make access easier.

#### **2.1.4.2 Visibility from the cockpit**

In VFR flight the pilot must have sufficient visibility to be able to choose the appropriate trajectory and also be able to avoid obstacles. In this way, it is necessary to evaluate the minimum viewing angles for cruise flight, take-off, landing and taxiing at the airport. The greatest difficulty is faced in the approach given that the plane descends with a certain slope and a considerable pitch angle while the pilot must be able to see all the different signals.

For example, when taxiing, the pilot should be able to see the ground at a maximum of 130 ft from the airplane, but preferably this distance should be less than 50 ft. When climbing, the pilot should be able to see at least  $10^\circ$  below the horizon and preferably  $15 - 20^\circ$  below it. Finally, when landing, the pilot should be able to see below the horizontal when the airplane is in the tail-down attitude.

#### **2.1.4.3 Flight deck dimensions and layout**

In order to design the flight deck, the minimum number of flight crew must be determined by taking into account the workload of the crew. The total amount of work is given by the sum of load of the flight path control, the collision avoidance, the navigation, the maintaining contact with the Air Traffic Control centers, the operation and supervision of systems and the decision taking concerning the execution of the flight. This is also affected by factors such as the degree of automation and complication of the systems and the operational limitations. Transport planes must have duplicated flight controls and in case of long-range flights it is required a third crew member seat. The flight deck must also provide adequate space for crew members baggage. In business aircraft, flight deck accommodation is limited so its length does not exceed 1.8 m. The current jet will need two crew

members to be piloted safely. In this way, according to [5], these are the typical measurements for the cabin:

<b>Number of flight deck seats</b>	2
<b>Length of flight deck (minimum/average) [m]</b>	1.60/1.78
<b>Distance between seat centerlines [m]</b>	0.76

TABLE 2.1: Characteristic flight deck distances.

#### 2.1.4.4 Emergency exits for crew members

In the case of a business jet, with a capacity of less than 20 passengers, the emergency exits for the crew can be the same as those for the passengers. This is due to the small dimensions of the plane, being the evacuation doors close enough for everyone.

## 2.2 Wing configuration

### 2.2.1 Vertical position of the wing

The vertical location of the wing relative to the fuselage is one of the first aspects to consider and it is to a very large extent determined by the operation requirements, although aerodynamic and structural differences are not without importance [5]. The aircraft developed in the present project is a private business jet, which cabin must be able to comfortably accommodate the passengers, as well as allowing a fluid living environment. To fulfil this purpose, a need is to provide the maximum possible height of the cabin.

The high wing is a design requirement for military and often cargo transports because it eases the movement of vehicles and personnel around the aircraft. However, this configuration is not the appropriate for a business jet because it would lead to a severe lowering of the cabin ceiling, as it is exemplified in Figure 2.3. Thus, this configuration is not convenient for the uncomfortability it would cause.



FIGURE 2.3: Air Force Reserve crewmembers board a C5-M Super Galaxy. Credit:  
Lisa Krantz/San Antonio Express-News

Mid wing is used when minimum drag in high-speed is required, so the aerodynamic interference between the boundary layers at small angles of attack is the lowest. Nevertheless, the wing may be continuous through the fuselage because the transfer of the loads from it may take place via “almost” solid bulkheads to which each winghalf is attached. From the inner point of view, this leads to an enormous physical obstacle that interferes with the functionality of the cabin.

The configuration that allows the maximum leverage, and which will be used for the present aircraft, will be low wing. From the service perspective, the interior space will lack of the physical obstacles that the other vertical positions of the wing generate. As regards functionality, the structural design will be of less complexity than in high-wing, where the weight of the fuselage is “hanged” from the wing. Additionally, the landing gear is able to be easily retracted and kept safe in the inner part of the wing.

However, an important disadvantage according to [1] is the interference drag in the case of a high-wing configuration is principally due to the interaction of the fuselage boundary layer with that from the wing’s lower surface. This latter layer is relatively thin at positive angles of attack. Meanwhile, for the case of low-wing is the boundary layer on the extrados the one that interferes with the fuselage boundary layer. This upper surface layer is appreciably thicker than the lower surface layer. Thus, the wing-fuselage interference drag for a low-wing configuration is usually greater than for a high-wing configuration.

Another inconvenience to take into account involves the security at the landing. The proximity of the engines and the wings (and in consequence the fuel) to the ground entails a higher risk of fire in case of damage caused by contact.

### 2.2.2 Wing plan shape

Since the first attempts to build the most efficient aircraft the discussion of which is the most efficient, in terms of consumption and production cost, wing shape has been present. The two types of wing shapes that have been repeated in all aircraft built since then have been the elliptical and the rectangular wings’ shape.

The wing shape becomes a key factor in the calculation of the coefficient lift  $C_l$  distribution around all the span wing. These two are related following the next equation:

$$C_l = \frac{l(y)}{q \cdot c(y)}$$

Where it can be appreciated terms like:

- **Lift distribution  $l(y)$ :** generated by the airfoils that make up all the wing cross-section, which will be considered constant for the preliminary

calculations.

- **Dynamic pressure  $q$ :** that will be also assumed constant for the first approximated calculations, considering the aircraft flying at a constant speed and altitude.
- **Chord distribution  $c(y)$ :** its variation all around the wing span is totally correlated with the wing shape.

It is easily observable that decreasing the chord as we move towards the tip of the wing will produce an increase of the  $C_l$  at the wing tip sections, generating the latter to stall earlier for the same angles of attack.

Our preliminary design idea is to use a rectangular wing shape instead of using an elliptical one. This decision is motivated by the idea that despite the elliptical wing shape offers better aerodynamic performance due to the production of the minimum aerodynamic induced drag for every angle of attack, it entails large costs of production that doesn't make up for the consumption decrease consequence of the drag reduction. Additionally the elliptical wing shape generates a constant total coefficient lift spanwise distribution  $C_L$  which will induce a total stall situation when the maximum angle of attack will be reached. This last effect also will disable all the control wing surfaces that could have been designed in the next sessions making the pilot not have any option to retake the plane's control.

In conclusion for our aircraft design it would be used the rectangular shape wing to which we will later add other aerodynamic design elements such as aspect ratio, taper ratio and others. However, despite being a less efficient plant distribution, the production process will be much cheaper and we consider that it is already enough for the design we are currently thinking.

### 2.2.3 Aspect ratio

The first geometrical parameter (and the most intuitive one) as regards the rectangular wing is the aspect ratio  $A$ , which is defined as the quotient of the squared wingspan  $b$  over the wing's surface  $S_w$ :

$$A = \frac{b^2}{S_w}$$

The aspect ratio is an indicative of the slenderness of the wing. In case of an elliptical wing, the induced drag coefficient is expressed as:

$$C_{D,i(el)} = \frac{C_L^2}{\pi A} \quad (2.1)$$

Mathematically, increasing  $A$  leads to a lessening of the induced drag. However, from a realistic perspective there exist the following set of restrictions:

- Structural limitations: if the length of the wing is increased, the lifting aerodynamic loads along it are able to produce a higher bending moment on the root mainly on the axial direction of the fuselage. Additionally, it may involve hazardous torsion on the wingtips.
- Maneuverability limitations: a higher aspect ratio leads to an increasing of the moment of inertia along the roll axis, which means that the rotation along this axis is more difficult to start but also to stop.
- Parasitic drag limitations: although the induced drag will decrease with higher aspect ratios, the normal surface to the wing, and consequently the parasite drag, will increase.
- Inner volume: low aspect ratios often imply a greater useful internal volume, since the maximum thickness is greater, which can be used to house the fuel tanks, retractable landing gear and other systems.
- Infrastructure limitations: airport legislation decrees a maximum allowable wingspan in order to fulfil the safety measures in hangars, taxiways and runways. In consequence, the manufacturers must adapt their aircraft to this conditions: for example, the A380 has lower aspect ratio than A320 or A350 due to its wider fuselage, though keeping similar wingspans.

The values found in commercial jet transport are mostly between 7 and 9 (view Table 7-1 in [5]), meanwhile in executive jet the interval is lowered down from 5.5 to 7. It will be this latter interval which may be taken as an orientative reference.

### 2.2.4 Taper ratio

The taper ratio  $\lambda$  is defined as the quotient of the tip chord  $c_t$  over the root chord  $c_r$ , that is:

$$\lambda = \frac{c_t}{c_r}$$

Although a tapered wing's visual appearance is not similar to an elliptical wing, the behavior may be very similar for certain values of  $\lambda$  in terms of the induced-drag coefficient  $C_{D,i}$ . It has been previously stated that the elliptical wing is the one that minimizes it, and for a non-elliptical wing the  $C_{D,i}$  may be expressed with a slight modification of expression (2.1):

$$C_{D,i} = \frac{C_L^2}{\pi A} (1 + \delta) \quad (2.2)$$

Where  $\delta$  is the induced drag factor. Figure 2.4 shows the evolution of  $\delta$  with  $\lambda$ , achieving a minimum between 0.35 and 0.45. In this interval, the aerodynamic behavior as regards induced-drag is in close proximity to the elliptical one. The mathematical reason is due to the elliptical similarity of the lift distribution along the wing.

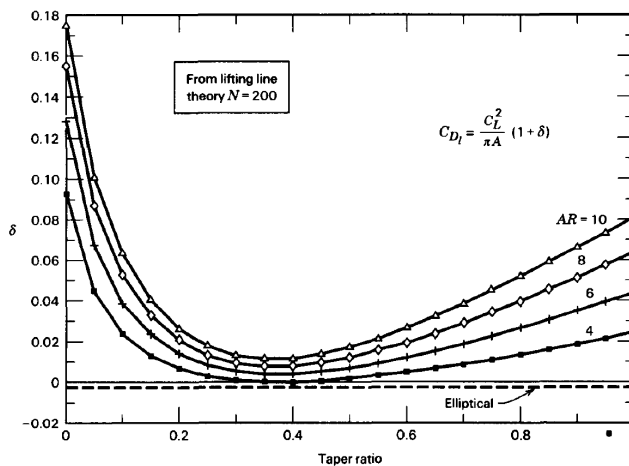


FIGURE 2.4: Numerical calculations of the induced drag factor for linearly tapered and elliptic wings. Source: [1]

The previous statement can be confirmed with the values shown in Table 7-1 in [5]. More precisely, for both jet transport and jet executive aircraft, there is no taper ratio lower than 0.2, being most of the values comprised between 0.3

and 0.4. The punctual planes that surpass the previous values develop military functions.

Following both the tendency of the current aircraft and taking into account the results of the graph, it follows that the resulting taper ratio for this aircraft must be found between 0.35 and 0.4.

### **2.2.5 Wing Sweep**

The wing sweep is usually defined with respect to the leading edge  $\Lambda_{L_E}$  or respect to an arbitrary line passing through the quarter chord points . Assuming a case of tapered wing with known taper ratio  $\lambda$ , it is possible to obtain the next relation:

$$\tan \Lambda_f = \tan \Lambda_{L_E} - \frac{4f(1-\lambda)}{A(1+\lambda)}$$

Where  $f$  is the quarter point from where sweep angle  $\Lambda_f$  at an arbitrary position is obtained.

At low speed flights wing sweep does not present any advantage, rather it decreases the efficiency due to an increase in the velocity field induced by the vortexes at the end of the wing, also known as downwash.

As it has been mentioned in the requirements section, we are trying to design an highly speed executive jet so the introduction of wing sweep will present more advantages than disadvantages. Wing sweep will introduce some negative effects like generation of two independent downwash areas, resulting from the both semi-wings, and producing some bad interference between their aerodynamic centers, that will be located inside this downwash areas. Despite of this big disadvantage, wing sweep is going to allow us to move back all the aerodynamic centers of all the sections that make up the wing and consequently also the Lift ( $L$ ) resultant force allowing us to control in a better way the longitudinal plane's stability. Moreover and possibly the most important, is the effect of delaying the sonic flow effects all over the wing allowing the aircraft flying at a higher speed. Due to the sweepback, the flow along the wing can be decomposed into two components, the first one along the chord direction and the second one along the span, which are independent between them if we assume inviscid flow. Accordingly to the

main aerodynamic principles, the pressure distribution along a wing section only depends on the normal/perpendicular component of the velocity or Mach number, which is related with the real Mach flight number by the expression 2.3 and is derived from the decomposition showed in the figure 2.5.

$$M_n = M_{flight} \cdot \tan \Lambda_{LE} \quad (2.3)$$

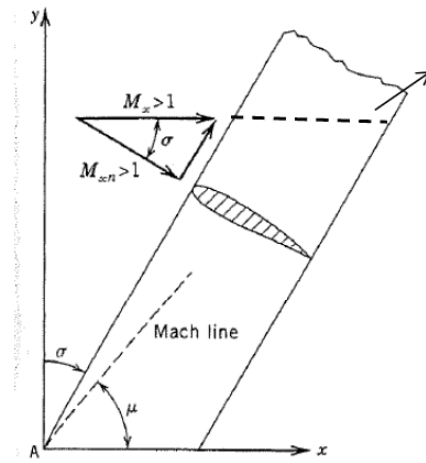


FIGURE 2.5: Decomposition of the velocity round the wing due to the wing sweep.

Source: [2]

In order to sum up we can state that by increasing the sweepback we are going to be able to achieve higher critical Mach numbers in our different wing sections delaying the appearance of shock waves and their undesirable effects.

The previous statement can be confirmed with the values shown in Table 7-1 in [5]. More precisely, for both jet transport and jet executive aircraft, the most of the wing sweepback values are comprised always between  $10^\circ$  and  $30^\circ$ . So in the same design line for that kind of aircraft and taking into account the benefits that wing sweep produces to the increase of Mach cruise flight number, the wing sweep angle for this aircraft must be found between  $20^\circ$  and  $30^\circ$ .

### 2.2.6 Wing twist

Wing twist is an strategy to make the angle of attack of the wing sections vary along the span. It can be geometric, so that the angle of attack  $\alpha$  is different at

different spanwise locations, or it can be aerodynamic, variating the airfoil along the wing. Negative geometrical twist on the extremes of the wing (wash-out) is recommendable as allows the proper functionality of the ailerons and flaps when the inner part of the wing enters in stall. Typical values of wash-out in general purpose aircraft are about -3 or -4 degrees.

### 2.2.7 Dihedral

The dihedral angle is commonly used in order to improve the longitudinal and lateral stability indices for an aircraft. It is also known as the strategy used to correct the negative interference between the fuselage and the main wing's aircraft. Introducing the dihedral to an aircraft is able to produce a rolling moment which is opposite to the one generated when the plane is performing a yaw maneuver. Basically, with the dihedral effect both semi-wings are able to appreciate two different wind relative velocity components, one bigger than the other, and this speed difference leads to two different attack angles. The side of the wing with the greater relative angle of attack will generate more lift and as a consequence will cause a yaw moment towards the opposite side, compensating the effect of the yaw movement.

When the dihedral angle is defined, it could be considered a negative or a positive angle and it will be totally related with the vertical position of the wing.

The dihedral angle definition is totally related to the vertical position of the wing. As it is shown in the Figure 2.6, for a high-wing configuration, the fuselage will produce an additional dihedral effect that may be compensated through a negative dihedral angle. The opposite case takes place in low-wing configurations, which need in terms of lateral stability a positive dihedral angle. Additionally in mid-wing configurations the fuselage effects cancel, thus dihedral effect is neutral and adding dihedral angle is not necessary.

For the case of the aircraft design that is being carried out, due to the selected low-wing configuration it will be necessary to introduce some positive dihedral to it. The most typical values for jet executive aircraft, where the most of them are low wing configured are dihedral angles between  $2^\circ$  and  $6^\circ$ .

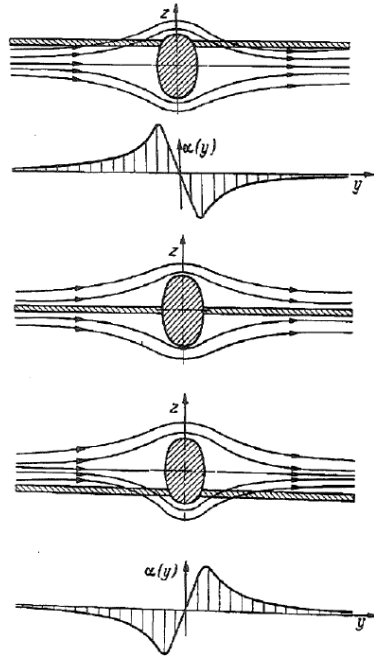


FIGURE 2.6: Additional dihedral effect produced by the interference of the Wing-Fuselage configuration. Source: [3]

### 2.2.8 Winglets

Winglets, also called wingtip devices, are complementary wing surfaces which are beneficial in terms of the aerodynamic drag. Often shaped like the dorsal fin of a shark, their purpose is to reduce the induced drag, which can be achieved by increasing the horizontal span or the vertical height of the lifting system. Winglets increase the length of the trailing edge, and thus the spread of the vortices along it, creating more lift at the wingtips.

In the race for approaching a close elliptical behavior as regards induced drag, for the same amount of structural material, non-planar wingtip devices can achieve a similar induced drag benefit as a planar span increase. As the wingspan is not enlarged, the structural affectation is less critical in this sense [15].

Winglets were firstly tested throughout the 80's decade, and were commercially introduced in the following one. As Figure 2.7 shows, the tendency is to introduce new shapes in order to progress in the efficiency they provide. This last fact is confirmed by the wide range of commercial aircraft: transport jets of all

sizes, as well as private jets and even gliders include these devices. It is highly recommendable to implement them in the current design, not as a general trait of the aircraft but more as a complement.



(A) Traditional shark-shaped (sharklet).  
Credit: Airbus

(B) Split-fence shape. Credit: Boeing

FIGURE 2.7: Different winglet shapes.

## 2.3 Power plant

Propulsion means the action of pushing forward or driving an object forward, so a propulsive system is a machine capable of creating thrust to achieve this goal. On airplanes and spacecraft, thrust is generated through the application of Newton's third law of action and reaction. This is, a working fluid is accelerated by the engine, and the reaction to this acceleration produces a force on the engine. The amount of thrust generated depends on the mass flow rate and the exit velocity of the fluid. Moreover, different propulsion systems produce thrust in slightly different ways. Below are detailed all the existing aircraft engines and its advantages and drawbacks.

The main reason why there are different types of engines is related to Newton's laws of motion. First, the thrust generated by the engine must balance the drag of the overall aircraft. Second, in order to accelerate the aircraft, the generated thrust must be higher than the drag. The excessive thrust is known as *excess thrust*. In fact, the greater the difference between thrust and drag, the faster the aircraft will accelerate.

Considering airliners and cargo planes, they spend most of the time in cruise condition. For these, excess thrust is not as important as high efficiency and low fuel usage. Since thrust depends on both the amount of gas moved and the exit velocity, it can be generated by accelerating a large amount of gas by a small amount or accelerating a small amount of gas by a large amount. Because aerodynamics of the fans, it is more efficient to accelerate a large amount of gas by a small amount. That is why they usually have large fans and tend to achieve high bypass ratio values. In contrast, fighter planes require high velocities, energy efficiency is not as important as excessive thrust. In addition, military aircraft usually have afterburners to increase thrust for short period of time [4].

### 2.3.1 Type of propellers

Aircraft powered with piston engines are quite obsolete nowadays. This is primarily due to the fact that turboprop engines are more efficient when creating thrust.

#### 2.3.1.1 Internal combustion engines

Briefly, the combustion process of internal combustion engines takes place in an enclosed cylinder where chemical energy is transformed into mechanical energy. Inside the cylinder there is a moving piston which compresses a mixture of fuel and air and is pulled back down due to the explosion of gases. On the power stroke, the piston is attached to a crankshaft which converts linear motion into circular motion that is used to turn the aircraft propeller. for a four stroke engine, usually 4 phases are distinguishable: intake, compression, combustion and exhaust. This process is repeated continuously in a thermodynamic motion called *Otto cycle*.

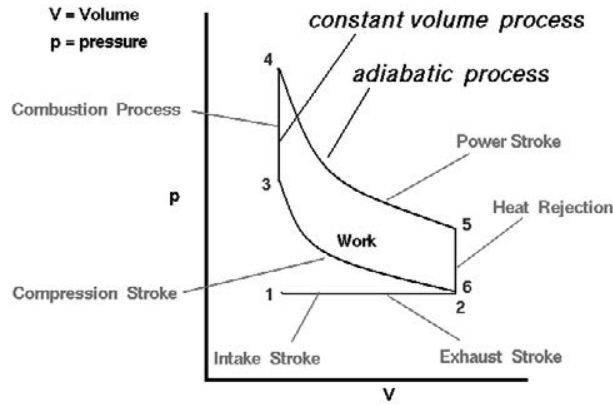


FIGURE 2.8: Ideal Otto Cycle. Source [4].

In an ideal Otto cycle, as shown in the diagram Figure 2.8, the area enclosed by the compression stroke (2-3) and the power stroke (4-5) is the work done by the engine. To achieve a greater amount of work and increase this area needs to be larger. Thus, adding more cylinders, decreasing the cylinders volume during compression, raising pressure, etc. can be accomplished. However, increasing the amount of engines increases aircraft's weight and creates more heat that needs to be dissipated. Even though radial engines enable a more efficient way of cooling, this configuration increases drag.



FIGURE 2.9: Radial engine. Source [4].

### 2.3.1.2 Turbine Engines

Jet propulsion is a practical application of Sir Isaac Newton's third law of motion which states that for every force acting on the body there is an opposite and equal reaction for aircraft propulsion. In which the "body" is the atmospheric air

that is accelerated as it passes through the engine. There are 4 types of turbine engines:

- Turbojet
- Turbofan
- Turboprop
- After-burning turbojets

### Turbojet Engines

Contrary to piston engines, instead of burning fuel in a confined space that is dependent upon precise timing of ignition, the turbojet engine is essentially an open tube that burns fuel continuously. Figure 2.10 shows a clear representations of the inner parts of a turbojet engine.

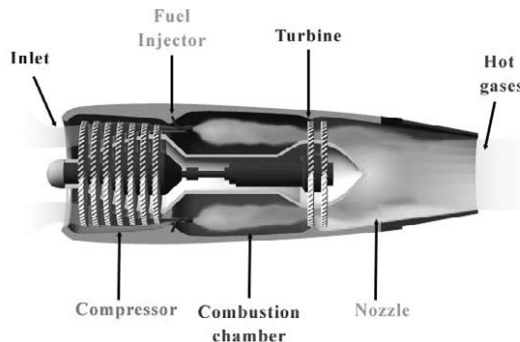


FIGURE 2.10: Cutaway view of turbojet engine. Source [4]

According to [4], turbojet consists of mainly 5 stages: First, a large mass of air is sucked through the *inlet* and is drawn to the *compressor*. The compressor raises the pressure of the air entering the combustion chamber by forcing the air to pass through rotating and stationary blades. As gas is forced to pass through smaller and smaller volumes, the pressure is increased heavily and the gas' temperature elevates as well. Today's compressors typically have a compression ratio of 40 : 1, the greater the value, the better efficiency. These values are far beyond of piston engines. Besides, in order to maximize efficiency, most aircraft usually have two different compressors operating at two different shafts, a low-pressure compressor followed by a high-pressure compressor.

Then, at the *burner* stage the fuel is injected and ignited with the air. This charges the gas with energy by raising its temperature dramatically and accelerated towards the turbine. In fact, the gas raises its temperature well over even turbines' materials melting point. Hence, only 12 % to 25 % of the air from the compression is combusted while the rest cools the combusted gases down to temperatures below turbine engines' damaging point. The larger the difference between the exhaust gas temperatures and the exterior air, the more thrust is created and more efficient is the engine.

The next stage is the *turbine*, where the gas passes across the turbine causing the blades to rotate, and in turn, to rotate the shaft that is connected to the compressor. Indeed, there remains still sufficient energy in the gas to make profit from it as it exits the nozzle.

Finally, the purpose of the *nozzle* is to convert kinetic energy into velocity and thereby produce thrust. The nozzle allows the gas to exit the engines and thus reach free-stream pressure which creates thrust of the engine. In addition, it controls the mass flow rate and the velocity which determines the amount of energy the engine produces.

Overall, turbine engines have a much higher power-to-weight ratio than piston engines. They can operate at much higher temperatures and can produce more thrust. However, they are less efficient at low speeds and low altitudes.

### Turbofan Engines

Turbofan engines are a modified version of a turbojet engine. Despite both of them share the main core stages, inlet, compressor, combustion chamber, turbine and nozzle, the turbofan has an additional turbine to turn a large many-bladed fan located in front of the engine. This is known as "two spool" engine, one spool is used to power the compressor whereas the other is used to power the fan. This means the flux is separated into a primary flux that enters to the combustion chamber and a secondary flux which bypasses the large fan. Indeed, over 75 % of the total thrust of the engine comes from the bypass air. Although little air passes over the core of the engine, large thrust is created for very little additional fuel. This why turbofans are more fuel efficient than turbojets since commercial aircraft operate primarily in cruise.

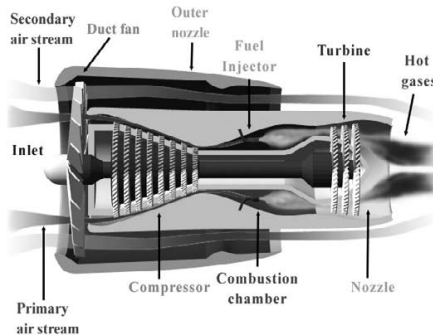


FIGURE 2.11: Cutaway view of turbofan engine

### 2.3.1.3 Turboprop Engines

A turboprop engine is a hybrid between a turbojet and a propeller engine. It has at its heart a turbojet core to produce power, but with two turbines. The first turbine powers the compressor while the second powers the propeller through a separate shaft and gear reduction. The gears are necessary to keep the propeller from going supersonic and losing efficiency.

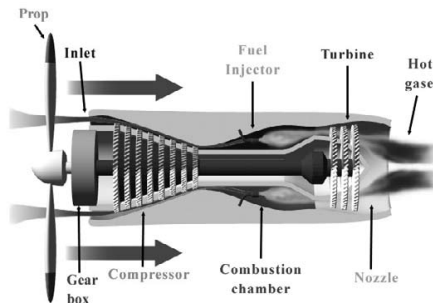


FIGURE 2.12: Cutaway view of turboprop engine

Unlike a basic turbojet, the second turbine removes most of the remaining energy from the flow to power the propeller and less than 10% of actual thrust is produced by the core. Turboprops operate well in the low subsonic range, with much more power than a piston-driven propeller aircraft.

### Afterburning turbojets

This engine is a turbojet with an additional modification with a capability of injecting hot fuel into the hot gases after they have passed through the turbine. This produces an additional thrust up to 50 %. The afterburner does not burn fuel as efficiently as the combustors do, so its operation dramatically increases fuel consumption.

There are other types of engines that are not mentioned above due to the fact that these engines (ramjet and scramjet) operate at supersonic speeds.

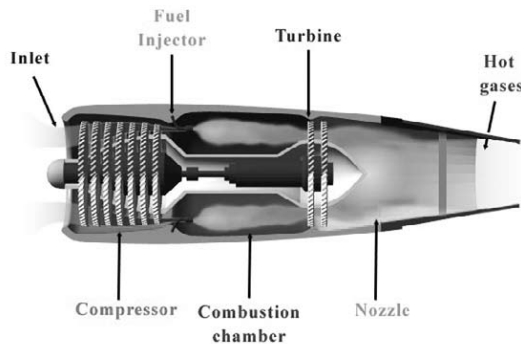


FIGURE 2.13: Cutaway view of the afterburning turbojet

#### 2.3.2 Position of the engines

Regarding the use of turbofan engines for civil aircraft, the relatively large diameter of modern high-bypass engines prohibits the installation of engines buried in the wing roots. Therefore, the engines are generally installed in pods, often detachable for maintenance. The engines and the pods are connected to the airframe by means of pylons, that are required to withstand heavy loads.

When talking about private jets, the engines are not required to be extremely large. Thus, the compactness of podded jet engines allow the designers some freedom in the location of the nacelles in a favourable position. As a result, two layouts are commonly seen: wing-mounted engines and aft-mounted engines. The second refer to engines pods attached to the rear end of the fuselage, while the first refer to the pods attached under the wings of the aircraft.

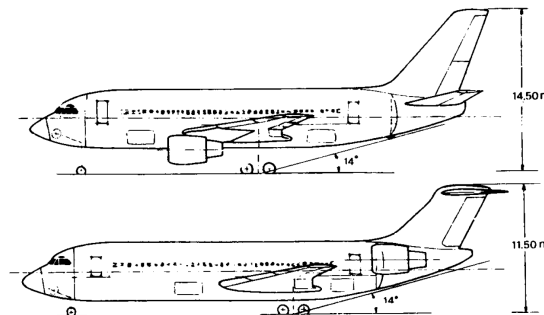


FIGURE 2.14: Installation of high-by-pass-ratio engines on the wing and in the rear fuselage. Source: [5]

### 2.3.2.1 Wing-mounted podded engines

When choosing the location of the engines, the following points shall be considered if the aim is to place the engines mounted to the wings.

- Placing the engines further outwards reduces proportionally the bending moment at the wing root produced due to the lift. However, when the taxi loads become more predominant this moment is reversed on account of the weight of the engines. Moreover, when placing the engines excessively outwards, the vertical tail surfaces need to be increased in order to compensate the adverse yawing moment.
- When designing swept-back wings it is possible to favourably alter the position of the center of gravity by changing the positions of the engines in the spanwise direction.
- The distance between the nacelle and the wing affects the shape of the flow channel, which is a decisive factor for the interference drag between the two parts. As we can see in figure 2.15 an unfavorable position creates a considerable drag penalty.

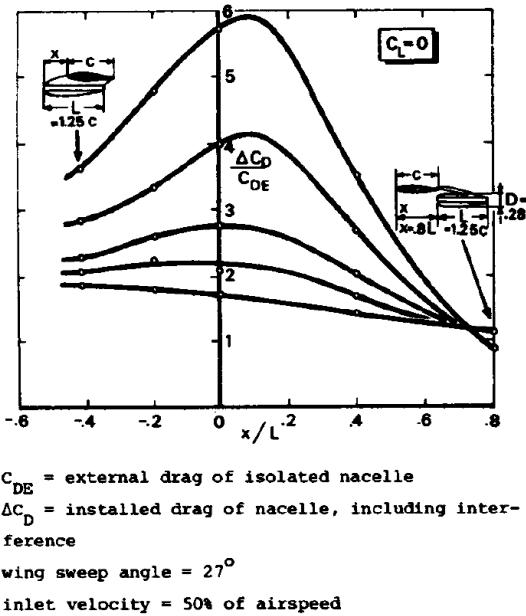


FIGURE 2.15: Location effects on interference drag of a wing-mounted nacelle.

Source: [5]

### 2.3.2.2 Fuselage-mounted podded engines

On the other hand, the following points must be considered if it is intended to place the engines at the rear part of the aircraft:

- The loads of the engines, approximately 10 times the installed weight, will be transferred into the fuselage in the forward and downward direction, thus a specific structure capable of withstanding the loads is needed.
- The location of the nacelles behind the aerodynamic center of the wing causes the aerodynamic center to move backwards. This stabilizing effect is beneficial for commercial aircraft.
- At large angles of attack, the wake created by the nacelles may reduce the effectiveness of the horizontal stabilizer. Thus, the location of the engines play a relevant role when talking about deep stalls.

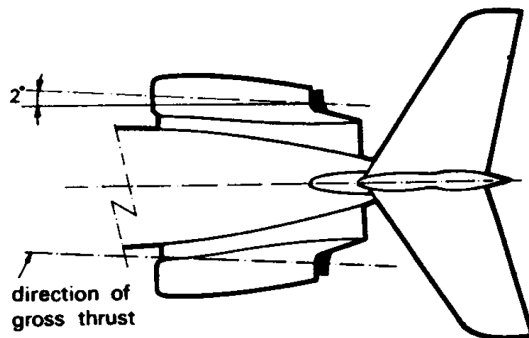


FIGURE 2.16: Example of the shape of engine nacelles mounted to the rear sides of the fuselage. Source: [5].

### 2.3.2.3 Private jet engines

Overall, when the engines are mounted way too below the wing this leads to a higher undercarriage and a larger vertical tailplane. Conversely, when the engines are placed at the end of the fuselage this can result in an unacceptably large centre of gravity.

Last but no least, engines attached to the fuselage or aft-mounted engines are solely used when the payload has a relatively small volume, and there is enough space for the engine and its inlet and exhaust ducts. With regard to civil aviation, the most useful case for aft-mounted engines is when talking about small private jets.

Taking all these factors into consideration, the conclusion is that although it will be required greater efforts on the rear pod structure, aft-mounted engines will be the most favourable case for the current private jet aircraft.

### 2.3.3 Number of engines

Since it has been decided to place the engines at the rear end of the fuselage, the number of engines is quite restricted. There are only two viable combinations: two engines as it is commonly seen in many aircraft and a three-engine configuration. Figure 2.17 illustrates both cases.

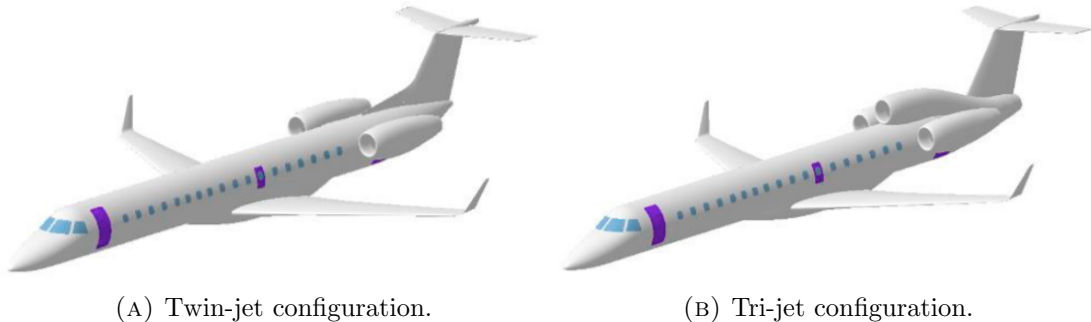


FIGURE 2.17: Available configurations for aft-mounted engines. Source [6].

When three engines are used, there is more difficulty when installing the third engine, for this it will have to be placed in the plane of symmetry. This adds a weight penalty and creates a problem as regards the design of the empennage. Some of the solutions to this problem are the S-duct engines or fitting the third engine buried in the vertical stabilizer.

On the other hand, although modern turbojet engines are very reliable, the possibility of an engine malfunction must never be ignored. An engine shutdown or an inability to operate can create a decrement in thrust, as well as may lead to extra yawing and rolling moments and extra drag. The airworthiness authorities must ensure that the aircraft are capable of operating in this unfavourable conditions and that the design provides an acceptable level of safety. Therefore, an extra engine implies a more direct solution to this problem, thus helping to certificate the aircraft more easily. Moreover, the tri-jet configuration allows the airlines to operate for more extended overseas flights when compared to twin-jet configurations.

Overall, the design team has decided to simplify the structural aspect of the engine pods and focus on the aerodynamic side of the project, as a consequence, a twin-jet configuration has been chosen.

## 2.4 Tail configuration

The empennage is formed by the horizontal and vertical stabilizer, as well as the elevators and rudders. Different tail configurations must be analysed in terms of aerodynamic and structural performance. Additionally, it must be mentioned

that the choice of a specific configuration will be highly influenced by the wing and engines layout.

## 2.4.1 Common configurations

### 2.4.1.1 Conventional tail

The conventional tail is the most common of all tail configurations, since it is used in about the 80% of total aircrafts ever built, as it ensures structural simplicity and stiffness. It is easily identifiable, as it presents a single fin with the stabilizer mounted on the fuselage itself. This configuration is often a default configuration unless the project call for alternative solutions due to the stated requirements.

The conventional tail configuration presents many advantages. First of all, it is provided with the safety that it is used in most of the existent aircrafts in the market.

By setting a conventional tail configuration, the position of the HT prevents the engines to be mounted on the fuselage aft of the cabin. This fact entails bringing down engine noise in the cabin.

Another advantage is that both the HT (horizontal tail, refers to a surface intended to control the pitch of the aircraft) and the VT (vertical tail, surface intended to control the yaw), are joined in the fuselage. This fact provides structural robustness to the tail, as the fuselage girth is large in the join. By this, the tail is provided with a huge torsional rigidity which also helps resisting empennage flutter. As explained below, other configurations join the HT directly to the VT. Hence, it is necessary to reinforce the VT.

Furthermore, it results an interesting configuration for single-engine propeller aircrafts, since it takes advantage of the propwash (it gives the aircraft a shove during the take off run). By this, it is possible to the aircraft to rotate at a lower airspeed. As a negative point, for propeller aircrafts the drag contribution increases if the tail is mounted inside the propwash.

At low angles of attack, the wake lies below the HT and presents a small thickness. However, when operating at high angles of attack, it is possible that the wing wake hits the tail due to the HT position in this configuration. Then, the thickness

of the wake experiences a great growth and wraps the HT. In this case, the turbulent airflow could cause the violent oscillation of the tail. Consequently, the pilot is warned of an imminent stall. At post-stall, the HT may exceed the lower boundary of the wake, although it depends on the geometry of the aircraft.

On the other hand, the main drawback of the conventional tail configuration is the possibility of getting a rudder blanketed by the separated wake emanating from the HT. This happens at angles of attack in the post-stall range. When the HT covers a substantial part of the rudder, the rudder authority gets reduced. Thus, a blanketed rudder is undesirable in abused flight conditions such as during a spin. In this case, the recovery becomes more challenging.

However, this fact is not a critical problem, as spin is a very complicated phenomenon and the blanketing of the rudder is not the only feature of the aircraft which affects in its development. Moreover, many aircraft are nowadays designed to guarantee that the rudder area susceptible to suffering the blanketing is outside the separated region in order to avoid this phenomenon.



FIGURE 2.18: Aircraft with a conventional tail. Source: [7]

#### 2.4.1.2 T-Tail

The T-Tail is based on the idea of joining the horizontal tail directly to the upper end of the vertical stabilizer. This configuration is the most used in business jets, basically due to the the efficient aerodynamic performance when mounting the engines in the rear fuselage part. As an example, Embraer Praetor 600, Cessna Citation X and Gulfstream G280, which are the potential competence of our aircraft, feature this specific configuration.

As regards its advantages, it is the most efficient tail in aerodynamic terms. This is mainly due to the high position of the HT, which receives undisturbed air by avoiding the jet efflux coming from the engines placed at the fuselage rear part.

In addition, the wing slipstream neither causes disturbance in the tail's coming flux because of its high position relative to the low wing.

Moreover, an additional positive aspect is the great spin recovery potential that this specific tail provides with. As a matter of fact, when the aircraft stall has ended, the horizontal stabiliser's turbulent slipstream does not blanket or interfere with the rudder due to HT's high position.

One of the main structural drawbacks of the T-Tail is the high torsional loads at the top end of the VT, which in turn also causes torsion in the rear fuselage part. This is due to asymmetric lift generated in yaw by the tail, basically explained by the HT high position coupled with the vertical stabilizer presence. This torsion implies the need of reinforcing the fuselage and vertical tail structure, resulting in an undesired weight increase.

Nevertheless, aeroelastic flutter is the most structurally demanding problem of this configuration. This phenomenon causes the need of reinforcing the vertical stabiliser and the joint with the horizontal one, which implies a further increase in weight.



FIGURE 2.19: Aircraft with T-tail configuration. Source: [7]

#### 2.4.1.3 Cruciform tail

This configuration is an intermediate option over the previous two, since the HT is located in the middle of the vertical stabilizer, creating in this way a cross in the tail of the aircraft. It is also quite common to see this structure in business jets, such as the Dassault Falcon 8X and the 2000LX or the Cessna Latitude, all of them similar models to the one developed in this project.

As with the T-Tail, raising the horizontal fin allows to have free space in the underside of the vertical tail, which can lead to aerodynamic advantages because of the placement of the engine regarding the HT. Nevertheless, unlike the previous configuration, the airflow to which the top of the rudder is exposed is not “clean”

at all, because the horizontal stabilizer is located in an intermediate position of the VT. This is an issue when it comes to spin recovery, as it has been explained in the conventional configuration.

Another major disadvantage, also shared with the high mounted HT, is that the vertical stabilizer needs to be reinforced, relative to the conventional type, in order to ensure the robustness of the tail and avoid aeroelastic flutter. In addition to that, the torsion loads are also greater than in the baseline configuration but less important than in the T-tail, since the latter is situated in a higher position.

One last aspect that should be taken into account is that the type of assembly between the elevator and the rudder has to ensure a free deflection of the last element. Thus, two options can be considered: a elevator with a removed part in the root or a rudder split in the position of the HT. The drawback of these alternatives is an increase in the complexity of the design as well as in the production costs.



FIGURE 2.20: Aircraft with a cruciform tail. Source: [7]

#### 2.4.2 Other configurations

There is a wide variety of other tail configurations to analyse yet, such as butterfly or V-Tail, twin vertical or H-Tail. Nonetheless, the usage of these more complex tails is not common in business jets. Basing on this fact and taking into account that there are no significant improvements in using these configurations, the mentioned tails will not be considered.

#### 2.4.3 Tail configuration choice

Taking into account the above performance of each tail configuration, the following comparative table is elaborated:

Configuration	Advantages	Disadvantages
<b>Conventional tail</b>	Highest stiffness among all tails Lightest tail configuration	Engine exhaust interference Interference with wing's slipstream Possible rudder blanketing (spin risk)
<b>T-Tail</b>	No engine exhaust interference No interference with wing's slipstream Spin recovery potential	Aeroelastic flutter problems Need of structural reinforcement in the VT Heaviest tail configuration
<b>Cruciform tail</b>	Slightly better stiffness than T-Tail No engine exhaust interference	Need of a complex rudder/elevator design Need of structural reinforcement in the VT Possible rudder blanketing (spin risk)

TABLE 2.2: Tail configurations performance comparison

It is evident that the conventional tail is the most structurally suitable due to its high stiffness and low weight. However, owing to the low wing configuration and engine positioning, it has been decided that a T-tail disposition is the most suitable one because of two main factors:

- Preventing engine's exhaust to disturb the tail's incoming air.
- Avoiding the interference of the slipstream coming from the low-wing on the HS.

It is true that this configuration is the most demanding in terms of structural loads, but a proper tail aerodynamic performance must be assured.

## 2.5 Landing gear configuration

Some of the typical configurations of undercarriage will be discussed in order to choose the more suitable one for our business jet.

### 2.5.1 Classic or tailwheel

This specific landing gear is now considered to be obsolete, although it was widely used years ago. Nowadays, business jets never feature this type of configuration due to its many drawbacks. Among them, we can highlight:

- It usually leads to aggressive braking, causing the plane to tip onto its nose.
- Since the center of gravity is located behind the front landing gear, there is a destabilizing effect when braking with a certain yaw angle relative to the runway. Therefore, the aircraft is expected to experiment a ground loop.
- Undesired bounces can appear in landing due to the additional lift generated. This is mainly caused when the touchdown is performed solely by the front wheels, which induces a tail-down moment.
- Difficulties when taxiing in strong wind conditions as a result of the high angle of attack attitude of the wing.
- Passenger discomfort because of the cabin floor inclination, as seen in Figure [2.21](#).
- Low pilot visibility when taxiing due to the mentioned inclination.
- High drag in take-off procedure until tail rising.

Nevertheless, this undercarriage configuration exhibits some worth considering advantages:

- Simple and light configuration.
- Notable ground manoeuvrability if the rear wheel is connected to the rudder control

- Easy attachment of the landing gear legs to the wing

However, these few positive aspects are not worth enough in order to consider the implementation of the classic configuration to our jet.



FIGURE 2.21: Classic or tailwheel configuration.

### 2.5.2 Nosewheel or tricycle

At the moment, this type of undercarriage is the most popular among the current configurations. This is mainly due to the improvement in performance compared to the other landing gear systems, as aircraft speeds have increased over time.

As mentioned above, there are several advantages that justify the use of this type of landing gear in front of the others models. These are stated as follows:

- Braking forces act behind the center of gravity (c.g.), so they have a stabilizing effect. Moreover, the pilot can make a full use of brakes during landing.
- The aircraft fuselage is leveled when grounded, and so the passenger cabin, increasing the comfort.
- Good pilot vision from cockpit.
- The nosewheel prevents the aircraft from turning over and protects the propellers from the ground.
- Low drag during initial phase of takeoff.
- When performed a two-point landing, the main gear creates a nose-down pitching moment.

However, the tricycle configuration has two main disadvantages:

- The nose unit takes between a 20 and 30 % of the aircraft weight. This implies that it is a considerably heavy element, due to the high loads it has to bear.
- Special structural modifications will be needed for the nose unit due to its location, especially when using retractable undercarriage in light aircraft.

In general, the advantages of this type of undercarriage clearly exceed its disadvantages. Aside, these can be solved if they are taken into account when designing the fuselage and the landing gear itself.



FIGURE 2.22: Aircraft with nosewheel undercarriage.

### 2.5.3 Tandem

The tandem landing gear is characterized by having its main wheels in the plane of symmetry, making them absorb nearly the same magnitude of force when performing the landing. It is important to note that its use is only recommended when its advantages suppose a real difference with the other systems:

- Its main legs are located at nearly the same distance of the center of gravity, creating a space for payload close to this point.
- Wheels can be retracted without interposing the wing structure. When talking about the weight, the landing gear will not cause an increase in fuselage weight, as it will depend on other factors, which are not strictly related to the gear itself, such as its control systems and its fastenings.

Counter to this advantages, several disadvantages can be highlighted:

- Need of outrigger wheels to stabilize the aircraft on the ground, resulting in a 1 % increase of weight. If two pairs of main legs are used, there is a reduction of load of the outriggers.
- The use of this undercarriage needs a proper touchdown attitude to avoid overstraining the gear. A small roll angle is also needed to prevent overstraining the outriggers. This disadvantage can be solved by placing the rear legs close to the center of gravity but this means losing unobstructed space for payload.
- A large tail-download moment is needed to rotate the aircraft. The attitude at rest of the aircraft will be chosen in order to fly itself off. Consequently, this will lead to an increase in drag during takeoff roll. If this moment is not achieved, an increase of the liftoff speed will be needed.

It is apparent that the disadvantages of this type of undercarriage outcome the advantages and, thus, its use is only recommended when the advantages mentioned above are mandatory needs.



FIGURE 2.23: Aircraft with simple-tandem undercarriage.



FIGURE 2.24: Aircraft with double-tandem undercarriage.

#### 2.5.4 Other unconventional configurations

There is a wide variety of other landing gear configurations to analyse yet, such as tricycle gear with double- or triple-axis boogie or even three- or four-leg landing gear. Nonetheless, since the stability and weight requirements are not truly demanding, the usage of these more complex undercarriage layouts is not common in business jets. Basing on this fact and taking into account that there are no necessary improvements to achieve by using these configurations, the mentioned landing gears will not be considered.

#### 2.5.5 Comparison and choice of landing gear configuration

Taking into account the above landing gear features the following comparative table is elaborated:

Configuration	Advantages	Disadvantages
Classic or tailwheel	<ul style="list-style-type: none"> <li>• Simple and light</li> <li>• Easy attachment to the wing</li> </ul>	<ul style="list-style-type: none"> <li>• Destabilizing effect when braking</li> <li>• Possible ground loops</li> <li>• Tail-down moment in two-point landing (causes bounces)</li> <li>• Low pilot visibility</li> <li>• Inclined fuselage (passenger discomfort)</li> <li>• High drag during take-off</li> </ul>
Tricycle or nosewheel	<ul style="list-style-type: none"> <li>• Stabilizing effect when braking</li> <li>• Leveled fuselage and cabin</li> <li>• Tail-up moment in two-point landing (prevents bounces)</li> <li>• Good pilot visibility</li> <li>• Prevention of turning over the aircraft</li> <li>• Low drag during take-off</li> </ul>	<ul style="list-style-type: none"> <li>• Heavy configuration (20 – 30% of aircraft's weight)</li> <li>• Need of additional structure to fit the front gear</li> </ul>
Tandem	<ul style="list-style-type: none"> <li>• More payload space due to legs positioning</li> <li>• Wheels retraction do not interfere with wing structure</li> </ul>	<ul style="list-style-type: none"> <li>• Need of stabilising outrigger wheels</li> <li>• Demanding touchdown attitude in landing</li> </ul>

TABLE 2.3: Landing gear configurations comparison

It is evident that the most suitable landing gear configuration for our business jet is the tricycle, just as every other aircraft of this kind. This decision is mainly due to the stability, visibility and passenger comfort that this layout provides with. Furthermore, at this moment, classic and tandem configurations have been almost completely superseded by the mentioned tricycle gear.



# Chapter 3

## Weights and performance

### 3.1 First estimation

#### 3.1.1 Weights and fuselage dimensions

The main weights of the aircraft must be estimated in an initial state of the project since they largely will condition the functional design and performance.

It must be taken into account that similar aircraft will be used to estimate the weight being, later, said weight one of the main parameters that will be used when searching estimated values through historical data. Table 3.1 shows the main specification parameters necessary to make the weight computations, corresponding to 8 of the most similar aircraft to the one who is planned to design.

Brand	Aircraft model	<i>OEW</i> [kg]	<i>MTOW</i> [kg]	<i>b_f</i> [m]	<i>h_f</i> [m]	<i>l_f</i> [m]	<i>V<sub>bagg</sub></i> [m <sup>3</sup> ]
Embraer	Praetor 600	11503.103	19440.062	2.08	1.82	20.75	4.39
Dassault	Falcon 8X	16374.685	33112.243	2.34	1.88	24.41	3.96
Dassault	Falcon 2000LX	11226.411	19413.753	2.34	1.88	20.22	3.79
Cessna	Longitude	10609.072	17916.899	1.96	1.83	22.30	3.17
Cessna	Citation X+	10038.453	16601.481	1.68	1.73	22.53	2.95
Cessna	Sovereign+	8271.257	13959.305	1.68	1.73	19.35	3.82
Gulfstream	G280	10954.256	17962.258	2.11	1.85	20.37	3.40
Hawker-beechcraft	4000	10341.906	17916.899	1.97	1.83	21.08	3.26

TABLE 3.1: Main fuselage and weight specifications of similar aircraft.

Brand	Model	Wing area [m <sup>2</sup> ]	Wing Span [m]
Embraer	Praetor 600	44.85	21.5
Dassault	Falcon 8X	70.70	26.29
Dassault	Falcon 2000LX	49.00	19.238
Cessna	Longitude	49.91	21.01
Cessna	Citation X+	48.96	19.39
Cessna	Sovereign+	50.40	22.04
Gulfstream	G280	46.00	19.21
Hawker-beechcraft	4000	49.30	18.82

TABLE 3.2: Wing specifications of similar aircraft.

It can be checked that the Operating Empty Weight has a typical value of around  $10^4$  kg, whereas the Maximum Total Operative Weight falls near to  $2 \cdot 10^4$  kg. However, there is an interesting exception, which is the Dassault Falcon 8X aircraft, that easily exceeds both figures. The three-engine configuration combined with the higher dimensions are oriented to achieve longer range; which leads to a higher weight. As regards the fuselage dimensions, the height  $h_f$  is between 1.7 – 1.8 m and the width  $b_f$  is commonly higher than 2 m. The fuselage section is thus a bit elliptical to allow better accommodation.

From the previous data, a set of expected values has been defined in Table 3.3 based on the arithmetic average, with the single exclusion of the *MTOW* and the *OEW* of the Falcon 8X.

<i>OEW</i> [kg]	<i>MTOW</i> [kg]	$b_f$ [m]	$h_f$ [m]	$l_f$ [m]	Wing area [m <sup>2</sup> ]	Wing Span [m]
10420.6	17601.5	2.0	1.8	21.4	51.1	20.9

TABLE 3.3: Expected set of characteristic parameters.

The baggage compartment volume  $V_{\text{bagg}}$  can be computed using the following expression:

$$V_{\text{bagg}} = k_b l_f b_f^2 \quad (3.1)$$

Where  $k_b$  is a constant term obtained from similar aircraft, as showed in the linear regression performed in Appendix A that provides the value  $k_b = 3,835 \cdot 10^{-2}$  for this study. Regarding the geometrical parameters, the ones from the reference set on Table 3.3 will be used. Replacing them in equation (3.1), the result is:

$$V_{\text{bagg}} = 3,835 \cdot 10^{-2} \cdot 21.376 \cdot 2.020^2 = 3.345 \text{ m}^3$$

This figure properly agrees with the reference values exposed in Table 3.3.

### 3.1.2 Power plant selection

Nowadays most aircraft designs are restricted to establish the main power plant parameters like those that have been mentioned in section 2.3. However, at any case, these designs consist on the manufacture of the engines. In order to simplify the constructive process, this task is entrusted to other specialised companies. An study based on the engines used in the similar aircraft has been implemented. Its results are shown in Tables 3.4 and 3.5 and will be used as reference data to base the future choice of the optimal engine in order to accomplish the preliminary requirements.

Brand	Aircraft model	Engine	Thrust [lbf]	$c_j$ [lb/(lbf · h)]
<b>Embraer</b>	Praetor 600	Honeywell HTF7000	7638	0.42
<b>Dassault</b>	Falcon 8X	Pratt-Whitney PW307D	6725	0.39
<b>Dassault</b>	Falcon 2000LX	Pratt-Whitney PW308C	7002.7	0.39 <sup>1</sup>
<b>Cessna</b>	Longitude	Honeywell HTF7000	7638	0.42
<b>Cessna</b>	Citation X+	Rolls-Royce AE 3007	7042	0.36
<b>Cessna</b>	Sovereign+	Pratt-Whitney PW306D	5907	0.39
<b>Gulfstream</b>	G280	Honeywell HTF7000	7638	0.42
<b>Hawker-beechcraft</b>	4000	Pratt-Whitney Canada PW306D	5907	0.39

TABLE 3.4: Operative engine specifications at sea level for similar aircraft.

<sup>1</sup> This value is extrapolated from the others due to no official data available.

Brand	Aircraft model	Engine	Bypass ratio	Engine weight [kg]
Embraer	Praetor 600	Honeywell HTF7000	4.3	696
Dassault	Falcon 8X	Pratt-Whitney PW307D	4.5	551
Dassault	Falcon 2000LX	Pratt-Whitney PW308C	4.1	540
Cessna	Longitude	Honeywell HTF7000	4.3	696
Cessna	Citation X+	Rolls-Royce AE 3007	5	744
Cessna	Sovereign+	Pratt-Whitney PW306D	4.5	450
Gulfstream	G280	Honeywell HTF7000	4.3	696
Hawker-beechcraft	4000	Pratt-Whitney Canada PW306D	4.5	450

TABLE 3.5: Engine specifications for similar aircraft.

Recalling the procedure followed in section 3.1.1, the average values will be computed and considered as a reference. An additional conversion of units from the Imperial System to the international one will be applied.

Thrust [N]	S.F.C. $c_j$ [kg / (N · s)]	Engine Weight [kg]
31128.655	$1.126 \cdot 10^{-5}$	634.225

TABLE 3.6: Reference set of characteristic propulsive parameters at sea level.

As regards the cruise stage, Table 2.2 in [8] suggests a wide interval of  $c_j$  from 0.5 to 0.9 lb / (lbf · h), which in International System (IS) units are  $1.416 \cdot 10^{-5}$  to  $2.549 \cdot 10^{-5}$  kg / (N · s). A first interesting detail is that the lower limit of the range is higher than the computed average value. The reason is that the latter is based on sea-level values, whereas the bibliography is already considering the operation at cruise height. As the height increases, the air density decreases and the invested power on air breathing raises, thus increasing the consumption. [16] proposes values between  $1.8 \cdot 10^{-5}$  and  $2 \cdot 10^{-5}$  kg / (N · s) for the cruise stage. The current regulations establish severe restrictions as regards combustion-gas emissions, and furthermore the consumption and efficiency in nominal performance is a key aspect to earn a presence in the market, the lowest value will be chosen due to the need of fulfilling this conditions.

However, it shall also be considered the loiter stage, which interval of  $c_j$  is from 0.4 to 0.6 lb / (lbf · h), or in IS from  $1.133 \cdot 10^{-5}$  to  $1.700 \cdot 10^{-5}$  kg / (N · s). These values of consumption are lower than for the cruise owing to the shorter heights the loiter is performed at. Under these conditions, the air is denser but the

velocity has decreased to achieve better maneuverability. An low, arbitrary value will be chosen for the current study due to the age of the data presented in [8].

The set of cruise values is shown in Table 3.7:

Thrust (cruise) [N]	S.F.C. (cruise) $c_{j,c}$ [kg/ (N · s)]	S.F.C. (loiter) $c_{j,l}$ [kg/ (N · s)]	Engine weight [kg]
$\sim 10^4$	$1.8 \cdot 10^{-5}$	$1.1 \cdot 10^{-5}$	634.225

TABLE 3.7: Reference set of characteristic propulsive parameters.

The thrust has additionally been modified, as the quotient of the sea-level thrust over the cruise one is around 3. It must be stated that the low selected values agree with the more modern engine data provided by [16].

## 3.2 Weight determination

### 3.2.1 Take off weight (*TOW*)

The take off weight is the total weight of the aircraft when it is located in the heading of the runway, just before the beginning of the run. It can be determined according to the following expression:

$$TOW = FW + OEW + PL \quad (3.2)$$

Where the addends are:

- **Fuel Weight *FW***: The total mass of fuel the aircraft carries (will be defined in section 3.2.5).
- **Operating Empty Weight *OEW***: This encompasses the weight of the whole empty aircraft, including all the required equipment and the crew.
- **Payload *PL***: Includes the passengers, their luggage and the cargo for what the costumer pays.

However, as the payload and the fuel weight may vary based on the route and the service and cabin configuration it provides, the *TOW* is not a design parameter.

### 3.2.2 Maximum take off Weight (*MTOW*)

The maximum take off weight *MTOW* is one of the most determining aircraft design parameters. Its great importance is due to the operational and structural limitations it imposes, and its computing can be referred to the *TOW* expression, being the *MTOW* its the limit value. Recalling expression (3.2) the *MTOW* can be expressed as:

$$MTOW \geq FW + OEW + PL$$

Which can be rearranged to obtain:

$$MTOW \geq \frac{PL}{1 - \frac{OEW}{MTOW} - \frac{FW}{MTOW}} \quad (3.3)$$

The terms that appear in this expression are correctly determined and computed in the next sections whereas therefore the *MTOW* value would be also calculated at the same time.

### 3.2.3 Operative Empty Weight (*OEW*)

For the current design, the Torenbeek and similarities criterion will be the implemented methodologies to compute the *OEW*.

#### 3.2.3.1 Torenbeek criterion

This method is based in the use of an empirical factor related with the empty weight increment ( $\Delta W_E$ ) depending on fuselage data of similar aircraft. The equation that defines the *OEW* is:

$$OEW = 0.2MTOW + W_{\text{engines}} + 500 + \Delta W_E(b_f, l_f, h_f) \quad (3.4)$$

This equation depends on some factors the value of which should be *ad hoc* computed in order to find adequate *OEW* and *MTOW* values. These factors, specially the  $\Delta W_E$ , could be estimated by the correlations shown in [5]. Nevertheless, these are old correlations and due to the constant improvements and innovations that are being implemented in current executive jet aircraft, this value must be recalculated using data from current aircraft similar to the model to be designed. The MATLAB code in Appendix E performs a regression based on the fuselage dimensions data of Table 3.1. The resultant graphical representation is shown in Appendix B.

According to the estimated fuselage data selected ( $b_f = 2.0$  m,  $l_f = 21.4$  m), the obtained increment value is  $\Delta W_E = 5476.942$  kg. In addition, the engines weight is computed by using data extracted from Table 3.7 and considering a twinjet configuration.

Therefore, the resulting *OEW* expression is such that:

$$OEW = 0.2 \cdot MTOW + 500 + 2 \cdot 634.225 + 5476.942 \quad [\text{kg}]$$

Solving the addition leads to:

$$OEW = 0,2 MTOW + 7245.392 \quad [\text{kg}] \quad (3.5)$$

This last expression may complement the  $MTOW$  inequality (3.3) and may be replaceable with the equation obtained from the other criteria. Then, and as long as the quotient  $FW/MTOW$  is computed, both  $MTOW$  and  $OEW$  can be computed.

### 3.2.3.2 Similarities criterion

The similarities criterion is based on the direct comparison with other airplanes which already exist. This method defines the  $OEW$  as a linear proportion of the  $MTOW$  through the factor known as  $\alpha$  as it is shown hereunder:

$$OEW = \alpha MTOW$$

In order to find the  $\alpha$  parameter, a linear regression is performed through the MATLAB code present in Annex E. As the previous equation shows, it is imposed on the regression a null origin ordinate. Table 3.8 shows the particular  $\alpha$  values computed from the similar airplane data from Table 3.1:

Brand	Model	$\alpha$
Embraer	Praetor 600	0.5917
Dassault	Falcon 8X	0.4945
	Falcon 2000LX	0.5783
Cessna	Longitude	0.5921
	Citation X+	0.6047
	Sovereign+	0.5925
Gulfstream	G280	0.6098
Hawker Beechcraft	4000	0.5772

TABLE 3.8:  $\alpha$  parameter for the different similar airplanes.

It can be checked that the factor is in close proximity to 0.6 with the exception of Dassault Falcon 8X, which value is near 0.5 due to its tri-engine configuration

and its greater dimensions, as it was stated in section 3.1.1.

The definitive computed value<sup>1</sup> of the factor is the following:

$$\alpha = 0.559$$

This means that the equation which relate both weights is:

$$OEW = 0.559 \text{ MTOW} \quad (3.6)$$

### 3.2.4 Payload

In order to compute the maximum payload  $MPL$  and as stated in [17], the following equation is used:

$$MPL = \#\text{pax} \cdot (W_{\text{pax}} + W_{\text{bagg}}) + \left[ k_{bd} V_{\text{bagg}} - \frac{\#\text{pax} \cdot W_{\text{bagg}}}{\rho_{\text{bagg}}} \right] \rho_{\text{cargo}} \quad (3.7)$$

According to the current aircraft's requirements, the number of passengers ranges from 6 (standard configuration) to 10 (maximum capacity). Since the calculated payload must be the maximum, the value to use will be 10.

According to [17], typical values for passenger ( $W_{\text{pax}}$ ) and baggage weights  $W_{\text{bagg}}$  are:

$$W_{\text{pax}} = 77 \text{ kg/pax} \quad W_{\text{bagg}} = 20 \text{ kg/pax}$$

It must be mentioned that the selected baggage value is corresponding to a long range flight.

In terms of the hold occupancy performance ( $k_{bd}$ ), common values are 0, 85 – 0, 90 as stated in [17]. Since reference [5] also mentions the first value,  $k_{bd} = 0, 85$  is selected. As regards the baggage compartment volume, it has been computed in section 3.1.1 and its value is  $V_{\text{bagg}} = 3.345 \text{ m}^3$ .

Finally, the baggage density is  $\rho_{\text{bagg}} = 200 \text{ kg/m}^3$  following the recommendation stated in [5]. As for the cargo, in the case of business jets there is no presence of “commercial” cargo since there is not a specifically dedicated hold space. Instead, the possible cargo needed (such as sport equipment or leisure objects) is loaded

---

<sup>1</sup>Using a linear regression with null ordinate at origin.

together with the baggage in its corresponding compartment at the rear part of the fuselage cabin. Taking this consideration into account, an estimated cargo density is  $\rho_{cargo} = 160 \text{ kg/m}^3$  as stated in [5]. Due to this fact, the second term in the right-hand side of equation (3.7) is the remaining cargo weight that the baggage compartment can fit apart from the already loaded passenger baggage.

Taking into account all the above mentioned values, the maximum payload is:

$$MPL = 10 \cdot (77 + 20) + \left[ 0,85 \cdot 3.345 - \frac{10 \cdot 20}{200} \right] 160 = 1264.884 \text{ kg} \quad (3.8)$$

Comparing this value to the corresponding ones for similar aircraft included in Table 1.1, a mean value of 1651 kg is obtained. Thereby, it can be clearly observed that our aircraft value is a 23,1% smaller than the commonly found.

However, this can be caused by the influence of some of the considered as similar aircraft, with slightly more passenger capacity, hold occupancy performance and baggage compartment volume. Obviously, the aircraft is designed to sacrifice payload and passenger capacity in order to reach larger range and Mach values.

### 3.2.5 Fuel Weight

The fuel weight ( $FW$ ) is one of the parameters that dictates the aircraft's range. According to [8], there are two types of fuel weight that needs to be considered:

$$FW = TF + RF \quad (3.9)$$

where  $TF$  stands for *trip fuel* (fuel actually used during the trip) and  $RF$  stands for *reserve fuel* (fuel reserves required for the mission).

Fuel reserves are normally specified in the mission specification. However, according to ICAO Annex 6, Part I, section 4.3.6 "Fuel Requirements", airplanes should calculate their required fuel quantity as follows: *Final reserve fuel (45 minutes of holding flight for turbine engines, 30 minutes for jets)*

- 2) to fly for 30 minutes at holding speed at 450 m (1500 ft) above the alternate aerodrome under standard temperature conditions , and approach and land ; and
- 3) to have an additional amount of fuel sufficient to provide for the increased

*consumption on the occurrence of any of the potential contingencies specified by the operator to the satisfaction of the State of the Operator (for either alternate destination aerodrome is required or not)*

In other words, this is an additional weight that must be taken into consideration while computing *MTOW*. Nevertheless, this *Reserve Fuel* shall only be used in an emergency scenario and not considered in normal operation. [18]

To determine the fuel weight actually used during the mission, the so-called *fuel-fraction method* will be used. In this method, the airplane mission is divided into a number of mission phases. The fuel used in each operation is found from simple calculation and historical data.

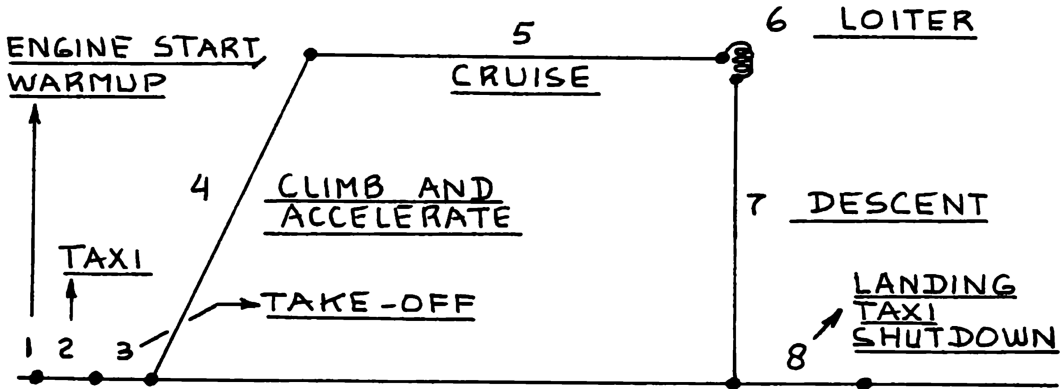


FIGURE 3.1: Mission Profile

The fuel-fraction method will be illustrated by applying it to our jet. Figure 3.1 defines the mission profile for this aircraft.

The fuel-fraction for each phase is defined as the ratio of end weight to begin weight. Next step is to assign numerical value to the fuel-fraction corresponding to each mission phase. Below are listed all the phases and the estimated values proposed by [8]:

1. **Engine Start and warm-up.** Begin weight is *TOW* and the end weight is  $W_1$ . Fuel fraction in this phase is given by  $W_1/TOW$ .

The fuel fraction for this phase and considering airplane type as business jets is 0.990.

2. **Taxi.** Begin weight is  $W_1$  and the end weight is  $W_2$ . Fuel fraction in this phase is given by  $W_2/W_1$ .

The fuel fraction for this phase and considering airplane type as business jets is 0.995.

3. **Take off.** Begin weight is  $W_2$  and the end weight is  $W_3$ . Fuel fraction in this phase is given by  $W_3/W_2$ .

The fuel fraction for this phase and considering airplane type as business jets is 0.995.

4. **Climb to cruise altitude and acceleration to cruise speed.** Begin weight is  $W_3$  and the end weight is  $W_4$ . Fuel fraction in this phase is given by  $W_4/W_3$ .

The fuel fraction for this phase and considering airplane type as business jets is 0.980.

5. **Cruise.** Begin weight is  $W_4$  and the end weight is  $W_5$ . Its computation can be done using the alternative forms of Breguet equation shown in Appendix C.

6. **Loiter.** This stage will be also analyzed through the Breguet's equation, but in this case in terms of endurance following the recommendation on [8].

7. **Descent.** Fuel fraction for this phase is given by  $W_7/W_6$ , following the current cardinal enumeration. Considering airplane type as business jets the corresponding value is 0.990.

8. **Landing, taxi and shut-down.** For the last stage of the flight, the fuel fraction in this phase is given by  $W_8/W_7$  and the corresponding figure in Table 3.3 is 0.992.

The mathematical form of the computation of the mission fuel-fraction  $M_{ff}$  encompasses the following product sequence:

$$M_{ff} = \frac{W_1}{TOW} \prod_{i=1}^{i=7} \frac{W_{i+1}}{W_i} \quad (3.10)$$

Then, the fuel weight used during the mission,  $W_{Fused}$  can be found as:

$$FW_{\text{used}} = TF = (1 - M_{ff}) TOW$$

The value for mission fuel weight,  $FW$  can finally be determined from:

$$FW = (1 - M_{ff}) TOW + RF$$

The current interest dwells on the expansion of expression (3.10):

$$M_{ff} = \frac{\underbrace{W_1}_{\substack{\text{Phase 1:} \\ \text{Engine start}}}}{\underbrace{W_{TO}}_{\substack{\text{Phase 2:} \\ \text{Taxi}}}} \cdot \frac{\underbrace{W_2}_{\substack{\text{Phase 3:} \\ \text{Take off}}}}{\underbrace{W_1}_{\substack{\text{Phase 4:} \\ \text{Climb}}}} \cdot \frac{\underbrace{W_3}_{\substack{\text{Phase 5:} \\ \text{Cruise}}}}{\underbrace{W_4}_{\substack{\text{Phase 6:} \\ \text{Loiter}}}} \cdot \frac{\underbrace{W_4}_{\substack{\text{Phase 7:} \\ \text{Descend}}}}{\underbrace{W_5}_{\substack{\text{Phase 8:} \\ \text{Shutdown}}}} \cdot \frac{\underbrace{W_5}_{\substack{\text{Phase 1:} \\ \text{Engine start}}}}{\underbrace{W_6}_{\substack{\text{Phase 2:} \\ \text{Taxi}}}} \cdot \frac{\underbrace{W_6}_{\substack{\text{Phase 3:} \\ \text{Take off}}}}{\underbrace{W_7}_{\substack{\text{Phase 4:} \\ \text{Climb}}}} \cdot \frac{\underbrace{W_7}_{\substack{\text{Phase 5:} \\ \text{Cruise}}}}{\underbrace{W_8}_{\substack{\text{Phase 6:} \\ \text{Loiter}}}} \cdot \frac{\underbrace{W_8}_{\substack{\text{Phase 7:} \\ \text{Descend}}}}{\underbrace{W_9}_{\substack{\text{Phase 8:} \\ \text{Shutdown}}}}$$

In case of necessity of reaching an alternate airport, it shall be included the weight ratios for the cruise to the new aerodrome  $W_{6.1}/W_6$  and for the loiter  $W_{6.2}/W_{6.1}$ .

Particularizing to a business jet aircraft, all the available fuel-fraction values extracted from Figure 3.3 will be replaced:

$$M_{ff} = \underbrace{0.990}_{\substack{\text{Phase 1:} \\ \text{Engine start}}} \cdot \underbrace{0.995}_{\substack{\text{Phase 2:} \\ \text{Taxi}}} \cdot \underbrace{0.995}_{\substack{\text{Phase 3:} \\ \text{Take off}}} \cdot \underbrace{0.980}_{\substack{\text{Phase 4:} \\ \text{Climb}}} \cdot \underbrace{\frac{W_5}{W_4}}_{\substack{\text{Phase 5:} \\ \text{Cruise}}} \cdot \underbrace{\frac{W_6}{W_5}}_{\substack{\text{Phase 6:} \\ \text{Loiter}}} \cdot \underbrace{0.990}_{\substack{\text{Phase 7:} \\ \text{Descend}}} \cdot \underbrace{0.992}_{\substack{\text{Phase 8:} \\ \text{Shutdown}}} \quad (3.11)$$

Next, as mentioned beforehand, Phase 5 (Cruise) and Phase 6 (Loiter) shall be solved using Breguet's Range and Endurance expressions.

	<b>Engine Start, Warm-up</b>	<b>Taxi</b>	<b>Take-off</b>	<b>Climb</b>	<b>Descent</b>	<b>Landing Taxi, Shutdown</b>
<b>Mission</b>						
<b>Phase No. (See Fig. 2.1)</b>	<b>1</b>	<b>2</b>	<b>3</b>	<b>4</b>	<b>7</b>	<b>8</b>
<b>Airplane Type:</b>						
1. Homebuilt	0.998	0.998	0.998	0.995	0.995	0.995
2. Single Engine	0.995	0.997	0.998	0.992	0.993	0.993
3. Twin Engine	0.992	0.996	0.996	0.990	0.992	0.992
4. Agricultural	0.996	0.995	0.996	0.998	0.999	0.998
5. Business Jets	0.990	0.995	0.995	0.980	0.990	0.992
6. Regional TBP's	0.990	0.995	0.995	0.985	0.985	0.995
7. Transport Jets	0.990	0.990	0.995	0.980	0.990	0.992
8. Military Trainers	0.990	0.990	0.990	0.980	0.990	0.995
9. Fighters	0.990	0.990	0.990	0.96-0.90	0.990	0.995
10. Mil. Patrol, Bomb, Transport	0.990	0.990	0.995	0.980	0.990	0.992
11. Flying Boats, Amphibious, Float Airplanes	0.992	0.990	0.996	0.985	0.990	0.990
12. Supersonic Cruise	0.990	0.995	0.995	0.92-0.87	0.985	0.992

**Notes:** 1. The numbers in this table are based on experience or on judgment.  
 2. There is no substitute for common sense! If and when common sense so dictates, the reader should substitute other values for the fractions suggested in this table.

FIGURE 3.2: Suggested fuel-fractions for several mission phases. Source: [8]

### 3.2.5.1 Cruise resolution

#### Single height methodology

The simplest approach for the ratio  $W_5/W_4$  is assuming constant height, consumption and aerodynamic efficiency, which leads to the following form of the Breguet's equation:

$$R_{\text{cruise}} = \left( \frac{V}{g c_j} \frac{L}{D} \right)_{\text{cruise}} \ln \left( \frac{W_4}{W_5} \right)$$

Where the values for the specific consumption  $c_j$  and for the aerodynamic efficiency  $E$  may be obtained from Figure 3.3. As regards the range  $R_{cr}$  and the cruise speed  $V$ , these are given in the mission specifications.

The ratio can be easily isolated, leading to:

$$\frac{W_5}{W_4} = e^{-R_{\text{cruise}}/\phi_{TF}} \quad \text{where} \quad \phi_{TF} = \left( \frac{V}{g c_j} \frac{L}{D} \right)_{\text{cruise}}$$

Table 3.9 shows the result of this analytical computation. It can be seen that the Mach number is not the maximum achievable, as well as the range also is not. The reason for the first one is the elevated consumption it may lead due to the

increase on the drag, and for the second shall be considered that the cruise is not the only stage of the flight, and the total covered distance has the contributions of the take off, the climb and the descent.

Mach number	Height [km]	Range [km]	Efficiency $L/D$	Weight ratio $W_5/W_4$
0.8	12	6667	15	0.514

TABLE 3.9: Performance characteristics at cruise stage (analytically computed).

The selected efficiency is a high value in comparison to the interval from 10 to 12 proposed by [8]. Nevertheless, and as it will be seen later, the numerical resolution shows that this figure is acceptable.

### Piecewise height methodology

A more precise approach consists on the separation of the whole cruise stage in stretches of different height in order to more precisely fulfil the assumption of constant efficiency. It shall be considered that the real cruise stages are performed throughout phases of constant height, but the latter may be increased in several occasions (always with the ATM permission) to maintain the aerodynamic efficiency.

The mathematical formulation of this method would require a product sequence:

$$\frac{W_5}{W_4} = \prod_{p=1}^{p=n} \frac{W_{4,p+1}}{W_{4,p}}$$

Where  $n$  is the number of phases the cruise has been divided in and the subscript  $p$  denotes a specific phase. It must be taken into account that  $W_{4,1} = W_4$  and  $W_{4,n+1} = W_5$  due to the coincidence with the beginning and the ending of the cruise.

#### 3.2.5.2 Loiter resolution

##### Single height methodology

The weight ratio of the final  $W_6$  over the initial  $W_5$  may be obtained using the analytical expression derived in Appendix C. For

$$E_{\text{loiter}} = \left( \frac{1}{gc_j} \frac{L}{D} \right)_{\text{loiter}} \ln \left( \frac{W_5}{W_6} \right)$$

Where the reference values to be replaced are again provided by Table 3.3.

The isolation of the weight ratio leads to:

$$\frac{W_6}{W_5} = e^{-E_{\text{loiter}}/\varphi_{TF}} \quad \text{where} \quad \varphi_{TF} = \left( \frac{1}{gc_j} \frac{L}{D} \right)_{\text{loiter}}$$

The loiter is a stage of the flight which does not usually have a long duration, from 20 up to 30 minutes, thus the constant height assumption is perfectly acceptable.

Loiter time [min]	Weight ratio $W_6/W_5$
30	0.979

TABLE 3.10: Performance characteristics at loiter stage.

For this computation, a preventive value of 30 minutes of holding has been chosen.

Mission Phase No. (See Fig. 2.1)	Cruise			Loiter				
	L/D	$c_j$	$c_p$	$\eta_p$	L/D	$c_j$	$c_p$	$\eta_p$
<b>Airplane Type</b>								
1. Homebuilt	8-10*		0.6-0.8	0.7	10-12		0.5-0.7	0.6
2. Single Engine	8-10		0.5-0.7	0.8	10-12		0.5-0.7	0.7
3. Twin Engine	8-10		0.5-0.7	0.82	9-11		0.5-0.7	0.72
4. Agricultural	5-7		0.5-0.7	0.82	8-10		0.5-0.7	0.72
5. Business Jets	10-12	0.5-0.9			12-14	0.4-0.6		
6. Regional TBP's	11-13		0.4-0.6	0.85	14-16		0.5-0.7	0.77
7. Transport Jets	13-15	0.5-0.9			14-18	0.4-0.6		
8. Military Trainers	8-10	0.5-1.0	0.4-0.6	0.82	10-14	0.4-0.6	0.5-0.7	0.77
9. Fighters	4-7	0.6-1.4	0.5-0.7	0.82	6-9	0.6-0.8	0.5-0.7	0.77
10. Mil. Patrol, Bomb, Transport	13-15	0.5-0.9	0.4-0.7	0.82	14-18	0.4-0.6	0.5-0.7	0.77
11. Flying Boats, Amphibious, Float Airplanes	10-12	0.5-0.9	0.5-0.7	0.82	13-15	0.4-0.6	0.5-0.7	0.77
12. Supersonic Cruise	4-6	0.7-1.5			7-9	0.6-0.8		

Notes: 1. The numbers in this table represent ranges based on existing engines.  
2. There is no substitute for common sense! If and when actual data are available, these should be used.  
3. A good estimate for L/D can be made with the drag polar method of Sub-section 3.4.1.  
\* Homebuilts with smooth exteriors and/or high wing loadings can have L/D values which are considerably higher.

FIGURE 3.3: Suggested values for  $L/D$ ,  $c_j$ ,  $\eta_p$  and for  $c_p$  for several mission phases.

Source: [8]

### 3.2.5.3 General weight ratio

#### Single height methodology

Recovering expression (3.11) and replacing the values obtained through the single height, constant speed and efficiency, the following numerical weight ratio is found:

$$M_{ff} = \underbrace{0.990}_{\substack{\text{Phase 1:} \\ \text{Engine start}}} \cdot \underbrace{0.995}_{\substack{\text{Phase 2:} \\ \text{Taxi}}} \cdot \underbrace{0.995}_{\substack{\text{Phase 3:} \\ \text{Take off}}} \cdot \underbrace{0.980}_{\substack{\text{Phase 4:} \\ \text{Climb}}} \cdot \underbrace{0.494}_{\substack{\text{Phase 5:} \\ \text{Cruise}}} \cdot \underbrace{0.979}_{\substack{\text{Phase 6:} \\ \text{Loiter}}} \cdot \underbrace{0.990}_{\substack{\text{Phase 7:} \\ \text{Descend}}} \cdot \underbrace{0.992}_{\substack{\text{Phase 8:} \\ \text{Shutdown}}} = 0.456 \quad (3.12)$$

And in case of having to reach an alternate aerodrome, the mission fuel fraction is around  $M_{ff,aa} = 0.44$ .

Which leads to:

$$FW = (1 - 0.456) TOW + RF = 0.544 TOW + (0.456 - 0.440) TOW = 0.56 TOW \quad (3.13)$$

The  $TOW$  is fair to be replaced by the  $MTOW$  in case of studying the limit performance.

### 3.2.6 Final weight computation

#### 3.2.6.1 Roskam's method

In order to finally compute the design weights of the current aircraft, an adaptation of the methodology proposed in [8] will be done.

This procedure is initiated by the determination of the payload mass  $MPL$ , which depends on the number of passengers, their luggage and the cargo the aircraft carries. Next, a value of the maximum take off weight  $MTOW$  is guessed from the data provided by aircraft manufacturers. The following step is one of the most important, as it consists on the computation of the fuel weight  $FW$  computation, which can be achieved both through an analytical approach of the flight or by using a numerical method that allows greater precision.

Once these three values are obtained, a tentative value of the operating empty weight  $OEW$  is obtained as a subtraction of the  $FW$  and the  $MPL$  from the

$MTOW$ . However, there exist correlations, such as the Torenbeek and the similarites criteria, that set a dependency between the  $OEW$  and the  $MTOW$ . Thus, an allowable  $OEW$  shall be obtained using one of the previous criteria. Both  $OEW$  may be compared, and if their relative deviation is greater than a certain value  $\xi$ , an adjustment must be applied over the  $MTOW$  in order to lead the comparison towards the convergence. The whole algorithm is graphically represented in Figure 3.4.

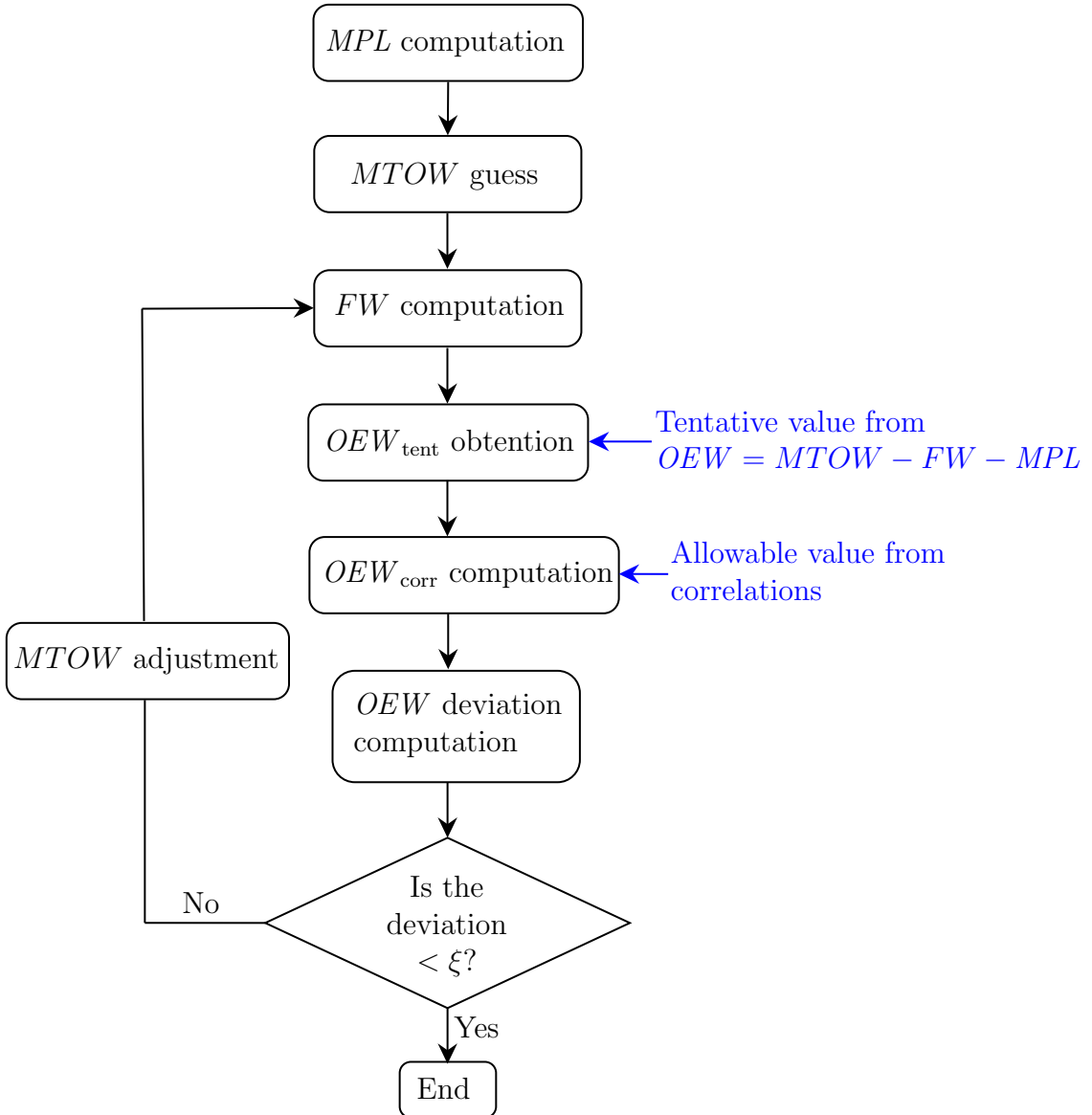


FIGURE 3.4: Roskam's algorithm for computing the design weights.

### 3.2.6.2 Single height methodology (SHA)

#### Torenbeek criterion

To finally compute the design weights of the aircraft, Torenbeek criterion will be firstly used. Equation (3.5) will be implemented inside the previously presented Roskam's algorithm. However, it shall be remembered that the computation of the fuel fractions for both cruise and loiter stages can be performed through analytical and numerical analysis.

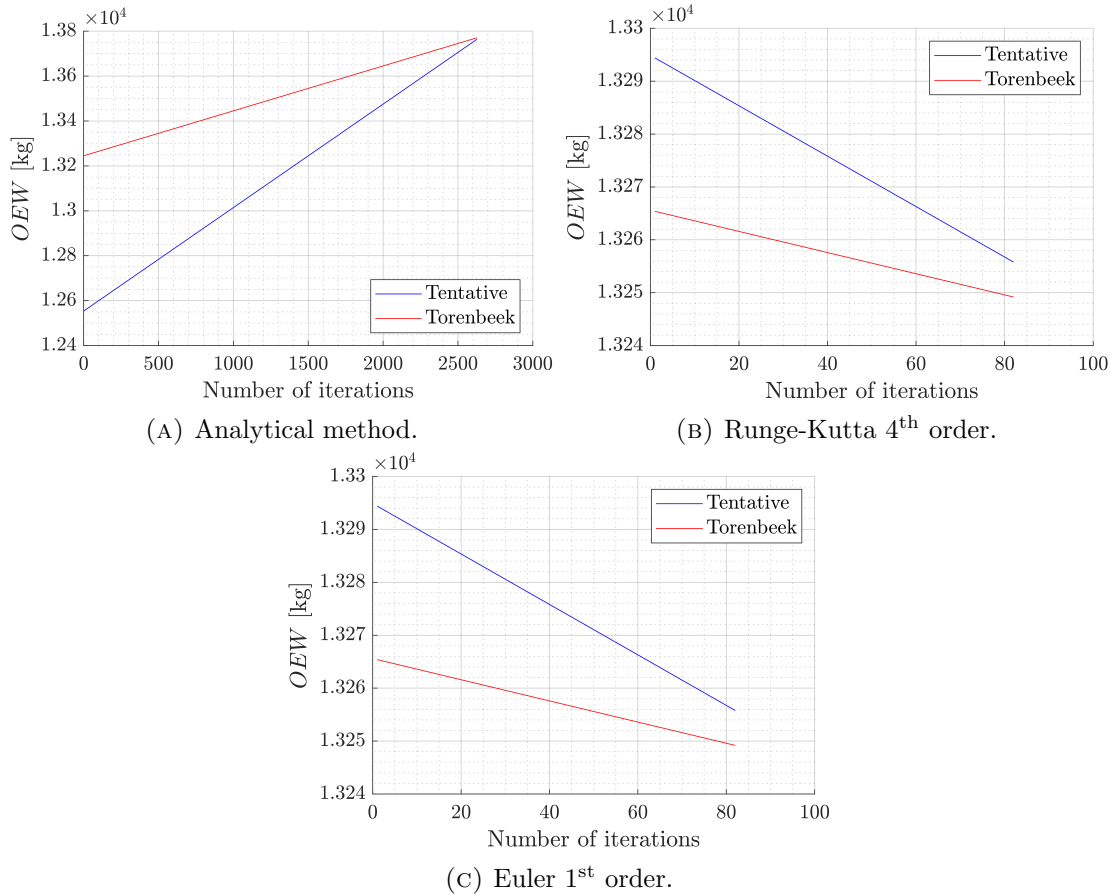


FIGURE 3.5: Convergence of the operating empty weight  $OEW$  using Torenbeek criterion.

Figure 3.5 shown the convergence plots for the operative empty weight using Roskam's criterion to compute the allowable  $OEW$  but with different methodologies to compute the key weight fractions (i.e. cruise and loiter). In this case, the convergence criterion was set on a relative deviation of 0.05 % towards the allowed value. it can be seen a clear convergence for the three methods used.

Analytic	Runge-Kutta (4 <sup>th</sup> order)	Euler (1 <sup>st</sup> order)
<i>OEW</i> [kg]	13764	13256
<i>MTOW</i> [kg]	32626	30019

TABLE 3.11: Exact values of the *MTOW* and *OEW* for a SHA analysis.

Table 3.11 shows the exact value of the design weights of the current aircraft. It can be seen that the analytic results are around 5 % and 10 % greater as regards *OEW* and *MTOW*, respectively, towards the numerical-obtained values. Furthermore, the difference between Runge-Kutta and Euler is trivial as it is in the order of units. The definitive values that will be used and considered onwards are the ones computed by the Runge-Kutta method, as its precision is greater due to its second order and the lack of partially unrealistic assumptions. Nevertheless, both of the numerical resolutions, the Euler and the Runge-Kutta method require a big amount of computational capacity to achieve its convergence. In order to simplify this fact, the Weight to Range diagram, presented in the chapter 5, will be computed with the analytical resolution method assuming that its calculated values, taking into account that not exceed more than 10 % from the numerical and more realistically ones, are also acceptable for the design project.

### Similarities criterion

The similarities criterion suggests a linear correlation with no independent term. The slope of this correlation is called  $\alpha$  and was determined in section 3.2.3.2. The convergence results are shown in Figure 3.6.

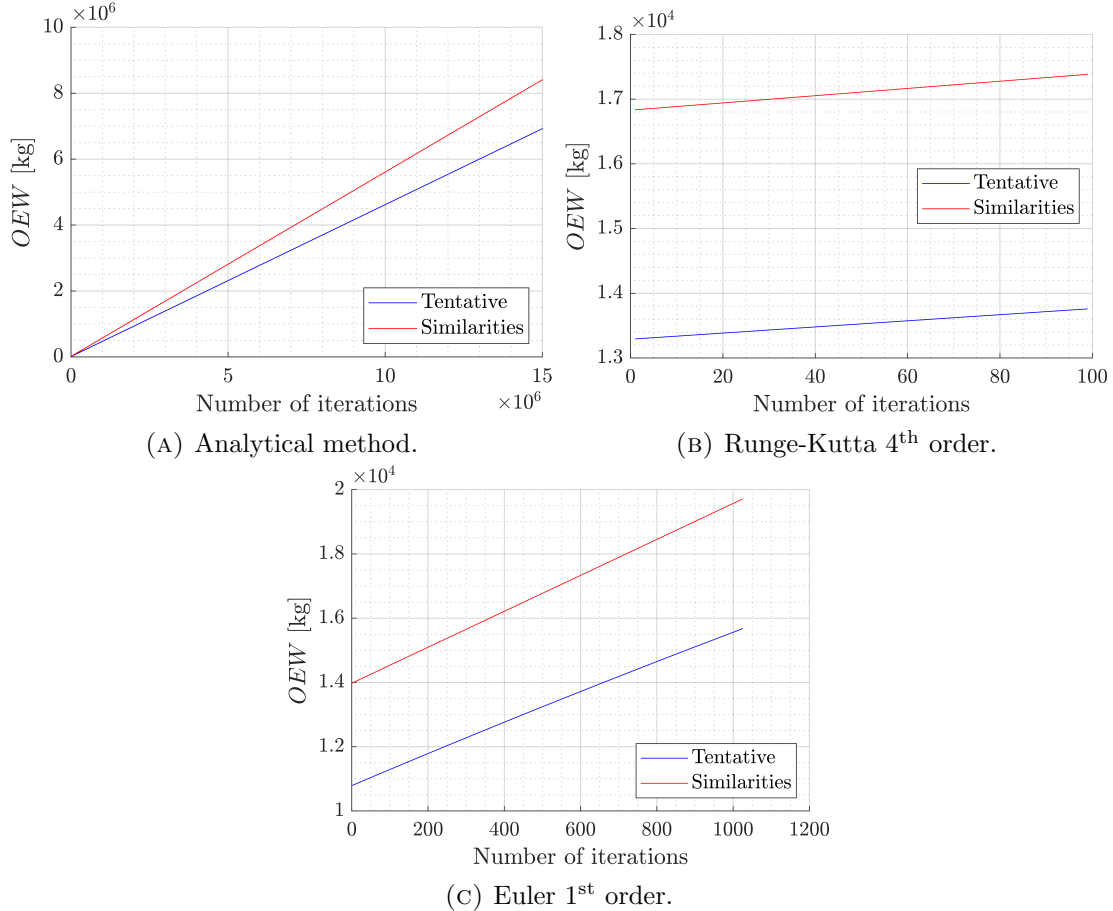


FIGURE 3.6: Convergence of the operating empty weight  $OEW$  using similarities criterion.

These results are decisive: convergence cannot be achieved using the similarities criterion. It can be checked that the curves for the tentative  $OEW$  and the allowable by correlation progressively diverge as the number of iterations increases. Mathematically, this fact can be explained comparing the  $\alpha$  coefficient obtained from a range of similar aircraft, and which value was 0.559, to the result determined by the data in Table 3.11. For the latter,  $\alpha \approx 0.44$ , which is a lower value than the obtained by regression. This is indeed a proof that the current aircraft is not absolutely similar as regards its performance, more exactly the range is greater; and additionally its nominal capacity has been considered the maximum. However, from the computational point of view, the required time is strongly higher due to the huge number of calculations this numerical method involves.

The results obtained by this criterion concludes on the limitation that the correlation will be only valid when the intended aircraft to design is extremely average

between the models in the market. In the current study, the idea is to fill a gap with a long-range, medium-capacity business jet. Thus, this method is not recommendable if the aim is to innovate.

### 3.2.6.3 Multiple height methodology (MHA)

Real flights are not entirely performed in a single height (i.e. flight level). The reason can be checked in Figure 3.7: as the flight goes on, the mass of the aircraft decreases because it is consuming fuel. Thus, the weight progressively diminishes, and with it also does the lift coefficient. It shall be considered that the drag coefficient is squared proportional to the latter. However, the tendency of  $C_L/C_D$  is also decreasing, fact that the graph clearly represents.

Greater efficiency translates into further range, and in order to achieve this upgrade, the cruise height is raised in several occasions during this stage. Results shown in Figure 3.7 are exaggerated due to the prompt change applied on the flight level, although in reality a climb phase would be required.

For the current study, the cruise has been divided in the following chronological heights: 12 km, 12,5 km and 13 km, where each interval covers the same longitudinal distance: a third of the cruise range. The result of applying this strategy is a decrease on both *MTOW* and *OEW* for the same range, as the figures in Table 3.12 show when they are compared to the ones in Table 3.11.

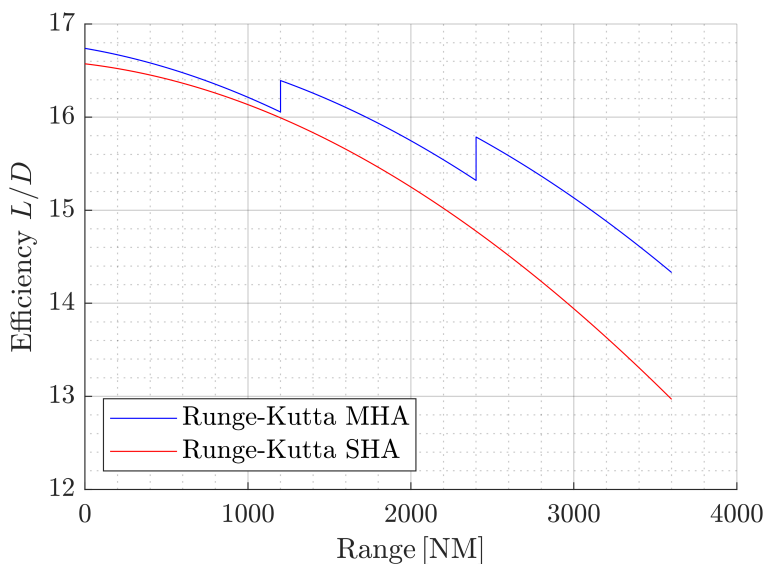


FIGURE 3.7: Evolution of the aerodynamic efficiency along the cruise stage.

	Runge-Kutta (4 <sup>th</sup> order)	Euler (1 <sup>st</sup> order)
<b>OEW</b> [kg]	12968	12968
<b>MTOW</b> [kg]	28643	28643

TABLE 3.12: Exact values of the *MTOW* and *OEW* for a MHA analysis.

### 3.3 Centering

The center of gravity CG is not necessarily a fixed point since its location depends on the weight distribution of the aircraft. Thus, the next step is to set the limits for the location of the CG along the longitudinal axis.

It must be highlighted that the CG position is highly dependent on the weight configuration used, thereby resulting in the elaboration of the called “Load and balance diagram” or “CG Limits Envelope Graph”. In general terms, the most critical CG positions are the fore-and-aft locations, which define such limits. For each likely loading condition the actual CG must remain inside these fore-and-aft limitations.

Precisely due to the aforementioned loading condition dependence, *MTOW*, *MLW*, *MZFW* and *OEW* have been considered when computing the mean CG limits to be used as an estimation for our aircraft. As a preliminary approximation and in order to determine the CG range of variation, data from similar aircraft have been taken into account. The estimated CG limits of our aircraft correspond to the mean values of Tables 3.13 and 3.14:

LOADING CONDITION	<i>MTOW</i>		<i>MLW</i>	
CG LIMIT	$\bar{x}_{CG, \min}$ (%)	$\bar{x}_{CG, \max}$ (%)	$\bar{x}_{CG, \min}$ (%)	$\bar{x}_{CG, \max}$ (%)
<b>Embraer Praetor 600</b>	21	32	21	34
<b>Dassault Falcon 2000LX</b>	16.9	22.75	16	25.5
<b>Cessna Citation X+</b>	17	21	17	28.5
<b>Cessna Sovereign+</b>	21.2	31	19.7	30
<b>MEAN VALUE</b>	<b>19.0</b>	<b>26.7</b>	<b>18.4</b>	<b>29.5</b>

TABLE 3.13: CG limits data from similar aircraft (1). Sources: [10][11][12][13]

LOADING CONDITION	MZFW		OEW	
CG LIMIT	$\bar{x}_{CG, \text{min}} (\%)$	$\bar{x}_{CG, \text{max}} (\%)$	$\bar{x}_{CG, \text{min}} (\%)$	$\bar{x}_{CG, \text{max}} (\%)$
Embraer Praetor 600	26.5	47	37	47
Dassault Falcon 2000LX	16	31.5	32.5	32.5
Cessna Citation X+	24.5	35.5	35.5	35.5
Cessna Sovereign+	18	31	18	31
MEAN VALUE	<b>21.3</b>	<b>36.3</b>	<b>30.8</b>	<b>36.5</b>

TABLE 3.14: CG limits data from similar aircraft (2). Sources: [10][11][12][13]

As mentioned before, the most critical limits are the fore- and aft- CG locations, which in the case of the current business jet are the mean values specified in the above table. To make it more visual, the data from the previous tables has been represented in Figure 3.8. The enclosed area on the graph represents the CG position envelope, and it defines the combinations of weight and CG position along the MAC that prove the aircraft is safe to fly:

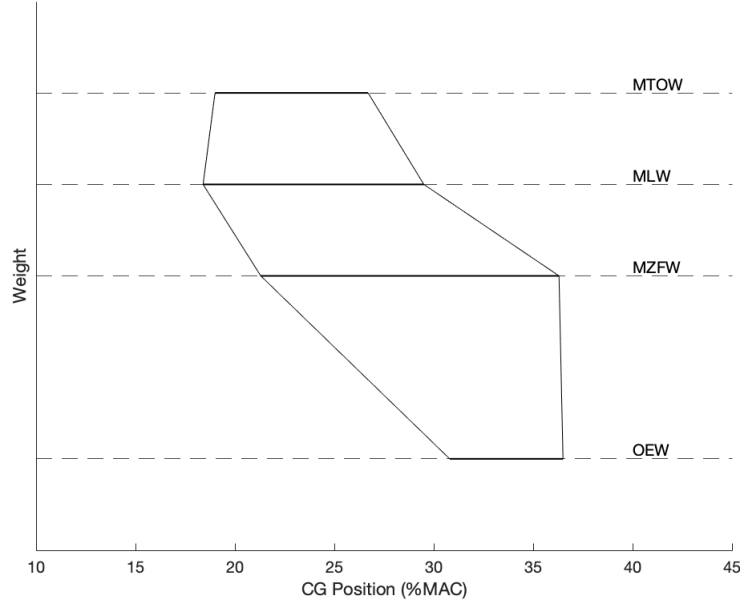


FIGURE 3.8: CG Weight Versus CG Position Chart

Comparing these CG limits with the ones provided in [17] (17 – 40 %MAC), it can be clearly seen that the estimated limits are contained in the commonly found range.

### 3.3.1 Impact of power plant on the position of the CG

The location of the engines highly influences the layout of the load and balance diagram due to their considerable weight.

As seen in Figure 3.9, if engines are located in the rear fuselage part, just as in the case of a business jet, both wing and cabin's useful space are displaced towards the front of the aircraft. Therefore, this position of the engines leads to a CG shift to the rear part, which will affect on the general layout of the load and balance diagram, analysed in the following sections.

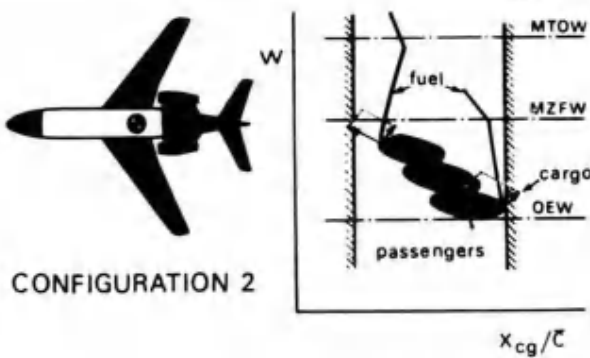


FIGURE 3.9: Power plant effect on load and balance diagram. Source: [5]

### 3.3.2 Impact of passenger on the position of the CG

The CG position is highly influenced by the movement and location of each passenger. In order to quantify the corresponding CG limits, the called “Window seating rule” is followed. This criterion is based on two main aspects: the seating occupation order regarding rows and also columns. As regards to our aircraft, the resulting passenger effect is represented in Figure 3.10.

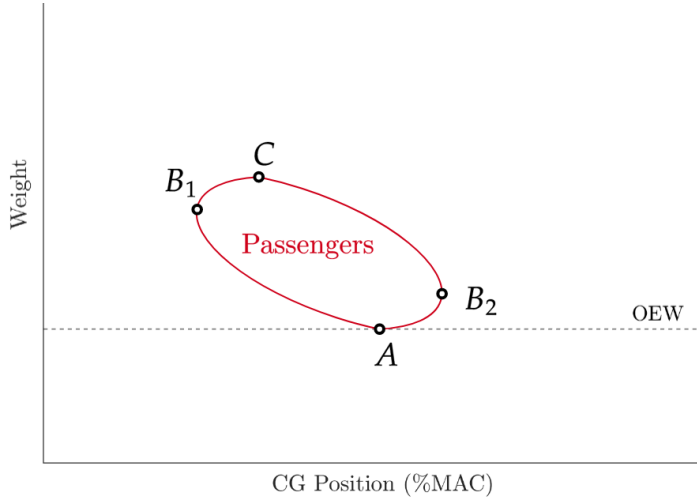


FIGURE 3.10: Passenger effect on load and balance diagram.

### 3.3.2.1 Rows order

Since the aircraft's empty cabin is known to be occupied by starting from the windows seats, the logical order is to fill from this row towards the aisle's nearest row.

Nevertheless, in the current case of a 10-seater business jet there is only one seat row at each side, which are in turn the window seats. This filling order would cause a CG shift to the left abscissa ( $A \rightarrow C$ ) as shown in Figure 3.10. This behaviour of the CG is basically due to the cabin layout in terms of seating. As Figure 3.9 shows, the CG is located at the rear part of the cabin, hence, seat row loading contributes to shift the CG towards the front.

### 3.3.2.2 Columns order

In terms of the seat columns, there are two possible occupation orders depending on the side of the aircraft (rear or front) the seats are filled from.

If the airplane is occupied by starting from the rear part ( $A \rightarrow B_2 \rightarrow C$ ), there will be firstly a CG shift towards the rear ( $A \rightarrow B_2$ ). Then, when seats start to get filled from the CG onwards until all the seat columns of the corresponding seat row are full, there is a larger shift towards the front part ( $B_2 \rightarrow C$ ).

On the contrary, if the seats are occupied by starting from the front part, the path ( $A \rightarrow B_1 \rightarrow C$ ) is followed.

### 3.3.3 Impact of Baggage compartment on the position of the CG

The addition or removal of weight in the cargo hold or baggage compartment presents a CG change problem which must be calculated before flight.

The loading of baggage and cargo in the compartment increases the weight and causes a shift of the CG which depends upon the location of the variable load. As the aircraft which is object of this project only has one rear hold, the CG position will be displaced towards the back whenever baggage or cargo are added (see Figure A.1).

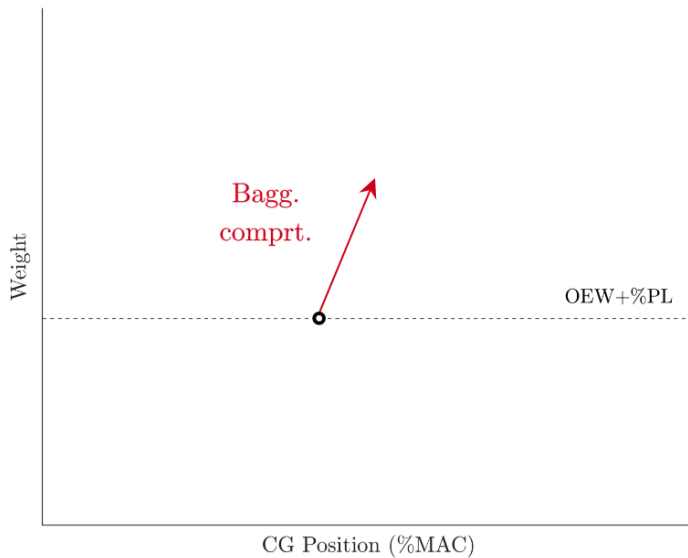


FIGURE 3.11: Baggage compartment effect on load and balance diagram

### 3.3.4 Impact of fuel weight on the position of the CG

Fuel is usually housed in a pair integral tanks on the wing, between the anterior and rear lengths. These two tanks are called the *inside tank*, which is the one closest to the join between the wing and the fuselage, and the exterior one, which is the one closest to the wing tip.

Bigger aircraft also count on a third fuel tank located inside the tail. Taking into account that the object of this project is a business jet and not a large aircraft, this extra fuel tank will not be considered in the preliminary design.

Going back to the fuel tanks located in the wing, in regards of the weight distribution, it is worth noting that the fuel which is firstly consumed is the one from the interior tank. Holding fuel as far as possible from the root of the wing is profitable from the structural point of view, as this mass will create a stronger bending moment that partially compensates the one created by the lift distribution.

As mentioned above, one of the requirements that this project must fulfil is reaching a slightly higher Mach than other existent aircraft in the sector. Thus, as explained, the wing sweep angle for this aircraft must be found between  $20^\circ$  and  $30^\circ$ . As the wing presents this geometry, the outer tank must be shifted backwards relative to the position of the center of gravity (see Figure 3.9), which implies a larger lever arm and, thus, a greater contribution to the CG shift along the MAC.

Indeed, the weight of the aircraft evolves mainly as fuel is burned. Not only does the amount of fuel available in tanks affect the range of values the CG can take, since a tank full in volume does not always correspond to the same weight, as its density is quite sensitive to temperature. Moreover, this difference can lead to a significant impact on the CG. However, at this stage of the project, this last consideration is not going to be taken into account.

A solution for the problems mentioned above, which is valid for small aircraft, is to position the fuel tanks close to the CG. Thus, the consumption of fuel does not affect the CG to any great extent.

In order to make a qualitative study on the impact of the Fuel Weight on the position of the CG, a Fuel Weight vs CG position chart is developed in Figure 3.12. Assuming that a fuel management procedure has been realized in order to minimize the movement of the CG along the MAC, the center of gravity shift will be represented by straight lines in the diagram.

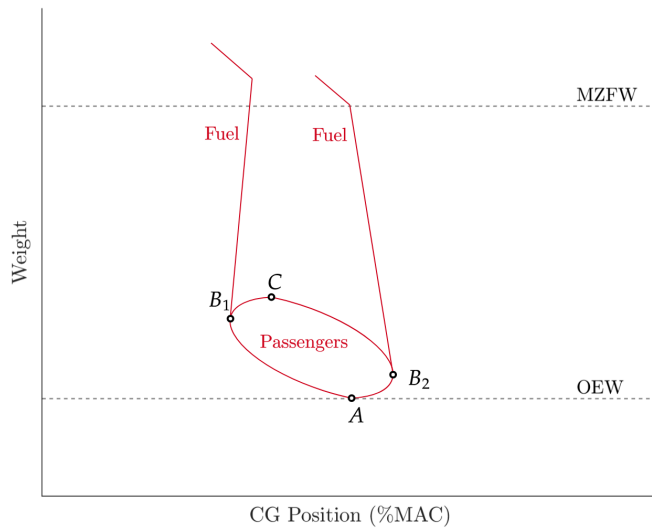


FIGURE 3.12: Fuel effect on load and balance diagram

The first point to consider is the ZFW, which includes the total weight of the airplane and all its contents, minus the total weight of the usable fuel on board. The outer tank is the first to be filled. Since the wing presents a sweep angle, the exterior fuel tank is displaced backwards from the actual CG, so the center of gravity position will be shifted towards the rear as the tank is filled.

Then, the inner tank fuel is filled. As its CG is now advanced from the aircraft CG, the center position will move to lower values of %MAC.

### 3.3.5 Resulting load and balance diagram

Bearing in mind the already analysed effect of passenger, baggage compartment, fuel and engines, the general estimated loading and balance distribution is such that:

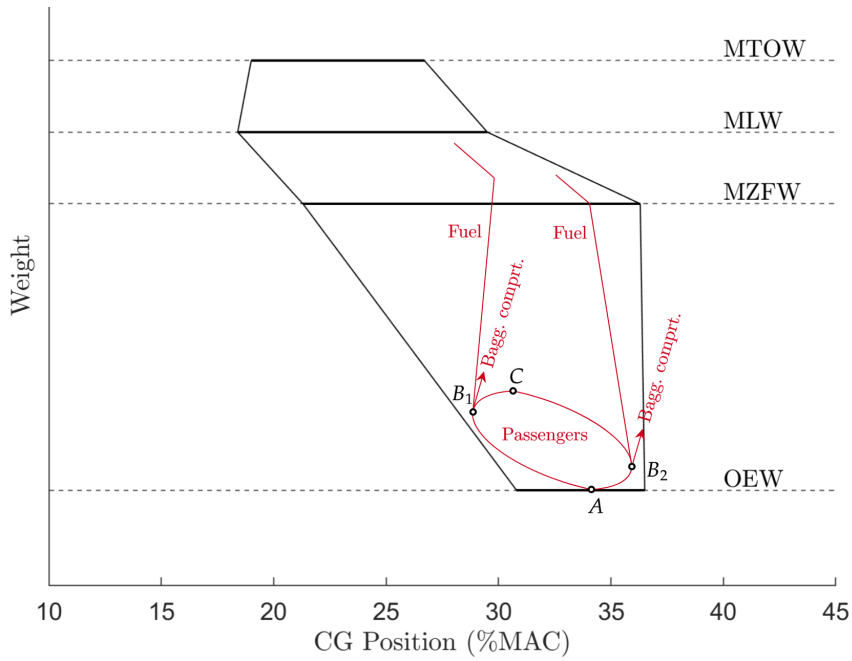


FIGURE 3.13: Resulting load and balance diagram

It must be mentioned that the provided graph is just a representative illustration, that is to say, the loading values used and the positioning of the loading variation (represented as red curves) are a mere estimation. In addition, a worth-mentioning aspect is that the mentioned loading variation do remain inside the CG limitations, thereby resulting in safe flight conditions.

# Chapter 4

## Design point selection

In order to determine the the design point of the aircraft, a graph *thrust-to-weight* ratio (T/W) versus wing loading (W/S) at take-off is going to be developed. With this in mind, the different requirements related to the operations performed by the jet are going to be taken into account, such as take-off, cruise, second segment and landing.

It is worth mentioning that thee developed code corresponding to this chapter is added in Appendix K.

### 4.1 Take-off

The expression that relates the *thrust-to-weight* ratio  $T/W$  with the wing loading (W/S) is:

$$\frac{T_{to}}{W_{to}} \geq k_{to} \frac{W_{to}/S_W}{\sigma C_{L,\max_{to}} s_{toFL}} \quad (4.1)$$

where  $T_{to}/W_{to}$  is the *thrust-to-weight* ratio at take-off,  $k_{to}$  is a given parameter from experimental data,  $W_{to}/S_W$  is the wing loading,  $\sigma$  is the the density ratio assuming International Standard Atmosphere,  $C_{L,\max_{to}}$  is the maximum lift coefficient at take-off and  $s_{toFL}$  is the take-off distance.

With the aim of estimating the take-off distance required by the aircraft, data from similar business jets have been taken into account (see Table 1.2). Thus, the mean value obtained is 4972.75 ft  $\equiv$  1515.69 m. nevertheless, the selected design

criterion used is:

$$s_{toFL} = 1515 \text{ m}$$

at sea-level conditions and considering *MTOW*.

Regarding the maximum lift coefficient at take-off, Table 3.1 from reference [8] offers a range of values suitable for business jets. As an estimation, a mean value of that range is chosen, so  $C_{L,\max_{to}} = 1.9$ .

To determine the value of the density ratio  $\sigma$ , it is going to be considered that the take-off takes place at sea-level conditions. Therefore, the relation between the local density and the one at sea level is  $\sigma = 1$ .

The last parameter that remains to determine is  $k_{to}$ . Its value corresponds to the slope of the straight line from Figure 3.7 of [8], which shows the proportionality between the take-off field length  $s_{toFL}$  and the take-off parameter for FAR 25 certified planes,  $TOP_{25}$ . It should be pointed that:

$$TOP_{25} = \frac{W_{to}/S_W}{\sigma C_{L,\max_{to}}(T_{to}/W_{to})} \quad (4.2)$$

According to expression 3.8 of [8],  $k_{to} = 37.5 \text{ ft}^3/\text{lb}$ , nonetheless, its equivalent in units of the International System (SI) is going to be used. Thus,  $k_{to} = 2.34 \text{ m}^3/\text{kg}$ .

Hence, replacing the previous values in equation 4.1 and having in mind that the units for the wing loading are  $N/m^2$ , it is obtained the following expression:

$$\frac{T_{to}}{W_{to}} \geq 8.37 \cdot 10^{-5} \cdot \frac{W_{to}}{S_W} \quad (4.3)$$

The graphic representation of this inequality is presented in Figure 4.1. The progression is linear with  $W_{to}/S_W$ , which means that higher wing loads require greater minimum thrust-to-weight ratio. In detail, for a given weight and with an increment in thrust, the wing section needed to accomplish the take-off requirements decreases and, consequently, the wing loading increases. This behaviour is logical, as greater loadings are meant to be compensated through higher thrust capacities.

Furthermore, it should be noted that the design point, according to inequality 4.3, has to be located in the region above the straight line.

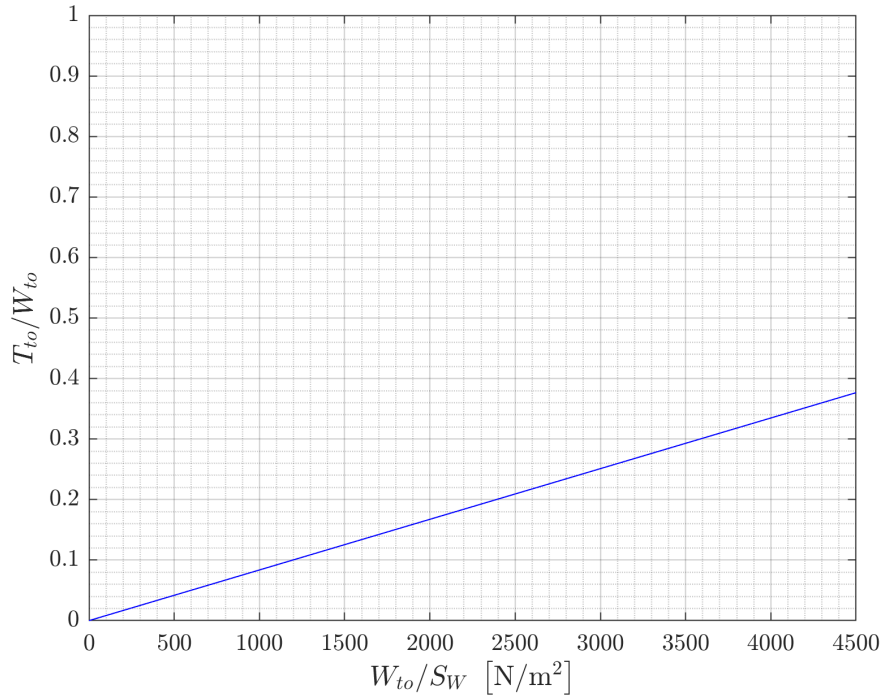


FIGURE 4.1: Graph regarding the take-off limitation.

## 4.2 Second segment

This phase takes place immediately after ascend and before achieving cruise flight (36 ft or 11 km height), also taking into consideration that the undercarriage system is collected and flaps are in ascend configuration.

The following dimensions are set based on FAR 25 specifications. This specification contemplates two scenarios. The first one considers a common take-off whereas the second scenario considers an aborted landing (balked landing). Thus, bearing in mind that the proposed business jet is a two-engine turbofan, thereupon are listed the requisites derived from the norm.

Norm	Description	CGR [rad]
FAR 25.121 (OEI)	Ascend First segment	$CGR > 0$
FAR 25.121 (OEI)	Ascend Second segment	$CGR > 0.024$
FAR 25.111 (OEI)	Final Ascend segment	$CGR > 0.012$

TABLE 4.1: Ascend requirements set by FAR 25.111 and FAR 25.121

Where  $CGR$  is the required climb gradient (this is the same as the flight path angle  $\gamma$ ), while OEI stands for one engine inoperative (one motor).

As stated in [8], according to FAR 25 the so called *second segment climb ascend* demands a climb gradient with one engine inoperative of no less than:

- 2.4 % for two-engine airplanes
- 2.7 % for three-engine airplanes
- 3.0 % for four-engine airplanes

with the following configuration:

1. Take-off flaps extended
2. Landing gear retracted
3. Remaining engines at take-off thrust or power
4. At  $V_2 (= 1.2V_{sTO})$
5. Out of the ground effect
6. Ambient atmospheric conditions
7. At maximum take-off weight

The dynamic equation that describes this stage's aircraft forces, projected to the aircraft's *wind axis* are the following equations:

$$\begin{cases} T = D + W \sin \gamma_2 + \frac{W}{g} \frac{dV}{dt} \\ L = W \cos \gamma_2 \end{cases}$$

Under the subsequent hypothesis,

- Small angle of attack
- Bi-dimensional motion and no lateral lift contribution

it is possible to express the *thrust-to-weight* ratio in terms of the parameters that dictate this stage. Thereby, second segment rise with critical engine failure:

$$\frac{T_{to}}{W_{to}} \geq \frac{N_e}{N_e - 1} \frac{T_{to,1e}}{T_{2,1e}} \frac{W_2}{W_{to}} \left[ \left( \frac{C_D}{C_L} \right)_2 + \gamma_2 \right]$$

where  $T_{to}/W_{to}$  is the *thrust-to-weight* ratio at take-off,  $N_e$  is the number of engines the aircraft has,  $T_{to,1e}$  expresses the take-off thrust for a single engine,  $T_{2,1e}$  happens to be the second segment thrust for a single engine,  $W_2/W_{TO}$  is the ratio between second segment weight and take-off weight and finally, as mentioned before,  $\gamma_2$  expresses the second segment ascend angle.

In the light of this stage, the norm set a minimum ascend angle  $\gamma_2$  including critical engine failure. This angle varies depending on the number of engines the aircraft has. For twin engine aircraft, this values is set to be at least 2.4 %.

$$CGR_2 = \gamma_2$$

$$\gamma_2 = 2.4\% = 0.024 \text{ rad} = 1.375 \text{ deg}$$

The values for this equation are listed below:

$$\frac{N_e}{N_e - 1} = 2 \quad \frac{T_{to,1e}}{T_{2,1e}} = 1 \quad \frac{W_2}{W_{TO}} \approx 0.98 \quad \frac{C_D}{C_L} = 0.1015 \quad (4.4)$$

According to [19], the thrust relation between take-off and second segment climb ascend  $T_{to,1e}/T_{2,1e} = 1$ . That is, the required thrust is the same during this two stages, and the difference is very small. Nevertheless, the main difference between these two stages are the aircraft configuration and the height. While during take.off, take-off flaps and gears are deployed, during second segment those landing gears are retracted.

Usually,  $\frac{W_2}{W_{TO}}$  is around  $\approx 98\%$ , take a look back to equation (3.12). This relation is equivalent to the weight loss of Phase 1, Phase 2 and Phase 3:

$$\frac{W_2}{W_{TO}} = \underbrace{0.990}_{\substack{\text{Phase 1:} \\ \text{Engine start}}} \cdot \underbrace{0.995}_{\substack{\text{Phase 2:} \\ \text{Taxi}}} \cdot \underbrace{0.995}_{\substack{\text{Phase 3:} \\ \text{Take-off}}} = 0.98 \quad (4.5)$$

As regards the efficiency, its value is:

$$C_D/C_L = \frac{C_{D0} + kC_L^2}{C_L} = \frac{(0.020 + 0.015) + 0.0437 \cdot 1.9^2}{1.9} = 0.1015 \quad (4.6)$$

where  $C_D$  is determined by the calculations performed in Appendix ??.

Thereby, the resulting second segment limitation is the following:

$$\frac{T_{to}}{W_{to}} \geq \frac{2}{2-1} \cdot 1 \cdot 0.98 \left[ \left( \frac{C_D}{C_L} \right)_2 + 0.024 \right]$$

Finally, the graphic representation of the aforementioned limitation is such that:

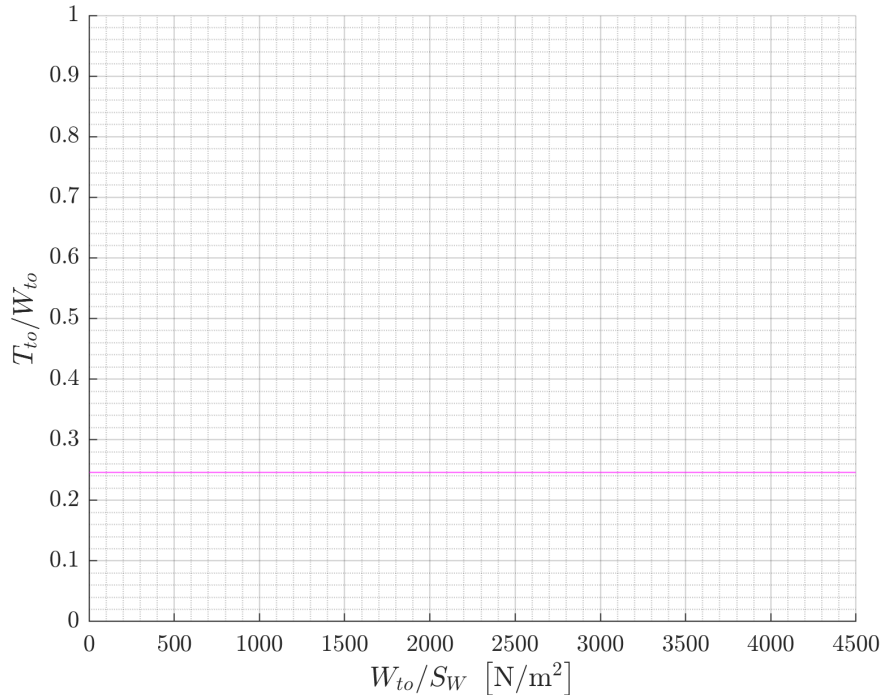


FIGURE 4.2: Graph regarding the second segment limitation

### 4.3 Cruise

The cruise flight phase is the longest in the mission. The aircraft develops a Rectilinear Horizontal Flight, in which the four main forces (resistance/thrust and support/weight) are in equilibrium.

The altitude at which this stage will be carried out will be determined in the flight plan, and the imposed speed is the design speed ( $M = 0.8$ ).

Thus, the two dynamic laws governing this phase of the mission (in both axes) are the following ones:

$$L_{cr} = W_{cr} \quad (4.7)$$

$$T_{cr} \geq D_{cr} \quad (4.8)$$

By developing both equilibrium Equations above, the following expression is obtained:

$$\frac{T_{to}}{W_{to}} \geq \frac{T_{to}}{T_{cr}} \frac{\frac{1}{2}\rho V^2}{\frac{W_{to}}{S_W}} \left( C_{D0} + \frac{\left( \frac{W_{to}}{S_W} \frac{W_{cr}}{W_{to}} \right)^2}{(\frac{1}{2}\rho V^2)^2 \pi A \varphi} \right) \quad (4.9)$$

In order to get Equation 4.9, the following steps have been followed. By definition:

$$L = C_L \bar{q} S_w \quad D = C_D \bar{q} S_w$$

If a parabolic drag polar is assumed  $\left( C_D = C_{D0} + \frac{C_L^2}{\pi A \varphi} \right)$ , we get (from 4.8):

$$T_{cr} \geq C_{D0} \bar{q} S_w + \frac{C_L^2 q S_w}{\pi A \varphi}$$

Dividing by weight and solving  $C_L$  from Equation 4.7, it is read:

$$\frac{T_{cr}}{W_{cr}} \geq \frac{C_{D0} q}{W_{cr}} + \frac{\frac{S_w}{S_W}}{q \pi A \varphi}$$

The next relation must be taken into consideration:

$$\frac{W_{to}}{S_w} = \frac{1}{k} \frac{W_{cr}}{S_w} \quad (4.10)$$

where  $k$  is a number  $0 < k < 1.0$ . Then:

$$\frac{T_{cr}}{W_{cr}} \geq \frac{1}{k} \left[ \frac{C_{D_0} q}{\left( \frac{W_{to}}{S_W} \right)} + \frac{\left( \frac{W_{to}}{S_W} \right)}{q \pi A \varphi} k^2 \right]$$

The parameter  $k$  is defined by the following expression:

$$k = \frac{W_{cr}}{W_{to}} \quad (4.11)$$

So,

$$\frac{T_{cr}}{W_{cr}} \geq \frac{1}{\frac{W_{cr}}{W_{to}}} \left[ \frac{C_{D_0} q}{\left( \frac{W_{to}}{S_W} \right)} + \frac{\left( \frac{W_{to}}{S_W} \right)}{q \pi A \varphi} \cdot \left( \frac{W_{cr}}{W_{to}} \right)^2 \right]$$

By developing the expression above:

$$\frac{T_{cr}}{W_{cr}} \geq \frac{1}{\frac{W_{cr}}{W_{to}}} \frac{q}{\frac{W_{to}}{S_W}} \left[ C_{D_0} + \frac{\left( \frac{W_{to}}{S_W} \right)^2 \left( \frac{W_{cr}}{W_{to}} \right)^2}{q^2 \pi A \varphi} \right]$$

Finally,

$$\frac{T_{cr}}{W_{cr}} \cdot \frac{T_{to}}{W_{to}} \cdot \frac{W_{to}}{T_{to}} \geq \frac{q}{\frac{W_{cr}}{W_{to}} \frac{W_{to}}{S_W}} \left[ C_{D_0} + \frac{\left( \frac{W_{to}}{S_W} \right)^2 \left( \frac{W_{cr}}{W_{to}} \right)^2}{q^2 \pi A \varphi} \right]$$

By developing the expression above and using the dynamic pressure expression in it ( $\bar{q} = \frac{1}{2} \rho V^2$ ), Equation 4.9 is obtained.

As the cruise ceiling is set at 12 km, if International Standard Atmosphere is assumed, the physical properties take the following value:

$$\rho = 0.3108 \text{ kg/m}^3 \quad T = 216.65 \text{ K} \quad P = 19.33 \text{ kPa} \quad a = 295.07 \text{ m/s}$$

In terms of the cruise speed:

$$V_{cr} = 0.8a = 236.06 \text{ m/s}$$

In regards of the parameters  $A$  and  $\varphi$ , according to [8] and as stated in Table I.1, the following values are assumed. For the calculation of the parameter  $A$ , the considered wingspan results for an average value of the similar existent aircrafts ( $\bar{b} = 20.94 \text{ m}$ ):

$$\varphi = 0.85 \quad A = \frac{b^2}{S_W} = \frac{20.94^2}{51.14} = 8.57$$

$T_{cr}/T_{to}$  can be read off engine diagrams for a given altitude and Mach number, but an equation is provided by reference [20]. For a cruise Mach number of  $M_{cr} = 0.8$ :

$$\frac{T_{cr}}{T_{to}} = (0.0013\lambda - 0.0387) h_{cr} - 0.0248\lambda + 0.7125 \quad (4.12)$$

, where  $\lambda$  is the bypass ratio. For the engine we are interested in,  $\lambda = 4.3$ .

By imposing  $h_{cr}$ , the following result is obtained:

$$\frac{T_{cr}}{T_{to}} = 0.1965$$

Thus,

$$\frac{T_{to}}{T_{cr}} = 5.09$$

On the other hand, the relation  $\frac{W_{cr}}{W_{to}}$  can be obtained from (3.12):

$$\frac{W_{cr}}{W_{to}} = \underbrace{0.990}_{\substack{\text{Phase 1:} \\ \text{Engine start}}} \cdot \underbrace{0.995}_{\substack{\text{Phase 2:} \\ \text{Taxi}}} \cdot \underbrace{0.995}_{\substack{\text{Phase 3:} \\ \text{Take off}}} \cdot \underbrace{0.980}_{\substack{\text{Phase 4:} \\ \text{Climb}}} = 0.9605 \quad (4.13)$$

Regarding to  $C_{D_0}$ , as explained above, it takes a value of  $C_{D_0} = 0.021$ .

At this point, we know the value of each parameter from Equation 4.9. Then, the graphic representation of the inequality is presented in Figure 4.3.

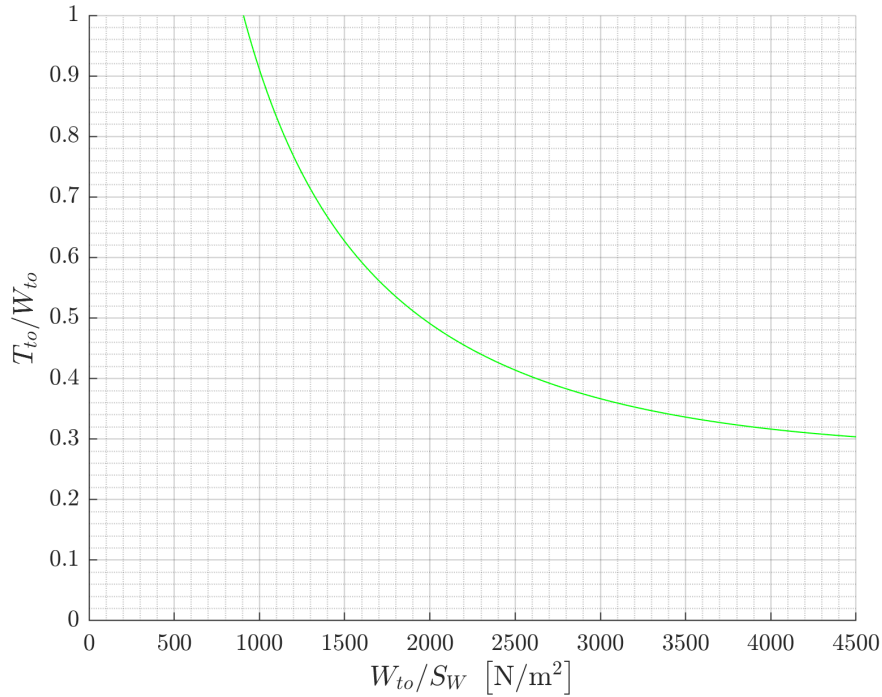


FIGURE 4.3: Graph regarding the cruise limitation

## 4.4 Landing

In order to estimate the landing distance, data from similar aircraft (see Table 1.2) have been considered. As a result, the obtained mean landing distance is 2886.75 ft  $\equiv$  879.88 m, being 4484 ft  $\equiv$  1367 m the maximum by Falcon 2000LX. Thereby, bearing in mind that our aircraft has a 47,5% larger *MTOW* than the mentioned model (see Table 3.1), as design criterion, the following estimated value is chosen:

$$s_l = 1750 \text{ m}$$

In the matter of sizing, the FAR 25 regulation must be followed. Specifically, it is stated that the FAR landing field length, as stated in Figure 4.4, is such that:

$$s_{lFL} = \frac{s_l}{0.6} = 2916.67 \text{ m} \quad (4.14)$$

where the 0.6 coefficient stands for the factor of safety set to considerate the variations in pilot technique that cannot be quantified with accuracy by FAA.

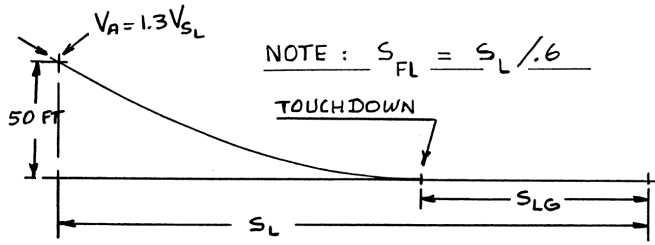


FIGURE 4.4: Definition of FAR 25 landing distances. Source: [8]

Moreover, an approximation speed relation is also required. According to Figure 3.17 of reference [8], the following expression can be used for this purpose:

$$s_{l FL} = 0.3 v_A^2 \quad (4.15)$$

where the units to use are  $s_{l FL}$  (ft) and  $v_A$  (kts).

From equations (4.14) and (4.15), the approximation speed can be calculated as indicated:

$$v_A = \sqrt{\frac{s_{l FL}}{0.3}} = \sqrt{\frac{1750 \cdot 3.2808/0.6}{0.3}} = 178.60 \text{ kts} \equiv 91.88 \text{ m/s}$$

However, the speed we are interested in is the stall speed in landing ( $V_{s_l}$ ). Therefore, according to Figure 4.4, the approximation speed is defined as the  $V_{s_l}$  increased by a 30%, thus:

$$v_{s_l} = v_A / 1.3 = 70.67 \text{ m/s}$$

Since this initial sizing is performed according to stall speed requirements, and there are no requirements for minimum stall speed in the case of FAR 25 certified airplanes, the next expression is used:

$$v_s = \sqrt{\frac{2W/S}{\rho C_{L,\max}}}$$

This equation refers to a generic power-off stall speed, but in our case it will be used for landing conditions.

As regards the typical values for the maximum lift coefficient in landing, Table 3.1 from reference [8] is used. A value of 2.6 is the maximum among the commonly

found in business jets, nevertheless, this data is probably outdated. That is to say, for the sake of compensating this coefficient we will use a slightly higher value of  $C_{L,\max_l} = 2.9$ . Hence, by rewriting the above formula, the wing load in landing can be obtained as:

$$\frac{W_l}{S_W} = \frac{v_{s_l}^2 \rho_0 C_{L,\max}}{2} = \frac{70.67^2 \cdot 1.225 \cdot 2.9}{2} = 8872.22 \text{ N/m}^2$$

Once this wing load limitation value has been computed, a relation between  $W_l$  and  $W_{to}$  has to be set. Specifically,  $W_{to}/W_l$  ratio is obtained from Equation (3.12), resulting in a value of  $W_{to}/W_l = 0.456$ . As also stated in [8], by using this factor the landing limitation can be computed as follows:

$$\frac{W_{to}}{S_W} = \frac{W_l}{S} \frac{W_{to}}{W_l} = 8872.22 \cdot 0.456 = 4045.73 \text{ N/m}^2$$

Therefore, the following inequality can be used as the mentioned landing limitation factor:

$$\frac{W_{to}}{S_W} \leq 4045.73 \text{ N/m}^2$$

It is worth noting that a different expression can be used in order to determine the aforementioned limitation. In this case, according to [21] the following inequality must be used:

$$\frac{W_{to}}{S_W} \leq k_l \frac{W_{to}}{W_l} \sigma C_{L,\max_l} s_{lFL}$$

Nevertheless, in this case the coefficient  $k_l$  in landing must be obtained from similar aircraft. Due to the obvious difficulty that carries the fact of finding the values for every variable appearing in the above formula, this landing limitation won't be used.

Finally, the graphic representation of the landing limitation is shown in Figure 4.5. It consists on a vertical line as it an independent limitation that must be all the time respected for questions of safety and structural integrity.

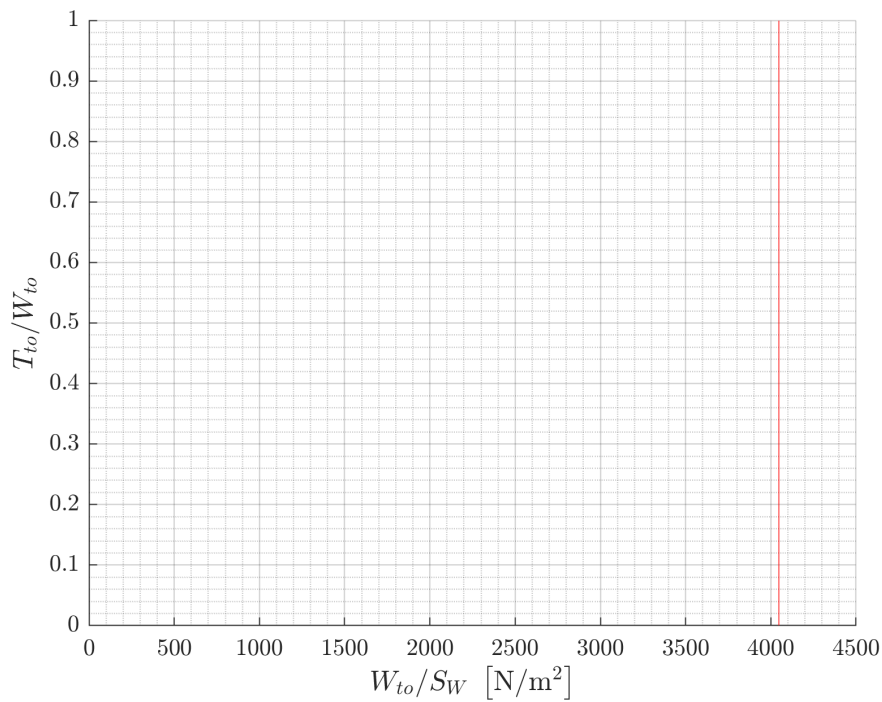


FIGURE 4.5: Graph regarding the landing limitation

## 4.5 Final selection (1st iteration)

In order to finally determine the design point, the previously analysed limitations must be considered. As a result, the highlighted area in Figure 4.6 ensures the compliance of the mentioned performance limitations.

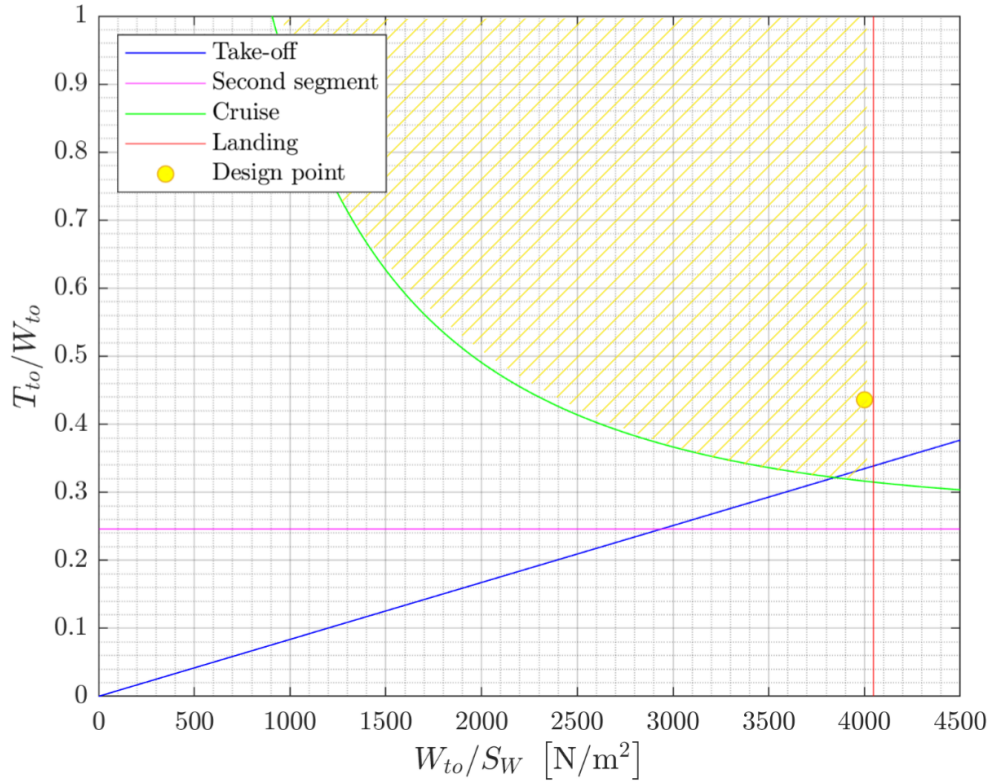


FIGURE 4.6: Design point selection (1st iteration)

As it can be observed, the point marked in yellow is the design point, this choice will be justified in the following sections. As stated in [21], the optimum design point needs to fulfil two basic conditions:

- Minimum  $T_{to}/W_{to}$ : to reduce the required thrust with a given  $MTOW$
- Maximum  $W_{to}/S_W$ : to reduce the required wing surface with a given  $MTOW$

#### 4.5.1 Thrust at take-off required

In first place, a *thrust-to-weight* ratio in take-off must be selected in order to vertically position the design point. In this case, the cruise limitation is the most critical one. Thus, the following ratio is selected:

$$\left( \frac{T_{to}}{W_{to}} \right)_{\text{design}} = 0.436$$

It is worth mentioning that there is the possibility of selecting a lower value nearer to the cruise curve so that  $T_{to}/W_{to} > 0.322$ . Nonetheless, this would imply a required total thrust of  $T_{to} > 90.5 \text{ kN} \equiv 45.2 \text{ kN/engine}$ . As previously showed in Table 3.4, engines mounted in similar jets only reach  $7665 \text{ lbf} \equiv 34.1 \text{ kN}$ , resulting in the need of a more powerful engine. Among the typical engines used in business jets that have been found, none of them provides a thrust around the required  $45.2 \text{ kN/engine}$ , that is to say a more powerful engine will have to be selected even if it is slightly overpowered. In this matter, the design point needed to be risen up to the mentioned 0.436 value according to the next available engine in terms of thrust, with a value of:

$$T_{to} = MTOW \cdot 9.81 \left( \frac{T_{to}}{W_{to}} \right)_{\text{design}} = 122.5 \text{ kN} \equiv 61.3 \text{ kN/engine}$$

where  $MTOW = 28643 \text{ kg}$  as showed in Table 3.12. This thrust value is the corresponding to the power plant specified in 4.5.1.1.

As a matter of fact, the choice of this specific point implies the use of a slightly overpowered engine relative to our thrust needs, nevertheless, this is not a major problem since the extra weight of this more powerful engine is minimal.

#### 4.5.1.1 Engine selection

Once the results are obtained, an engine meeting the requirements has to be chosen and installed. The General Electric CF34 is a civilian high-bypass turbofan developed by GE Aircraft Engines from its TF34 military line. This engine is used on a number of business and regional jets, including the Bombardier CRJ series, the Embraer E-Jets, and the Chinese ARJ21.



FIGURE 4.7: CF34-8C5B1 Engine. Source: [9]

The CF34 Engine series has a wide variety of models certified and analysed in EASA's type-certificate data sheet [9]. According to the aircraft's needs in terms of thrust at both sea level and cruise, specific consumption at also both phases and weight restraints, two engines meet the required criteria:

#### Performance Specifications

	-8C5B1	-8C5
Maximum takeoff thrust with APR <sup>†</sup>	13,790 lb	14,500 lb
Bypass ratio	5:1	5:1
Overall pressure ratio	28:1	28.5:1
Thrust/weight ratio	5.7:1	6:1
Maximum diameter	52 in	52 in
Fan diameter	46.2 in	46.2 in
Length	128 in	128 in
Weight	2,400 lb	2,450 lb
Noise	Meets or surpasses ICAO Chap. 4 requirements	
Emissions	Meets or surpasses ICAO CAEP/6 requirements	
Mounting	Fuselage	Fuselage
Specific fuel consumption 35K/0.8 max cruise	.67	.68

<sup>†</sup>Uninstalled. Sea level flat-rated to 86°F/30°C.

FIGURE 4.8: CF34-8C5 Engine comparison. Source: [9]

The results indicate that the maximum takeoff thrust ought to be superior to 10 klb so the variation between both is not significant. As the CF34-8C5B1's specific consumption is lower and the weight a bit lower, this engine meets all criteria with astounding results.

### 4.5.2 Wing surface required

Finally, a wing load in take off needs to be chosen. As regards this value, the most critical limitation is the landing, which sets a condition of  $\frac{W_{to}}{S_W} < 4045.7 \text{ N/m}^2$ . In line with this, the selected value is such that:

$$\left( \frac{W_{to}}{S_W} \right)_{\text{design}} = 4000 \text{ N/m}^2$$

It is relevant to mention that this value is not the maximum that can be chosen, basically in order to left a certain safety margin in relation with the landing limitation.

Then, using the MTOW the required wing surface is:

$$S_W = \frac{MTOW \cdot 9.81}{\left( \frac{W_{to}}{S_W} \right)_{\text{design}}} = 70.2 \text{ m}^2$$

This value is significantly higher than the initially estimated, of  $51.1 \text{ m}^2$ , but considerably similar to the one used by the analogous aircraft Falcon8X, with  $70.7 \text{ m}^2$ . We are well aware of the big surface that the selected value represents, nevertheless, this number is achievable.

## 4.6 Second iteration and sizing results summary

In the first iteration of the design point, the MTOW value used was computed with the estimated wing surface of  $51.1 \text{ m}^2$ . Obviously this differs vastly from the surface obtained by means of the design point. Hence, a second iteration of the design point will be carried out by recalculating the MTOW with the following data:

$$S_W = 70.2 \text{ m}^2; \quad b = 23 \text{ m} \quad A = 7.5$$

Thus, considering this new MTOW = 26720 kg and bearing in mind the above data, the resulting design point graph is:

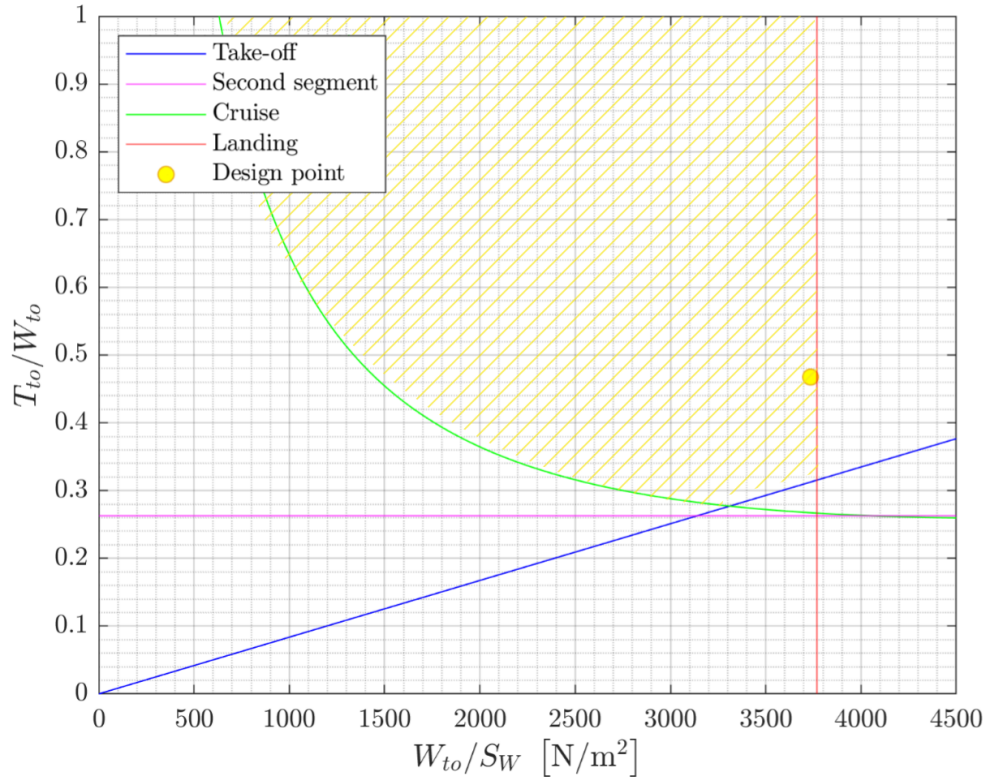


FIGURE 4.9: Design point selection (2nd iteration)

The slight variation of the landing limitation enables the possibility of reducing the landing variables  $C_{L,Max_l} = 2.83$  and  $s_l = 1670$  m. In terms of thrust, the results do not need to vary from the original ones, so the already selected engine is valid. To sum up, the resulting sizing data is:

Parameter	$C_{L,Max_{to}}$	$C_{L,Max_l}$	$\left(\frac{T_{to}}{W_{to}}\right)_{design}$	$T_{to}$ [kN]	$\left(\frac{W_{to}}{S_W}\right)_{design}$ [N/m <sup>2</sup> ]	$S_W$ [m <sup>2</sup> ]
Value	1.9	2.83	0.4675	122.5	3735	70.2

TABLE 4.2: Summary of the design point parameters

# Chapter 5

## Weight-Range Diagrams

For each possible flight that our aircraft could operate, some weight criteria must be totally respected and this would determine all the operational capabilities for the plane. Talk about the aircraft's capabilities is, in other words, the same that referring to the possible ranges which it would be capable to reach for different take off, fuel and payload weight conditions.

The Weight-Range Diagrams provide this very useful information with the aim of providing briefly idea of all this relations mentioned above. Also is necessary to mention that all the calculations will be performed using the code in Annex L which is based in the study that has been developed in the previous two chapter calculations accordingly to the analytical weight computation results.

### 5.1 Weight to Range Diagram

This diagram is meant to relate the different possible weight values, plotted in the y-axis with the reachable ranges according tot the Breguet's equation for range and all the other weight relation involved during the aircraft's fly.

This Weight to Range diagram could be subdivided into three different sections, separated by three of the most interested range values: range for maximum payload  $R_{PL}$ , range for maximum take off Weight  $R_{MTOW}$  and maximum Range  $R_{MAX}$ .

### 5.1.1 TOW ascending section

The first section of the diagram would be defined by an ascending tendency for the Take off weigh value.

The starting point values are easily obtained thanks to the Weight estimation and calculation mentioned above and shown in the Analytical results column of the table 3.11. With these two values and the resulting mass consumed fraction  $M_{ff}$ , the maximum zero fuel weight  $MZFW$  and the reserve fuel, estimated, (RF) can also be calculated. These values are calculated and shown with the expressions and the table below.

$$MZFW = OEW + MPL$$

$$FW = TF + RF = M_{ff}MTOW$$

Where the total Fuel Weight can be expressed by the summation of the trip fuel ( $TF$ ) and the reserve Fuel ( $RF$ ) with both fractions known and computed in the referenced Matlab code.

<b>MTOW</b> [kg]	<b>OEW</b> [kg]	<b>MZFW</b> [kg]	<b>RF</b> [kg]	<b>MPL</b> [kg]
32626	13764	15028.88	394.31	1264.88

TABLE 5.1: Starting weight values for the Weight to Range diagram

By the start of this segment the trip fuel value is considered 0 kg. Logically, at the same time that the aircraft is filled with the necessary trip fuel, the range performance which is associated to this operational starting weight conditions will be increasing till the maximum Payload range. This value is known owing to the way that the weight values have been computed. This maximum payload range must fullfill with the initial requirement which states that the range value carrying the maximum payload should be at least 4500 NM. Additionally the maximum payload range would be also associated with the maximum take off conditions. As it has been mentioned before, this section is characterised by a constant increase of the trip fuel weight, and starting from the Maximum payload

conditions. It only results in finishing in the conditions of maximum load of the plane, which is the same that saying the Maximum take off weight (*MTOW*).

### 5.1.2 *MTOW* constant section

This constant segment would last till the range value associated to the maximum take off Weight value. In order to increase the range and exchange between payload, reserve fuel and trip fuel would been computed. This weight change will take place up to the point where the value of the payload is equal to the initial payload requirement with the maximum possible fuel *MFW*. This is equal to a 1700 lb payload with the maximum fuel weight.

Executing the subroutine that has been created in order to compute the weight estimation, and modifying with the objective of obtaining the range as in output value with a fixed *MTOW* and *OEW* values is easily obtaining the constant *MTOW* section till the maximum take off range value where any combination with the payload maximum fuel requirement, *MTOW* and *OEW* is not far possible.

These last values are shown in the next table.

<b><i>MTOW</i> [kg]</b>	<b><i>OEW</i> [kg]</b>	<b><i>R<sub>MTOW</sub></i> [NM]</b>	<b><i>PL</i> [kg]</b>	<b><i>MWF</i> [kg]</b>
32626	13764	4783	771.11	1895.33

TABLE 5.2: Inter medium weight values for the Weight to Range diagram

### 5.1.3 *TOW* descending section

The diagram objective is to find the maximum possible range of the aircraft. With the aim of computing the best and longest possible performance, an hypothetical last case of carrying 0 [kg] Payload will be assumed.

Once the aircraft has been filled with the maximum fuel weight the only way of increasing the range is continue with the idea of decreasing the starting Payload conditions. This proceeding way will be assumed until the Payload weight achieve its minimum value of 0 [kg]. Intuitively this take off weight conditions are related with a very unusual operations for the commercial and regional aircraft due to

the fact that surely, they will have been manufactured with the idea of carrying payload and producing some economical benefits to its owner.

Applying the local relations between *TOW*, Payload, *FW* and *OEW*, recently mentioned the *TOW* value is calculated with the expression below.

$$TOW = OEW + PL + FW$$

If Payload is considered 0 [kg] and the Fuel weight has reached its maximum value (*MFW*), the last weight point is obtained by:

$$TOW_{last} = OEW + MFW$$

Moreover the last range point of the diagram and also the descending tendency for the *TOW* are computed using the same relations that have been employed during all the project. Easily knowing the last *TOW* value and the fuel Weight at the same point the mass fuel final fraction (*M<sub>ff</sub>*) could be calculated. Taking inverse process used the analytical weight calculation the total maximum range will be computed resulting from the Breguet range equation for the fuel fraction during the cruise stage. These calculation procedure is shown with the expressions that continue.

$$M_{fff} = 1 - \frac{MFW}{TOW_{last}}$$

$$\frac{W_5}{W_4} = \frac{M_{ff}}{\frac{W_1}{W_{TO}} \cdot \frac{W_2}{W_1} \cdot \frac{W_4}{W_3} \cdot \frac{W_6}{W_5} \cdot \frac{W_7}{W_6} \cdot \frac{W_8}{W_7}}$$

where all the fractions are computed and with a known value. So using the Breguet equation for the range it is assumed:

$$\frac{W_5}{W_{4last}} = e^{-R_{cruise-max}/\phi_{TF}} \quad \text{where} \quad \phi_{TF} = \left( \frac{V}{gc_j} \frac{L}{D} \right)_{\text{cruise}}$$

$$R_{cruise-max} = \left( \frac{V}{gc_j} \frac{L}{D} \right)_{\text{cruise}} \ln \left( \frac{W_4}{W_5} \right)$$

Finally the Maximum range value is computed using the 80 % relation assumed between the cruise range and the total operation aircraft range.

$$R_{\max} = \frac{R_{\text{cruise-max}}}{0.8}$$

Using the Matlab code help this values are computed and resulting in the next values.

<b>TOW</b> [kg]	<b>OEW</b> [kg]	<b>R<sub>max</sub></b> [NM]	<b>PL</b> [kg]
31866	13764	4989	0

TABLE 5.3: Last weight values for the Weight to Range diagram

Finally the Weight to Range Diagram can be obtained. It is presented with two different axis limits. The first one is the real and total axis graphical representation. The second one is set in order to clearly appreciate the slope changes at the different diagram sections.

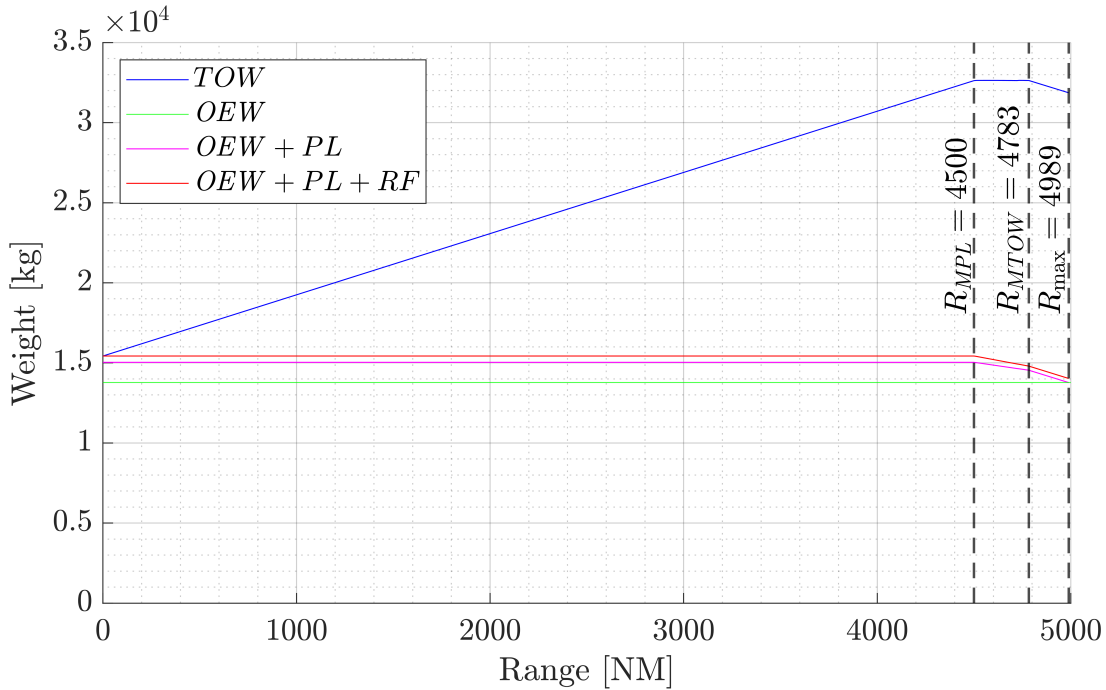


FIGURE 5.1: Weight to range diagram 1

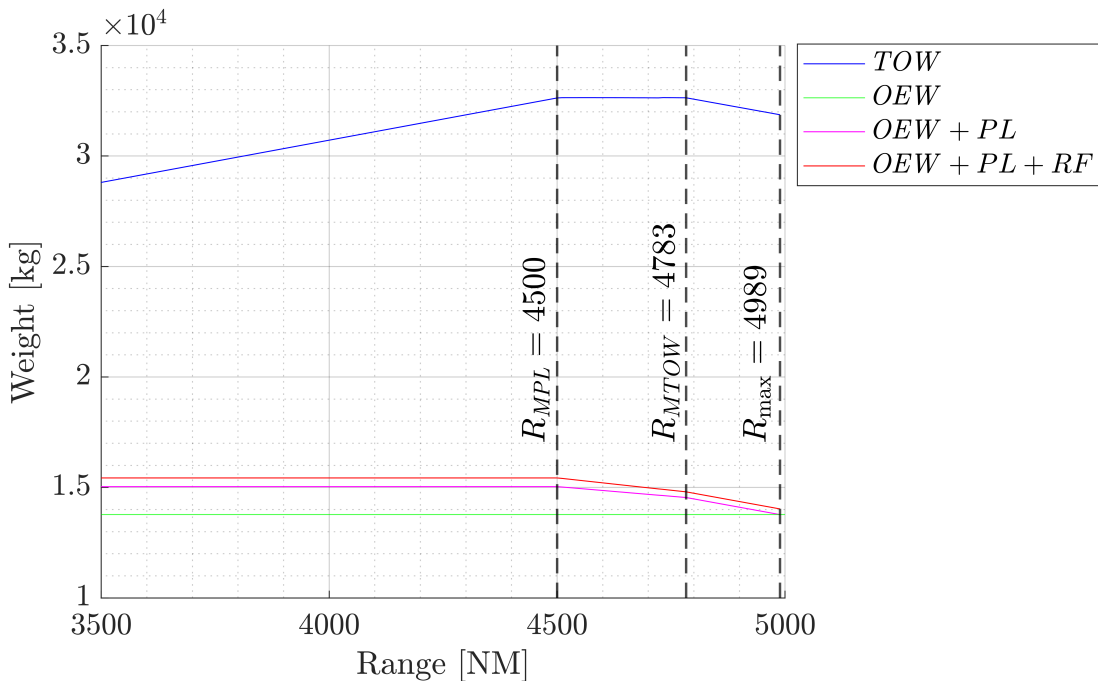


FIGURE 5.2: Weight to range diagram 2

## 5.2 Payload to Range Diagram

Talking about aircraft design projects is usually synonymous with the objective of transporting some kind of payload. This second diagram becomes an extraction of the payload evolution from the last diagram presented. At the same line evolution than the Take off weigh, the Payload is going to be limited different sections represented in the diagram below.

The first one is the associated operational conditions of carrying the maximum payload. In terms of the business jet that is being designed it would be the same than transporting the maximum passengers into the aircraft (10 passengers). This maximum Payload value, already mentioned above, is closely related with the maximum zero fuel weight, through the operational empty weight and its constant and defined value. So in terms of conclusion, as much as we increase this value of the Maximum zero fuel weight available the maximum payload would be increased. However these won't be an optimal operational conditions due to the fact that the maximum range achievable will be reduced.

The second section is limited by the maximum take off weight of the aircraft which is also already defined. As it has been specified before, in order to increase the range performance a reduction of the payload would be necessary to achieve the necessary fuel weight value. The maximum take off weight would limit this section till the moment when the aircraft is fully fuel loaded. Operating between these two payload and range values would be the most optimal conditions for the commercial planes. In our business jet case, taking into the account that the operational conditions are totally subject to owner's needs,

Finally the third section will be the less optimal conditions due to the fact that it is limited by the maximum fuel weight. At the moment that this weight value is reached, the only way of increasing the range is decreasing the payload making the operation of the aircraft less and less inefficient from an economic point of view.

In our business jet case, taking into the account that the operational conditions are totally subject to owner's needs, even knowing that they wouldn't be the most optimal and efficient conditions, the aircraft should be available to fly in all three payload conditions.

With the same idea of appreciating better the slope variations, below is presented the same Payload-Range diagram with two different axis distribution.

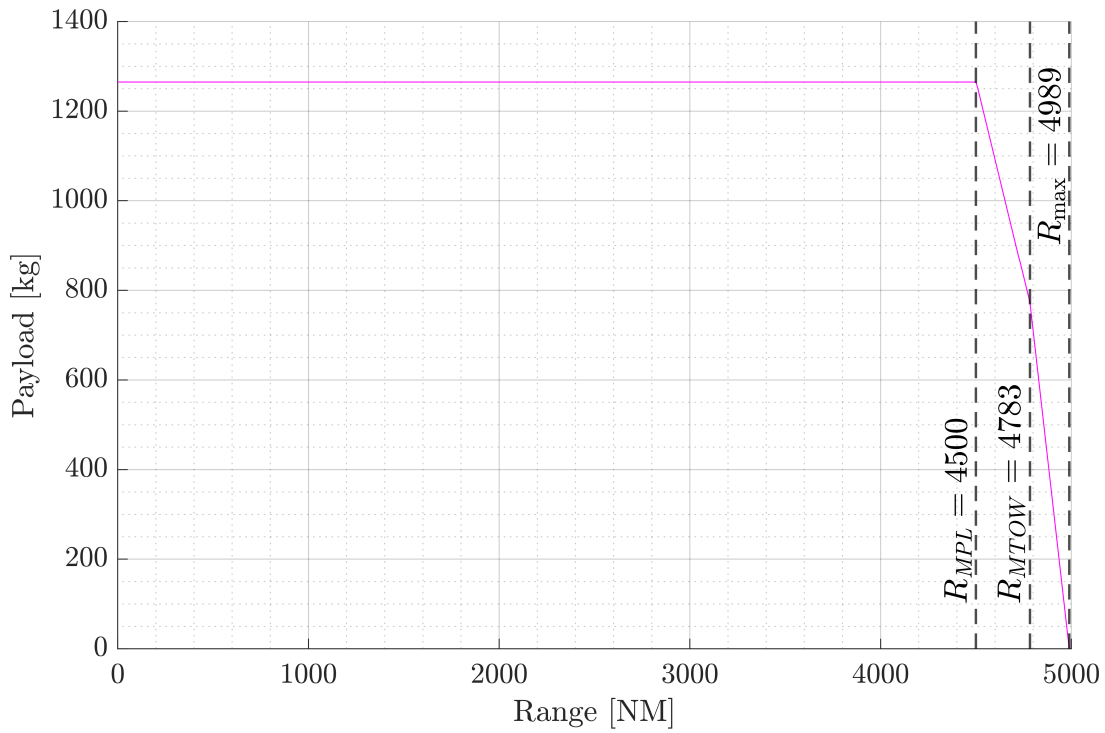


FIGURE 5.3: Payload to range 1

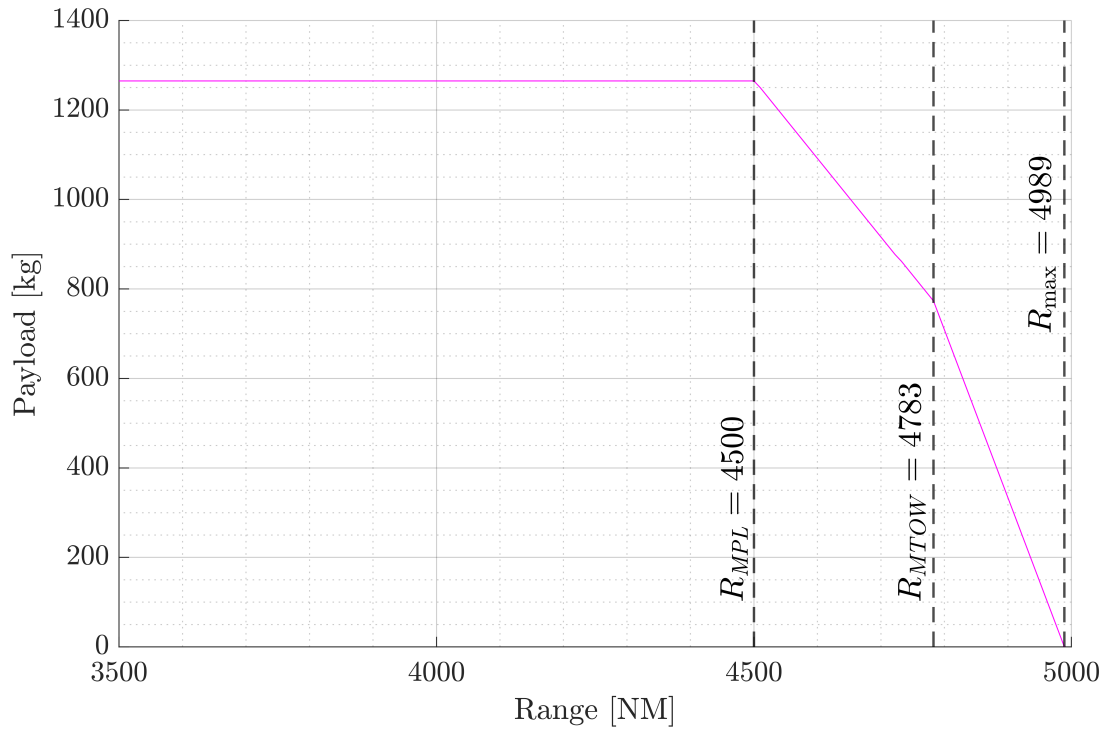


FIGURE 5.4: Payload to range 2

## Appendix A

### Baggage compartment volume

In order to determine the  $k_b$  coefficient, data from similar business jets have been used, as showed in Table 3.1. Taking into account the expression of the baggage compartment volume  $V_{bagg} = k_b l_f b_f^2$ , a linear regression can be performed as seen in the following graph:

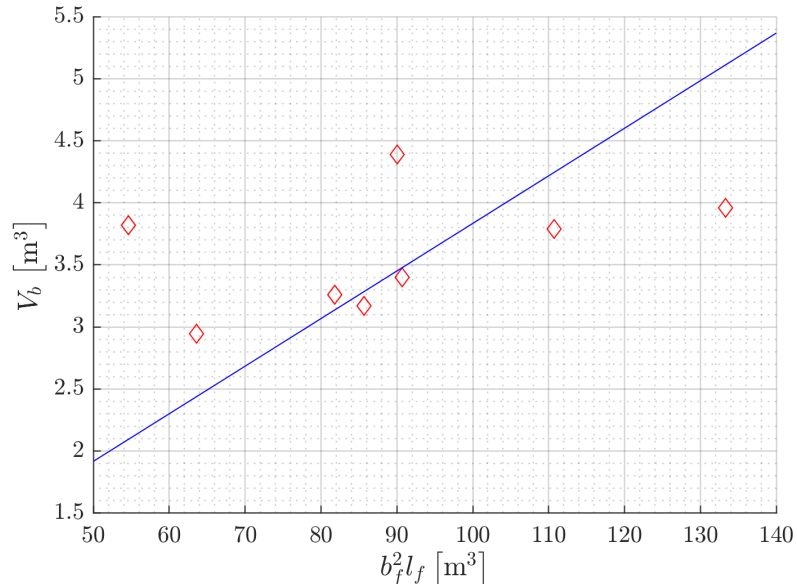


FIGURE A.1: Linear regression of the baggage compartment volume

As a result, the equation  $V_{bagg} = 0,03835l_f b_f^2$  is obtained, and so is the coefficient  $k_b$ .



## Appendix B

### Torenbeek criteria weight increment computation

The calculation of the  $\Delta W_E$  value from this study must be performed by using data from similar business jets exposed in Table 3.1. However, this variable's dependency may be a bit tricky, as Figure 5-3 in [5], which can be taken as a reference, shows a linear correlation when both the abscissa and ordinate axis are in a logarithmic scale.

Mathematically, this behavior can be expressed as:

$$\log_{10} \Delta W_e = A \log_{10} \left( l_f \frac{b_f + h_f}{2} \right) + B \quad (\text{B.1})$$

Where  $A$  and  $B$  are constant coefficients. MATLAB code detailed in Annex E performs a linear regression through the following sentence:

$$\text{polyfit}\left(\log_{10} \left( l_f \frac{b_f + h_f}{2} \right), \log_{10} \Delta W_e\right)$$

That gives as an outcome the parameters  $A$  and  $B$ . Nevertheless, expression (B.1) does not allow a fast and comfortable computations, so it will be transformed into an explicit form. Firstly, both sides of the identity will become the exponent of power of base 10.

$$10^{\log_{10} \Delta W_e} = 10^{A \log_{10} x + B} \quad \text{where, for simplicity} \quad x = l_f \frac{b_f + h_f}{2}$$

**APPENDIX B. TORENBEEK CRITERIA WEIGHT INCREMENT  
Aircraft Design COMPUTATION**

---

The left-hand side can be easily simplified, whereas the right-hand side can be developed following the properties of the power product:

$$\Delta W_e = (10^{\log_{10} x})^A \cdot 10^B$$

Which eventually leads to:

$$\Delta W_e = 10^B \left( l_f \frac{b_f + h_f}{2} \right)^A$$

The linear regression can be performed as seen in Figure B.1. Note that both axis are logarithmic.

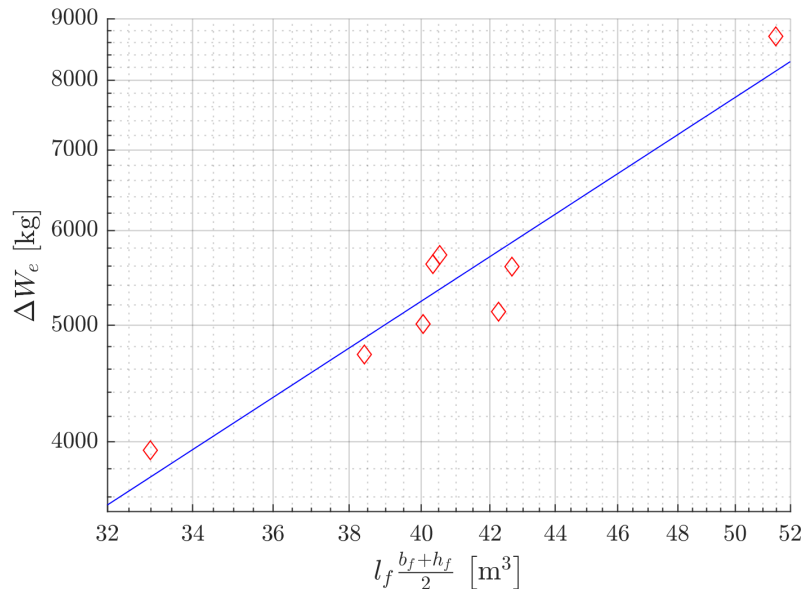


FIGURE B.1: Linear regression of the  $\Delta W_E$  value.

The estimate set of fuselage parameters for  $b_f$ ,  $h_f$  and  $l_f$  can be found in Table 3.3. The corresponding abscissa value results in  $41.031 \text{ m}^3$ . Using the regression provided by the MATLAB code in Annex E, it is easily observable that this value leads to a computed value of  $\Delta W_E = 5476.942 \text{ kg}$ .

# Appendix C

## Breguet's equation derivation

### C.1 Breguet's equation for range

The Breguet equation establishes a relation between the range and a set of design parameters of the aircraft. The simple, differential form states that the temporal variation of the weight is equal to the specific consumption  $c_j$  times the gravity acceleration  $g$  and the engine thrust  $T$ :

$$\frac{dW}{dt} = -gc_j T$$

However, the latter equation is time dependant, and the interest in this case is to analyze the performance in terms of range (distance). In order to achieve the desired dependence, the chain rule of the differential will be applied as follows:

$$dx = \frac{dx}{dt} dt = V dt$$

With this action the cruise speed of the aircraft  $v$  and the time differential  $dt$  are introduced into the Breguet's equation:

$$V \frac{dW}{dx} = -gc_j T \quad (\text{C.1})$$

Throughout the cruise stage, assuming horizontal flight, the following system of dynamic equations is fulfilled:

$$\begin{cases} T = D \\ L = W \end{cases} \xrightarrow{\text{dividing both eq.}} \frac{T}{W} = \frac{D}{L} \implies T = \frac{D}{L}W \quad (\text{C.2})$$

Where the quotient  $L/D$  is called the aerodynamic efficiency. The thrust can now be replaced in the Breguet equation:

$$V \frac{dW}{dx} = -gc_j \frac{W}{\frac{D}{L}}$$

Rearranging terms it can be obtained:

$$dx = -\frac{V}{gc_j} \frac{L}{D} \frac{1}{W} dW \quad (\text{C.3})$$

### C.1.1 Analytical resolution

The differential equation (C.3) allows a direct analytical integration if the following hypothesis are done:

- **Constant velocity:** this implies constant Mach number and height for the cruise stage and may be totally valid for a certain range.
- **Constant efficiency:** this assumption is not fully valid, as the weight decreases as the flight goes on due to the fuel consumption. According to the system of equations for horizontal flight (C.2), the lift must diminish too, fact that leads to a change on the lift coefficient  $C_L$  that influences the drag coefficient  $C_D$ . As a result of this, the aerodynamic efficiency  $L/D$  should also suffer a variation.
- **Constant specific fuel consumption:** the specific fuel consumption depends on the flight Mach number as it is shown hereunder:

$$\frac{c_j}{c_{j,\text{ref}}} = \left( \frac{M}{M_{\text{ref}}} \right)^\beta$$

Where the subscript *ref* denotes reference condition for a certain Mach number and the parameter  $\beta$  is encompassed between 0 and 1 and represents the compressibility effects on the consumption. Thus, if the Mach number remains constant the  $c_j$  also does, and the assumption becomes absolutely correct.

Applying a definite integral on equation (C.3):

$$\int_{x_0=0}^R dx = -\frac{V}{gc_j} \frac{L}{D} \int_{W_4}^{W_5} \frac{1}{W} dW$$

The primitive function of the integral on the right-hand side is a napierian logarithm which is able to absorb the negative sign:

$$R = \frac{V}{gc_j} \frac{L}{D} \ln \left( \frac{W_4}{W_5} \right)$$

It must be noted that the weights' subscript obey the cardinal enumeration used on [8] to designate the mission profile.

### C.1.2 Numerical resolution

A more faithful alternative to solve the Breguet's equation is using numerical methods such as Runge-Kutta or Euler. However, both require a form of the equation where the differential is isolated and all the dependencies are set exclusively on both the independent and dependent variables.

The departure point in this case will be expression (C.1), where the thrust has not been replaced yet. From system (C.2), it is known that in horizontal flight the thrust equals the drag:

$$V \frac{dW}{dx} = -gc_j D$$

Where the drag can be developed as:

$$D = \frac{1}{2} \rho V^2 S C_D(C_L)$$

And the drag polar can be assumed as parabolic with constant coefficients:

$$C_D(C_L) = C_{D0} + k C_L^2$$

Furthermore, and again from the dynamic system (C.2), it is known that the lift equals the weight:

$$\frac{1}{2}\rho V^2 S C_L = W$$

From the latter equation, the lift coefficient  $C_L$  can be isolated and replaced into the drag polar, which can in turn be substituted in the Breguet's equation, leading to:

$$\frac{dW}{dx} = -\frac{gc_j}{\gamma} \frac{1}{2} \rho V^2 S \left[ C_{D0} + k \left( \frac{2W}{\rho V^2 S} \right)^2 \right]$$

Defining the velocity as a function of the Mach number:

$$V = M \sqrt{\gamma R_g T}$$

It leads to:

$$\frac{dW}{dx} = -\frac{gc_j}{2} \rho S M \sqrt{\gamma R_g T_h} \left[ C_{D0} + k \left( \frac{2W}{\rho \gamma R_g T S} \right)^2 \right] \quad (\text{C.4})$$

This last result fulfils the initial requirements: the differential is isolated on the left-hand side and the dependence is set on the weight, which is the dependent variable; and on the range and height, which are the independent variable, as they are totally arbitrary.

## C.2 Breguet's equation for endurance

The differential equation for horizontal flight in terms of endurance (time) can be easily obtained from expression (C.3), but without considering the variable change, thus leading to:

$$dt = -\frac{1}{gc_j} \frac{L}{D} \frac{1}{W} dW \quad (\text{C.5})$$

### C.2.1 Analytical resolution

Considering the same exact assumptions than in section C.1.1, expression (C.5) can be definitely integrated as follows:

$$\int_{t_0=0}^E dt = -\frac{1}{gc_j} \frac{L}{D} \int_{W_5}^{W_6} \frac{1}{W} dW$$

Thus leading to:

$$E = \frac{1}{gc_j} \frac{L}{D} \ln \left( \frac{W_5}{W_6} \right)$$

Again, the subscripts are referred to the stages designated in the mission profile.

### C.2.2 Numerical resolution

Recalling expression (C.4), the only difference is that the velocity will be absent. In consequence, the final expression that should be solved through the numerical method will be:

$$\frac{dW}{dt} = -\frac{gc_j}{2} \rho S M^2 \gamma R_g T_h \left[ C_{D0} + k \left( \frac{2W}{\rho \gamma R_g T S} \right)^2 \right]$$



# Appendix D

## Numerical analysis

### D.1 Euler approximation

An initial value problem is considered:

$$\begin{cases} \frac{dy}{dx} = f(x, y(x)) \\ y(a) = y_0 \end{cases} \quad \begin{array}{l} (\text{D.1}) \\ (\text{D.2}) \end{array}$$

with  $x \in [a, b]$ ,  $y(x) \in \mathbb{R}$  i  $f: [a, b] \times \mathbb{R} \rightarrow \mathbb{R}$ . In general, the majority of the equations that are considered do not have an explicit solution  $y(x)$ . However, given the points  $x_0, \dots, x_n \in [a, b]$ , it is possible to obtain the value that  $y(x)$  has in those according to [22].

The Euler approximation is based on dividing the  $[a, b]$  interval in  $N$  subgroups defined by a width,  $h$ , where:

$$h = \frac{x_f - x_0}{N} \quad (\text{D.3})$$

so that a discreet group of  $N + 1$  points:  $x_0, x_1, x_2, \dots, x_N$  of the interval fulfillesthat:

$$x_i = x_0 + ih \quad 0 \leq i \leq N \quad (\text{D.4})$$

The initial condition  $y(x_0) = y_0$ , represents the point  $P_0 = (x_0, y_0)$  through which the solution of the equation intersects, which will be denoted as  $F(x) = y$ .

As a result, the first derivative which is equal to the slope of the function is obtained:

$$\frac{y_1 - y_0}{x_1 - x_0} = f(x_0, y_0) \quad (\text{D.5})$$

And then it is solved for  $y_1$ :

$$y_1 = y_0 + (x_1 - x_0)f(x_0, y_0) = y_0 + hf(x_0, y_0) \quad (\text{D.6})$$

Finally, looping this method a general result is obtained for each subdivision:

$$y_n = y_{n-1} + hf(x_{n-1}, y_{n-1}) \quad (\text{D.7})$$

## D.2 Runge Kutta method

An initial value problem is considered:

$$\begin{cases} \frac{dy}{dx} = f(x, y(x)) \\ y(a) = y_0 \end{cases} \quad (\text{D.8})$$

$$y(a) = y_0 \quad (\text{D.9})$$

with  $x \in [a, b]$ ,  $y(x) \in \mathbb{R}$  i  $f: [a, b] \times \mathbb{R} \rightarrow \mathbb{R}$ . In general, the majority of the equations that are considered do not have an explicit solution  $y(x)$ . However, given the points  $x_0, \dots, x_n \in [a, b]$ , it is possible to obtain the value that  $y(x)$  has in those according to [22].

The Runge-Kutta algorithms function as follows according to [22]:

$$\begin{cases} y(a) = y_0 \end{cases} \quad (\text{D.10})$$

$$\begin{cases} y_{n+1} = y_n + h \sum_{i=1}^k c_i k_i^n, & 0 \leq n \leq N - 1 \end{cases} \quad (\text{D.11})$$

with  $k \in \mathbb{N}$  previously defined, and the coefficients  $k_i^n$  are functions defined by:

$$\left\{ \begin{array}{l} k_1^n = f(x_n, y_n) \\ k_i^n = f \left( x_n + a_i h, y_n + h \sum_{j=1}^{i-1} b_{ij} k_j^n \right), \quad 2 \leq i \leq k \end{array} \right. \quad (\text{D.12})$$

$$\left\{ \begin{array}{l} k_1^n = f(x_n, y_n) \\ k_i^n = f \left( x_n + a_i h, y_n + h \sum_{j=1}^{i-1} b_{ij} k_j^n \right), \quad 2 \leq i \leq k \end{array} \right. \quad (\text{D.13})$$

The RK4 algorithm is a Runge-Kutta algorithm that is obtained for  $k = 4$ . It is expressed as follows:

$$\left\{ \begin{array}{l} y(a) = y_0 \\ y_{n+1} = y_n + \frac{h}{6} (k_1^n + 2k_2^n + 2k_3^n + k_4^n), \quad 0 \leq n \leq N - 1 \end{array} \right. \quad (\text{D.14})$$

$$\left\{ \begin{array}{l} y(a) = y_0 \\ y_{n+1} = y_n + \frac{h}{6} (k_1^n + 2k_2^n + 2k_3^n + k_4^n), \quad 0 \leq n \leq N - 1 \end{array} \right. \quad (\text{D.15})$$

where the coefficients are defined by:

$$\left\{ \begin{array}{l} k_1^n = f(x_n, y_n) \\ k_2^n = f \left( x_n + \frac{h}{2}, y_n + \frac{h}{2} k_1^n \right) \end{array} \right. \quad (\text{D.16})$$

$$\left\{ \begin{array}{l} k_1^n = f(x_n, y_n) \\ k_2^n = f \left( x_n + \frac{h}{2}, y_n + \frac{h}{2} k_1^n \right) \end{array} \right. \quad (\text{D.17})$$

$$\left\{ \begin{array}{l} k_1^n = f(x_n, y_n) \\ k_2^n = f \left( x_n + \frac{h}{2}, y_n + \frac{h}{2} k_1^n \right) \\ k_3^n = f \left( x_n + h, y_n + h k_2^n \right) \end{array} \right. \quad (\text{D.18})$$

$$\left\{ \begin{array}{l} k_1^n = f(x_n, y_n) \\ k_2^n = f \left( x_n + \frac{h}{2}, y_n + \frac{h}{2} k_1^n \right) \\ k_3^n = f \left( x_n + h, y_n + h k_2^n \right) \\ k_4^n = f(x_n + h, y_n + h k_3^n) \end{array} \right. \quad (\text{D.19})$$

Intuitively, the Runge-Kutta methods discretise the domain defined by the independent variable  $x$  in subgroups defined by  $h$  where, for each point  $x_n$  of the discretisation, calculate the value of  $y'$  in the surrounding points of  $x_n$ , i.e., the  $k_i^n$  coefficients. From the current value  $y_n$  of the function and the coefficients, the following value of the function,  $y_{n+1}$ , is calculated.

The numerical methods are, in general, approximations of the analytical solution of the problem. The precision of the approximation depends on  $h$ . However, the RK4 method is of global order 4, which mean that the error is also of order  $\mathcal{O}(h^4)$ . This implies that, if a  $h' = h/2$  is defined and the RK4 algorithm is reapplied, the error will be reduced 16 times.



# Appendix E

## Regression code

This code and its required Excel file can be found inside the folder *Regression code* which can be accessed through clicking [here](#).

```
1 % Code for obtaining auxiliar parameters involved in the weight  
2 % determination  
3  
4 % 2020, Aircraft Design  
5  
6 % Authors:  
7 % Cristian Asensio García  
8 % Juan Garrido Moreno  
9 % Yi Qiang Ji Zhang  
10 % Alexis Leon Delgado  
11 % Alba Molina Cuadrado  
12 % David Morante Torra  
13 % Teresa Peña Mercadé  
14 % Ferran Rubio Vallhonrat  
15 % Iván Sermanoukian Molina  
16 % Santiago Villarroya Calavia  
17  
18 % PREAMBLE  
19 clear  
20 clc
```

```

21 | close all
22 | format long
23 |
24 | %% DATA INPUT
25 |
26 | % Fuselage dimensions Excel reading
27 | fuselage_length=[xlsread('JET','Sheet1','W6');xlsread('JET','Sheet1',
28 | 'W8:W11');xlsread('JET','Sheet1','W13');xlsread('JET','Sheet1',
29 | 'W20');xlsread('JET','Sheet1','W22')];
30 | fuselage_width=[xlsread('JET','Sheet1','T6');xlsread('JET','Sheet1',
31 | 'T8:T11');xlsread('JET','Sheet1','T13');xlsread('JET','Sheet1',
32 | 'T20');xlsread('JET','Sheet1','T22')];
33 | fuselage_height=[xlsread('JET','Sheet1','U6');xlsread('JET','Sheet1',
34 | 'U8:U11');xlsread('JET','Sheet1','U13');xlsread('JET','Sheet1',
35 | 'U20');xlsread('JET','Sheet1','U22')];
36 |
37 | % Operative masses Excel reading
38 | MTOW=[xlsread('JET','Sheet1','N6');xlsread('JET','Sheet1',
39 | 'N8:N11');xlsread('JET','Sheet1','N13');xlsread('JET','Sheet1',
40 | 'N20');xlsread('JET','Sheet1','N22')];
41 | OEW=[xlsread('JET','Sheet1','P6');xlsread('JET','Sheet1',
42 | 'P8:P11');xlsread('JET','Sheet1','P13');xlsread('JET','Sheet1',
43 | 'P20');xlsread('JET','Sheet1','P22')];
44 | engine_mass=[xlsread('JET','Sheet1','X6');xlsread('JET','Sheet1',
45 | 'X8:X11');xlsread('JET','Sheet1','X13');xlsread('JET','Sheet1',
        |
        | % Baggage volume Excel reading
        |
        | baggage_volume=[xlsread('JET','Sheet1','S6');xlsread('JET','Sheet1',
        | 'S8:S11');xlsread('JET','Sheet1','S13');xlsread('JET','Sheet1',
        | 'S20');xlsread('JET','Sheet1','S22')];
        |
        | % Estimation of our aircraft fuselage data
        |
        | b_f_est=mean(fuselage_width);
        | l_f_est=mean(fuselage_length);
        |
        | %% LINEAR REGRESSION OF THE BAGGAGE COMPARTMENT
        | → VOLUME
        |
        | % Computation of the product of the squared fuselage width times the length

```

```

46 baggage_volume_abscissa=(fuselage_width.^2).*fuselage_length;
47
48 % Regression of a linear function that crosses the coordinate origin
49 kb_regression=fitlm(baggage_volume_abscissa,baggage_volume,'Intercept',false);
50
51 % Graphic plotting
52 fig1=figure(1);
53 set(fig1,'Renderer', 'painters', 'Position', [400 400 500 350]);
54 hold on
55
56 % Scatter plot
57 scatter(baggage_volume_abscissa,baggage_volume,'d','r')
58
59 % Regression line plot
60 plot(linspace(50,140,20),linspace(50,140,20)*kb_regression.Coefficients{1,1}, 'b')
61
62 % Axis format
63 set(gca,'TickLabelInterpreter','latex','fontsize',10)
64 ylabel('$V_b \left[ \mathrm{m}^3 \right]', 'interpreter','latex','FontSize',12)
65 xlabel('$b_f^2 l_f \left[ \mathrm{m}^3 \right]', 'interpreter','latex','FontSize',12)
66
67 % Grid format
68 grid on
69 ax = gca;
70 ax.GridColor = [0, 0, 0];
71 ax.GridAlpha=0.2;
72
73
74 %% LINEAR REGRESSION OF THE DELTA W_E
75
76 % Computation of the correspondent abscissa
77 Delta_W_e_abscissa=fuselage_length.* (fuselage_width+fuselage_height)/2;
78
79 % Delta W_e computation
80 Delta_W_e=OEW-0.2*MTOW-500-2*engine_mass;

```

```

81 % In the tri-engine case, another engine mass must be added
82 Delta_W_e(2)=Delta_W_e(2)+engine_mass(2);
83
84 % Regression of a standard linear function
85 %Delta_W_e_regression=polyfit(Delta_W_e_abscissa,Delta_W_e,1);
86 Delta_W_e_regression=polyfit(log10(Delta_W_e_abscissa),log10(Delta_W_e),1);
87
88 % Graphic plotting
89 fig2=figure(2);
90 set(fig2,'Renderer', 'painters', 'Position', [400 400 500 350]);
91 hold on
92
93 % Scatter plot
94 scatter(Delta_W_e_abscissa,Delta_W_e,'d','r')
95
96 % Regression line plot
97 plot(linspace(32,52,20),linspace(32,52,
20).^Delta_W_e_regression(1)*10.^Delta_W_e_regression(2),'b')
98
99 % Axis format
100 set(gca,'TickLabelInterpreter','latex','fontsize',10)
101 xlabel('$l_f \frac{b_f + h_f}{2} \left[ \mathrm{m}^3 \right]$', 'interpreter',
'latex', 'FontSize', 12)
102 ylabel('$\Delta W_e \left[ \mathrm{kg} \right]$', 'interpreter', 'latex', 'FontSize',
12)
103 set(gca,'yscale','log')
104 set(gca,'xscale','log')
105 xlim([32 52])
106 ylim([3500 9000])
107
108 % Grid format
109 grid on
110 grid minor
111 ax = gca;
112 ax.GridColor = [0, 0, 0];
113 ax.GridAlpha=0.2;

```

```

114
115 %% LINEAR REGRESSION OF THE ALPHA CONSTANT FOR THE
116 %→ SIMILARITIES CRITERIA
117
118 % Regression of a linear function that crosses the coordinate origin
119 alpha_regression=fitlm(MTOW,OEW,'Intercept',false);
120
121 % Graphic plotting
122 fig3=figure(3);
123 set(fig3,'Renderer', 'painters', 'Position', [400 400 500 350]);
124 hold on
125
126 % Scatter plot
127 scatter(MTOW,OEW,'d','r');
128
129 % Regression line plot
130 plot(linspace(10000,35000,20),linspace(10000,35000,
131 20)*alpha_regression.Coefficients{1,1}, 'b');
132
133 % Axis format
134 set(gca,'TickLabelInterpreter','latex','fontsize',10)
135 xlabel('$\mathrm{MTOW} \left[ \mathrm{kg} \right]$', 'interpreter', 'latex',
136 'FontSize',12)
137 ylabel('$\mathrm{OEW} \left[ \mathrm{kg} \right]$', 'interpreter', 'latex',
138 'FontSize',12)
139
140 % Grid format
141 grid on
142 grid minor
143 ax = gca;
144 ax.GridColor = [0, 0, 0];
145 ax.GridAlpha=0.2;

```



# Appendix F

## ISA atmosphere MATLAB code

The following MATLAB code computes the density and temperature for a given height using the International Standard Atmosphere (ISA) model.

```
1 function [T,rho]=ISA_atmosphere(Z)
2
3 % Physical constants definition
4 R_asterisc=8.31432; % [N m/(mol K)]
5 M_0=28.964420*1e-3; % [kg/mol]
6 N_A=6.02257e26*1e-3; % [1/mol]
7 g_0_geo=9.80665; % [m^2/(s^2 m)]
8 g_0=9.80665; % [m/s^2]
9 Gamma=g_0_geo/g_0; % [m'/m]
10 r_0=6.356766e6; % [m]
11
12 % Geopotential height vector
13 H_b=[0 11 20 32 47 51 71 80]*1e3; % [m']
14 % Temperature gradient vector
15 L_Mb=[-6.5 0.0 1.0 2.8 0.0 -2.8 -2.0]*1e-3; % [K/m']
16 beta_viscosa=1.458*10^(-6); % [kg /(s m K^1/2]
17 S=110.4; %[K] Sutherland's constant
18 gamma_aire=1.4;
19
20 % Computation of the base pressures (P_b) and the base temperatures at a
```

```

21 % mollecular scale (T_b) of each region of the atmosphere.
22 % Data obtained from ISO 2533:1975 (ISA atmosphere)
23 T_Mb=[288.15 zeros(1,length(L_Mb)-1)]; % [K]
24 P_b=[101325.0 zeros(1,length(L_Mb)-1)]; % [Pa]
25 for i=1:(length(L_Mb)-1)
26     T_Mb(i+1)=T_Mb(i)+L_Mb(i)*(H_b(i+1)-H_b(i));
27     if L_Mb(i)==0
28         P_b(i+1)=P_b(i)*exp((-g_0_geo*M_0*(H_b(i+1)-
29             H_b(i)))/(R_asterisc*T_Mb(i)));
30     else
31         P_b(i+1)=P_b(i)*(T_Mb(i)/(T_Mb(i)+L_Mb(i)*(H_b(i+1)-
32             H_b(i))))^(g_0_geo*M_0/(R_asterisc*L_Mb(i)));
33     end
34 end
35 % Geopotential altitude computation
36 H=Z*Gamma*r_0/(r_0+Z);
37 % Temperature and pressure computation according to the geopotential
38 % altitude according to ISO 2533:1975
39 for b=1:(length(L_Mb))
40     if H>=H_b(b) && H<H_b(b+1) % Es distingeix el tram de l'atmosfera
41         T_M=T_Mb(b)+L_Mb(b)*(H-H_b(b));
42         if L_Mb(b)==0 % Si existeix gradient de temperatura
43             P=P_b(b)*exp((-g_0_geo*M_0*(H-H_b(b)))/(R_asterisc*T_Mb(b)));
44         else % Si no existeix gradient de temperatura
45             P=P_b(b)*(T_Mb(b)/(T_Mb(b)+L_Mb(b)*(H-
46                 H_b(b))))^(g_0_geo*M_0/(R_asterisc*L_Mb(b)));
47         end
48         break
49     end
50 end
51 % Gravity acceleration computation according to Z
52 g=g_0*(r_0./(r_0+Z)).^2;
53

```

```
54 % Sound speed calculation from T_M
55 a=sqrt(gamma_aire*R_asterisc*T_M/M_0);
56
57 % Other termophysical properties
58 T=T_M;
59 rho=(P*M_0)./(T*R_asterisc);
60 mu=(beta_viscosa*T.^1.5)./(S+T);
61
62 end
```



# Appendix G

## Weight-computing MATLAB code (Runge-Kutta)

??

### G.1 Main code

The following MATLAB code encompasses the Roskam's iterative loop to compute the design weights of the aircraft. Inside this loop the functions [G.1.1](#) and [G.1.2](#), which implement the Runge-Kutta numerical resolution, are called. Additionally, functions **F** to compute the atmospheric properties and **I** to compute the drag coefficient have also been used.

```
1 % Code for obtaining the weight design parameters
2
3 % 2020, Aircraft Design
4
5 % Authors:
6 % Cristian Asensio García
7 % Juan Garrido Moreno
8 % Yi Qiang Ji Zhang
9 % Alexis Leon Delgado
10 % Alba Molina Cuadrado
```

## **APPENDIX** WEIGHT-COMPUTING MATLAB CODE (RUNGE-KUTTA)

```
11 % David Morante Torra
12 % Teresa Peña Mercadé
13 % Ferran Rubio Vallhonrat
14 % Iván Sermanoukian Molina
15 % Santiago Villarroya Calavia
16
17 % PREAMBLE
18
19 clear
20 clc
21 close all
22 format long
23
24 %% DATA INPUT
25
26 % Fuselage dimensions
27 b_f_expected=2.02;
28 a_f_expected=1.819125;
29 l_f_expected=21.376375;
30
31 % Payload parameters
32 pax = 10 ; % Number of passengers
33 W_pax = 77 ; % Mass of a passenger [kg]
34 W_bagg = 20 ; % Mass of a passenger's baggage [kg]
35 rho_cargo = 160 ; % Cargo density [kg/m^3]
36 rho_bagg = 200 ; % Baggage density [kg/m^3]
37 kbd = 0.85 ; % Hold occupation efficiency
38
39 % Performance data
40 % Expected total range
41 total_range=4500*unitsratio('meter','nauticalmile'); % [m]
42 M_cruise = 0.8; % Cruise Mach number
43 M_loiter = 0.6; % Cruise Mach number
44 R_cruise = 0.8*total_range; % Cruise range [m]
45
```

```

46 % Cruise height vector. All the heights will be tackled equitatively
47 h_cruise_vector=[12000]; % [m]
48 % Length of each phase of the cruise
49 R_stage=R_cruise/length(h_cruise_vector); % [m]
50
51 h_loiter = 10000 ; % Loiter height [m]
52 h_reserve = 450; % Height for the reserve flight, stablished by ICAO [m]
53 cj_cruise = 2*1.8 * 10^(-5); % Cruise specific consumption [kg/N/s]
54 cj_loiter = 2*1.1 * 10^(-5); % Loiter specific consumption [kg/N/s]
55 E_loiter = 20 * 60 ; % Loiter time [s]
56 Autonomy= 30 * 60 ; % Reserved time to reach alternate aerodrome [s]
57 MTOW_estimated = 30100 ; % MTOW estimation [kg]
58 engine_weight=634.225; % Average engine weight [kg]
59
60 % Termo-physical properties
61 R_g = 2.870528738362446e+02 ; % Constant for air
62 lambda = 1.4 ; % Heat relation for air
63 g = 9.80665 ; % Gravity acceleration [m/s^2]
64
65 S = 51.1; % Wing surface [m^2]
66 Wing_span=20.9; % Wing span [m]
67
68 % Data regression loading
69 load('k_b_baggage.mat'); % Constant for the baggage volume
70 load('alpha.mat'); % Constant for the similarities criterion
71 load('Delta_W_e_regression.mat'); % Term for the Torenbeek criterion
72
73 % Number of points to numerically study the cruise
74 N=1e6;
75 % Number of points for each phase of the cruise
76 M=round(N/length(h_cruise_vector));
77
78 %% WEIGHT FRACTIONS
79
80 % Baggage volume

```

## **APPENDIX** WEIGHT-COMPUTING MATLAB CODE (RUNGE-KUTTA)

```
81 V_bagg=k_b_baggage*b_f_expected^2*l_f_expected;
82
83 % Maximum payload calculation
84 MPL = pax * (W_pax+W_bagg) + (kbd*V_bagg -
85 ((W_bagg*pax)/rho_bagg))*rho_cargo ; % Computation fo Payload Weight
86
87 % Fuel fractions determination for each stage
88
89 fraction1 = 0.990 ; % Mass fuel fraction engine start phase
90 fraction2 = 0.995 ; % Mass fuel fraction taxi phase
91 fraction3 = 0.995 ; % Mass fuel fraction take off phase
92 fraction4 = 0.980 ; % Mass fuel fraction Climb phase
93 fraction7 = 0.990 ; % Mass fuel fraction descend phase
94 fraction8 = 0.992; % Mass fuel fraction shutdown phase
95
96 %% TORENBEEK CRITERION LOOP FOLLOWING ROSKAM'S METHOD
97
98 % Delta W_e abscissa calculation
99 x_fuselage = l_f_expected * 0.5 * (a_f_expected+b_f_expected);
100 % Delta_e computation
101 Delta_e = 10^Delta_W_e_regression(2) * x_fuselage^(Delta_W_e_regression(1));
102
103 % Initial error definition
104 error=true;
105 % Assigment of the estimated MTOW
106 MTOW_RK4_torenbeek=MTOW_estimated;
107 % Counter initialization
108 counter=0;
109 % Data storage matrix initialization
110 data_storage_RK4_torenbeek=[];
111
112 while error==true % Loop that is executed until convergence is achieved
113
114 counter=counter+1; % Counter addition
```

```

115
116 % Drag polar coefficients computation.
117 % It is only performed once, as it only depends on the MTOW
118 [C_D0,k] = Polar_parameters_function(MTOW_RK4_torenbeek,S,Wing_span);
119
120 % Mass at the beginning of the cruise stage
121 Mass_begin_cruise=fraction1*fraction2*fraction3*fraction4*MTOW_RK4_torenbeek;
122
123 % Fraction 5 initialization
124 fraction5_prod=1;
125
126 for stage=1:length(h_cruise_vector) % Loop that goes all over the phases of the
   ↪ cruise
127
128 % Cruise height assignation
129 h_cruise=h_cruise_vector(stage);
130
131 % Runge-Kutta resolution of this phase of the cruise
132 [~,~,fraction5(stage),Efficiency(stage,:)] = RK4_range.function(cj_cruise,
   M_cruise,C_D0,k,S,h_cruise,Mass_begin_cruise*9.81,R_stage,M);
133
134 % Mass at the end of the current stage =
135 % mass at the beginning of the next stage
136 Mass_begin_cruise=Mass_begin_cruise*fraction5(stage);
137
138 % Fraction 5 productory for phases
139 fraction5_prod=fraction5_prod*fraction5(stage);
140
141 end % End of the cruise loop
142
143 % The mass at the beginning of the loiter is the mass at the end of the
144 % cruise stage (i.e. the last cruise phase)
145 Mass_begin_loiter=Mass_begin_cruise;
146
147 % Runge-Kutta resolution of the loiter

```

## **APPENDIX WEIGHT-COMPUTING MATLAB CODE (RUNGE-KUTTA)**

```
148 [~,~,fraction6] = RK4_autonomy_function(cj_loiter,M_loiter,C_D0,k,S,h_loiter,  
    Mass_begin_loiter*9.81,Autonomy);  
149  
150 % Mass at the beginning of the reserve stage  
151 Mass_begin_reserve=Mass_begin_loiter*fraction6;  
152  
153 % Runge-Kutta resolution of the reserve stage  
154 [~,~,fraction_reserve] = RK4_autonomy_function(cj_loiter,M_loiter,C_D0,k,S,  
    h_reserve,Mass_begin_reserve*9.81,Autonomy);  
155  
156 % Mission fuel fraction  
157 M_ff_RK4=fraction1*fraction2*fraction3*fraction4*fraction5_prod*fraction6*fraction_reserve*fraction1  
158  
159 % Total fuel weight computation  
160 W_f_RK4 = (1-M_ff_RK4)*MTOW_RK4_torenbeek;  
161  
162 % Operating empty weight computation (tentative)  
163 OEW_tentative=MTOW_RK4_torenbeek-W_f_RK4-MPL;  
164  
165 % Allowable operating empty weight computation (according to Torenbeek  
    ↪ criterion)  
166 OEW_torenbeek = 0.2*MTOW_RK4_torenbeek + 2*engine_weight+  
    ↪ Delta_e+500;  
167  
168 % Relative deviation computation  
169 OEW_torenbeek_deviation=abs(OEW_torenbeek-  
    OEW_tentative)/OEW_torenbeek;  
170  
171 % Data storage  
172 data_storage_RK4_torenbeek(1,counter)=OEW_tentative; % Tentative result  
173 data_storage_RK4_torenbeek(2,counter)=OEW_torenbeek; % Torenbeek result  
174  
175 error=false;  
176  
177 % If the convergence criterion is not fulfilled, the error is set back to  
178 % true
```

```

179 if OEW_torenbeek_deviation>0.0005
180     error=true;
181
182 % Depending on the value, a different adjustment is made
183 if OEW_torenbeek>OEW_tentative
184     MTOW_RK4_torenbeek=MTOW_RK4_torenbeek+1;
185 else
186     MTOW_RK4_torenbeek=MTOW_RK4_torenbeek-1;
187 end
188
189 end % End of the conditional that checks the convergence
190
191 end % End of the loop
192
193 % Graphic plotting
194 fig1=figure(1);
195 set(fig1,'Renderer', 'painters', 'Position', [400 400 500 350]);
196 hold on
197
198 plot([1:1:size(data_storage_RK4_torenbeek,2)], data_storage_RK4_torenbeek(1,:), 'b')
199
200 plot([1:1:size(data_storage_RK4_torenbeek,2)], data_storage_RK4_torenbeek(2,:), 'r')
201
202 % Axis format
203 set(gca,'TickLabelInterpreter','latex','fontsize',13)
204 ylabel('$OEW\\left[\\mathrm{kg}\\right]$', 'interpreter','latex','FontSize',15)
205 xlabel('Number of iterations', 'interpreter','latex','FontSize',15)
206
207 % Grid format
208 grid on
209 ax = gca;
210 ax.GridColor = [0, 0, 0];
211 ax.GridAlpha=0.2;
212 grid minor

```

## **APPENDIX G WEIGHT-COMPUTING MATLAB CODE (RUNGE-KUTTA)**

```
213
214 legend('Tentative','Torenbeek','Location','northeast','interpreter','latex',
215 'fontsize',13)
216 %% SIMILARITIES CRITERION LOOP FOLLOWING ROSKAM'S
217 %→ METHOD
218 % Initial error definition
219 error=true;
220 % Assigment of the estimated MTOW
221 MTOW_RK4_similarities=MTOW_estimated;
222 % Counter initialization
223 counter=0;
224 % Data storage matrix initialization
225 data_storage_RK4_similarities=[];
226
227 while error==true % Loop that is executed until convergence is achieved
228
229 counter=counter+1; % Counter addition
230
231 % Drag polar coefficients computation.
232 % It is only performed once, as it only depends on the MTOW
233 [C_D0,k] = Polar_parameters_function(MTOW_RK4_similarities,S,Wing_span);
234
235 % Mass at the beginning of the cruise stage
236 Mass_begin_cruise=fraction1*fraction2*fraction3*fraction4*MTOW_RK4_similarities;
237
238 % Fraction 5 initialization
239 fraction5_prod=1;
240
241 for stage=1:length(h_cruise_vector) % Loop that goes all over the phases of the
242 %→ cruise
243
244 % Cruise height assignation
245 h_cruise=h_cruise_vector(stage);
```

```

245
246 % Runge-Kutta resolution of this phase of the cruise
247 [~,~,fraction5(stage),Efficiency(stage,:)] = RK4_range_function(cj_cruise,
248 M_cruise,C_D0,k,S,h_cruise,Mass_begin_cruise*9.81,R_stage,M);
249
250 % Mass at the end of the current stage =
251 % mass at the beginning of the next stage
252 Mass_begin_cruise=Mass_begin_cruise*fraction5(stage);
253
254 % Fraction 5 productory for phases
255 fraction5_prod=fraction5_prod*fraction5(stage);
256
257 end % End of the cruise loop
258
259 % The mass at the beginning of the loiter is the mass at the end of the
260 % cruise stage (i.e. the last cruise phase)
261 Mass_begin_loiter=Mass_begin_cruise;
262
263 % Runge-Kutta resolution of the loiter
264 [~,~,fraction6] = RK4_autonomy_function(cj_loiter,M_loiter,C_D0,k,S,h_loiter,
265 Mass_begin_loiter*9.81,Autonomy);
266
267 % Mass at the beginning of the reserve stage
268 Mass_begin_reserve=Mass_begin_loiter*fraction6;
269
270 % Runge-Kutta resolution of the reserve stage
271 [~,~,fraction_reserve] = RK4_autonomy_function(cj_loiter,M_loiter,C_D0,k,S,
272 h_reserve,Mass_begin_reserve*9.81,Autonomy);
273
274 % Mission fuel fraction
275 M_ff_RK4=fraction1*fraction2*fraction3*fraction4*fraction5_prod*fraction6*fraction_reserve*fraction7;
276
277 % Total fuel weight computation
278 W_f_RK4 = (1-M_ff_RK4)*MTOW_RK4_similarities;
279
280 % Operating empty weight computation (tentative)

```

## **APPENDIX WEIGHT-COMPUTING MATLAB CODE (RUNGE-KUTTA)**

```
278 OEW_tentative=MTOW_RK4_similarities-W_f_RK4-MPL;
279
280 % Allowable operating empty weight computation (according to similarities
281 % → criterion)
281 OEW_similarities= alpha*MTOW_RK4_similarities;
282
283 % Relative deviation computation
284 OEW_similarities_deviation=abs(OEW_similarities-
284 OEW_tentative)/OEW_similarities;
285
286 % Data storage
287 data_storage_RK4_similarities(1,counter)=OEW_tentative; % Tentative result
288 data_storage_RK4_similarities(2,counter)=OEW_similarities; % Similarities
288 % → result
289
290 error=false;
291
292 % If the convergence criterion is not fulfilled, the error is set back to
293 % true
294 if OEW_similarities_deviation>0.0005
295     error=true;
296
297     % Depending on the value, a different adjustment is made
298     if OEW_similarities>OEW_tentative
299         MTOW_RK4_similarities=MTOW_RK4_similarities+10;
300     else
301         MTOW_RK4_similarities=MTOW_RK4_similarities-10;
302     end
303
304 end % End of the conditional that checks the convergence
305
306 end % End of the convergence loop
307
308 % Graphic plotting
309 fig2=figure(2);
```

```

310 set(fig2,'Renderer','painters','Position',[400 400 500 350]);
311 hold on
312
313 plot([1:size(data_storage_RK4_similarities,2)], data_storage_RK4_similarities(1,
314      :, 'b')
314 hold on
315 plot([1:size(data_storage_RK4_similarities,2)], data_storage_RK4_similarities(2,
316      :, 'r')
316 legend('estimated','similarities')
317
318 % Axis format
319 set(gca,'TickLabelInterpreter','latex','fontsize',13)
320 ylabel('$OEW\\left[\\mathrm{kg}\\right]$', 'interpreter','latex','FontSize',15)
321 xlabel('Number of iterations', 'interpreter','latex','FontSize',15)
322
323 % Grid format
324 grid on
325 ax = gca;
326 ax.GridColor = [0, 0, 0];
327 ax.GridAlpha=0.2;
328 grid minor
329
330 legend('Tentative','Similarities','Location','east','interpreter','latex','fontsize',13)

```

### G.1.1 Range-solving function

This MATLAB function solves Breguet's differential equation for the cruise stage using a 4<sup>th</sup> order Runge-Kutta numerical method.

```

1 % Function to solve the Breguet's differential equation in terms of range
2 % using a 4th order Runge-Kutta numerical method
3
4 % 2020, Aircraft Design
5
6 % Authors:
7 % Cristian Asensio García

```

## APPENDIX WEIGHT-COMPUTING MATLAB CODE (RUNGE-KUTTA)

```
8 % Juan Garrido Moreno
9 % Yi Qiang Ji Zhang
10 % Alexis Leon Delgado
11 % Alba Molina Cuadrado
12 % David Morante Torra
13 % Teresa Peña Mercadé
14 % Ferran Rubio Vallhonrat
15 % Iván Sermanoukian Molina
16 % Santiago Villarroya Calavia
17
18 function [X_sol,W_sol,frac,Efficiency] = RK4_range_function(c_t,M,C_D0,k,S,H,
   W_0,Range,N)
19
20 %% 1. Definition of Constants, Parameters and Variables
21
22 % 1.1. CONSTANTS
23 Ru = 8.31432; % Universal Constant for Ideal Gases [J/mole*K]
24 % Earth
25 g = 9.80665; % Acceleration at Earth's surface [m/s^2]
26 T0 = 288.15; % US Standard Sea Level Temperature [K]
27 P0 = 101325; % Pressure at Sea Level [Pa]
28 Mm = 28.9644*10^-3; % Molecular Mass [kg*mole^-1]
29 H_layer = 1e3*[0 11 20 32 47 52 61 69 79 90 100 110 117.776]; % Earth's
   ↪ atmospheric layers
30 lambda = 1e-3*[-6.5 0 1 2.8 0 -2 -4 -3 0 2 4.36 16.4596 0]; % Earth's
   ↪ atmospheric layers altitude thermal gradient [k/m]
31 gamma = 1.4; % Earth's air specific heats relation [adim]
32 R = Ru/Mm; % Gas constant for Earth's air
33
34 %% 2. PHYSICAL DATA
35
36 % Atmospherical properties
37 [T_h,rho]=ISA_atmosphere(H);
38
39 %% 3. RUNGE-KUTTA RK4
```

```

40
41 % 3.1 Numerical data
42
43 % Declaration of solution vectors
44 X_sol= linspace(0,Range,N);
45 DeltaX=X_sol(2)-X_sol(1);
46 W_sol = zeros(1, length(X_sol));
47 Efficiency = zeros(1, length(X_sol));
48
49 % 3.2 Initial conditions
50 W_sol(1) = W_0;
51
52 % 3.3 Runge-Kutta RK4
53 for i = 1:length(X_sol)-1
54
55     % Functions
56     F1 = @(X, W) -
57         c_t*g/(M*sqrt(gamma*R*T_h))*(0.5*C_D0*rho*(M^2*gamma*R*T_h)*S+k*(2*W^2)/(rho
58     % Computation of coefficients sub 1
59     i1 = F1(X_sol(i), W_sol(i));
60     % Computation of coefficients sub 2
61     i2 = F1(X_sol(i)+ DeltaX/2, W_sol(i)+i1*DeltaX/2);
62     % Computation of coefficients sub 3
63     i3 = F1(X_sol(i)+ DeltaX/2, W_sol(i)+i2*DeltaX/2);
64     % Computation of coefficients sub 4
65     i4 = F1(X_sol(i)+ DeltaX, W_sol(i)+i3*DeltaX);
66     % Compute next step
67     W_sol(i+1) = W_sol(i) + (DeltaX/6)*(i1 + 2*i2 + 2*i3 + i4);
68
69     % Efficiency computation
70     C_L=(2*W_sol(i))/(rho*(M^2*gamma*R*T_h)*S);
71     C_D=C_D0+k*C_L^2;
72     Efficiency(i)=C_L/C_D;
73 end % End of the Runge-Kutta loop

```

## **APPENDIX G WEIGHT-COMPUTING MATLAB CODE (RUNGE-KUTTA)**

```
74 % Fraction between final and initial mass  
75 frac = W_sol(end)/W_0;  
76  
77  
78 end
```

### **G.1.2 Autonomy-solving function**

This MATLAB function solves Breguet's differential equation for the loiter stage using a 4<sup>th</sup> order Runge-Kutta numerical method.

```
1 % Function to solve the Breguet's differential equation in terms of endurance  
2 % using a 4th order Runge-Kutta numerical method  
3  
4 % 2020, Aircraft Design  
5  
6 % Authors:  
7 % Cristian Asensio García  
8 % Juan Garrido Moreno  
9 % Yi Qiang Ji Zhang  
10 % Alexis Leon Delgado  
11 % Alba Molina Cuadrado  
12 % David Morante Torra  
13 % Teresa Peña Mercadé  
14 % Ferran Rubio Vallhonrat  
15 % Iván Sermanoukian Molina  
16 % Santiago Villarroya Calavia  
17  
18 function [T_sol,W_sol,frac] = RK4_autonomy_function(c_t,M,C_D0,k,S,H,W_0,  
Autonomy)  
19  
20 %% 1. Definition of Constants, Parameters and Variables  
21  
22 % 1.1. CONSTANTS  
23 Ru = 8.31432; % Universal Constant for Ideal Gases [J/mole*K]
```

```

24 % Earth
25 g = 9.80665; % Acceleration at Earth's surface [m/s^2]
26 T0 = 288.15; % US Standard Sea Level Temperature [K]
27 P0 = 101325; % Pressure at Sea Level [Pa]
28 Mm = 28.9644*10^-3; % Molecular Mass [kg*mole^-1]
29 H_layer = 1e3*[0 11 20 32 47 52 61 69 79 90 100 110 117.776]; % Earth's
   ↪ atmospheric layers
30 lambda = 1e-3*[-6.5 0 1 2.8 0 -2 -4 -3 0 2 4.36 16.4596 0]; % Earth's
   ↪ atmospheric layers altitude thermal gradient [k/m]
31 gamma = 1.4; % Earth's air specific heats relation [adim]
32 R = Ru/Mm; % Gas constant for Earth's air
33
34 %% 2. PHYSICAL DATA
35
36 % Atmospheric conditions
37 [T_h,rho]=ISA_atmosphere(H);
38
39 %% 3. RUNGE-KUTTA RK4
40
41 % 3.1 Numerical data
42 DeltaT = 10;
43
44 % Declaration of solution vectors
45 T_sol = 0:DeltaT:Autonomy;
46 W_sol = zeros(1, length(T_sol));
47
48 % 3.2 Initial conditions
49 W_sol(1) = W_0;
50 %[C_D0,k] = Polar_parameters_function(W_sol(1)/9.81,S,Wing_span);
51
52 % 3.3 Runge-Kutta RK4
53 for i = 1:length(T_sol)-1
54
   % Functions

```

## APPENDIX G WEIGHT-COMPUTING MATLAB CODE (RUNGE-KUTTA)

```
56 F1 = @(T, W) -  
57 % Computation of coefficients sub 1  
58 i1 = F1(T_sol(i), W_sol(i));  
59 % Computation of coefficients sub 2  
60 i2 = F1(T_sol(i)+ DeltaT/2, W_sol(i)+i1*DeltaT/2);  
61 % Computation of coefficients sub 3  
62 i3 = F1(T_sol(i)+ DeltaT/2, W_sol(i)+i2*DeltaT/2);  
63 % Computation of coefficients sub 4  
64 i4 = F1(T_sol(i)+ DeltaT, W_sol(i)+i3*DeltaT);  
65 % Compute next step  
66 W_sol(i+1) = W_sol(i) + (DeltaT/6)*(i1 + 2*i2 + 2*i3 + i4);  
67  
68 end % End of the Runge-Kutta loop  
69  
70 % Fraction between final and initial mass  
71 frac = W_sol(end)/W_0;  
72  
73 end
```

# Appendix H

## Weight-computing MATLAB code (Euler)

??

### H.1 Main code

The following MATLAB code encompasses the Roskam's iterative loop to compute the design weights of the aircraft. Inside this loop the functions [G.1.1](#) and [G.1.2](#), which implement the Euler numerical resolution, are called. Additionally, functions [F](#) to compute the atmospheric properties and [I](#) to compute the drag coefficient have also been used.

```
1 % Code for obtaining the weight design parameters
2
3 % 2020, Aircraft Design
4
5 % Authors:
6 % Cristian Asensio García
7 % Juan Garrido Moreno
8 % Yi Qiang Ji Zhang
9 % Alexis Leon Delgado
10 % Alba Molina Cuadrado
```

```
11 % David Morante Torra
12 % Teresa Peña Mercadé
13 % Ferran Rubio Vallhonrat
14 % Iván Sermanoukian Molina
15 % Santiago Villarroya Calavia
16
17 % PREAMBLE
18
19 clear
20 clc
21 close all
22 format long
23
24 %% DATA INPUT
25
26 % Fuselage dimensions
27 b_f_expected=2.02;
28 a_f_expected=1.819125;
29 l_f_expected=21.376375;
30
31 % Payload parameters
32 pax = 10 ; % Number of passengers
33 W_pax = 77 ; % Mass of a passenger [kg]
34 W_bagg = 20 ; % Mass of a passenger's baggage [kg]
35 rho_cargo = 160 ; % Cargo density [kg/m^3]
36 rho_bagg = 200 ; % Baggage density [kg/m^3]
37 kbd = 0.85 ; % Hold occupation efficiency
38
39 % Performance data
40 % Expected total range
41 total_range=4500*unitsratio('meter','nauticalmile'); % [m]
42 M_cruise = 0.8; % Cruise Mach number
43 M_loiter = 0.6; % Cruise Mach number
44 R_cruise = 0.8*total_range; % Cruise range [m]
45
```

```

46 % Cruise height vector. All the heights will be tackled equitatively
47 h_cruise_vector=[12000 12500 13000]; % [m]
48 % Length of each phase of the cruise
49 R_stage=R_cruise/length(h_cruise_vector); % [m]
50
51 h_loiter = 10000 ; % Loiter height [m]
52 h_reserve = 450; % Height for the reserve flight, stablished by ICAO [m]
53 cj_cruise = 2*1.8 * 10^(-5); % Cruise specific consumption [kg/N/s]
54 cj_loiter = 2*1.1 * 10^(-5); % Loiter specific consumption [kg/N/s]
55 E_loiter = 20 * 60 ; % Loiter time [s]
56 Autonomy= 30 * 60 ; % Reserved time to reach alternate aerodrome [s]
57 MTOW_estimated = 27000 ; % MTOW estimation [kg]
58 engine_weight=634.225; % Average engine weight [kg]
59
60 % Termo-physical properties
61 R_g = 2.870528738362446e+02 ; % Constant for air
62 lambda = 1.4 ; % Heat relation for air
63 g = 9.81 ; % Gravity acceleration [m/s^2]
64
65 %S = 51.1; % Wing surface [m ^2]
66 S=70;
67 Wing_span=23;
68 %Wing_span=20.9; % Wing span [m]
69
70 % Data regression loading
71 load('k_b_baggage.mat'); % Constant for the baggage volume
72 load('alpha.mat'); % Constant for the similarities criterion
73 load('Delta_W_e_regression.mat'); % Term for the Torenbeek criterion
74
75 % Number of points to numerically study the cruise
76 N=1e6;
77 % Number of points for each phase of the cruise
78 M=round(N/length(h_cruise_vector));
79
80 %% WEIGHT FRACTIONS

```

```

81
82 % Baggage volume
83 V_bagg=k_b_baggage*b_f_expected^2*l_f_expected;
84
85 % Maximum payload calculation
86 MPL = pax * (W_pax+W_bagg) + (kbd*V_bagg -
87 ((W_bagg*pax)/rho_baggage))*rho_cargo ; % Computation fo Payload Weight
88
89 % Fuel fractions determination for each stage
90 fraction1 = 0.990 ; % Mass fuel fraction engine start phase
91 fraction2 = 0.995 ; % Mass fuel fraction taxi phase
92 fraction3 = 0.995 ; % Mass fuel fraction take off phase
93 fraction4 = 0.980 ; % Mass fuel fraction Climb phase
94 fraction7 = 0.990 ; % Mass fuel fraction descend phase
95 fraction8 = 0.992; % Mass fuel fraction shutdown phase
96
97 %% TORENBEEK CRITERION LOOP FOLLOWING ROSKAM'S
98 %→ METHOD (SINGLE HEIGHT ANALYSIS SHA)
99
100 % Delta W_e abscissa calculation
101 x_fuselage = l_f_expected * 0.5 * (a_f_expected+b_f_expected);
102 % Delta_e computation
103 Delta_e = 10^Delta_W_e_regression(2) * x_fuselage^(Delta_W_e_regression(1));
104
105 % Initial error definition
106 error=true;
107 % Assignation of the estimated MTOW
108 MTOW_Euler_torenbeek=MTOW_estimated;
109 % Counter initialization
110 counter=0;
111 % Data storage matrix initialization
112 data_storage_Euler_torenbeek=[];
113 while error==true % Loop that is executed until convergence is achieved

```

```

114
115 counter=counter+1; % Counter addition
116
117 % Drag polar coefficients computation.
118 % It is only performed once, as it only depends on the MTOW
119 [C_D0,k] = Polar_parameters_function(MTOW_Euler_torenbeek,S,Wing_span);
120
121 % Mass at the beginning of the cruise stage
122 Mass_begin_cruise=fraction1*fraction2*fraction3*fraction4*MTOW_Euler_torenbeek;
123
124 % Fraction 5 initialization
125 fraction5_prod=1;
126
127 for stage=1:length(h_cruise_vector) % Loop that goes all over the phases of the
    ↪ cruise
128
129 % Cruise height assignation
130 h_cruise=h_cruise_vector(stage);
131
132 % Euler resolution of this phase of the cruise
133 [~,~,fraction5(stage),Efficiency(stage,:)] = Euler_range_function(cj_cruise,
    M_cruise,C_D0,k,S,h_cruise,Mass_begin_cruise*9.81,R_stage,M);
134
135 % Mass at the end of the current stage =
136 % mass at the beginning of the next stage
137 Mass_begin_cruise=Mass_begin_cruise*fraction5(stage);
138
139 % Fraction 5 productory for phases
140 fraction5_prod=fraction5_prod*fraction5(stage);
141
142 end % End of the cruise loop
143
144 % The mass at the beginning of the loiter is the mass at the end of the
145 % cruise stage (i.e. the last cruise phase)
146 Mass_begin_loiter=Mass_begin_cruise;

```

```

147
148 % Euler resolution of the loiter
149 [~,~,fraction6] = Euler_autonomy_function(cj_loiter,M_loiter,C_D0,k,S,h_loiter,
150 Mass_begin_loiter*9.81,Autonomy);
151
152 % Mass at the beginning of the reserve stage
153 Mass_begin_reserve=Mass_begin_loiter*fraction6;
154
155 % Euler resolution of the reserve stage
156 [~,~,fraction_reserve] = Euler_autonomy_function(cj_loiter,M_loiter,C_D0,k,S,
157 h_reserve,Mass_begin_reserve*9.81,Autonomy);
158
159 % Mission fuel fraction
160 M_ff_Euler=fraction1*fraction2*fraction3*fraction4*fraction5_prod*fraction6*fraction_reserve*fraction7;
161
162 % Total fuel weight computation
163 W_f_Euler = (1-M_ff_Euler)*MTOW_Euler_torenbeek;
164
165 % Operating empty weight computation (tentative)
166 OEW_tentative=MTOW_Euler_torenbeek-W_f_Euler-MPL;
167
168 % Allowable operating empty weight computation (according to Torenbeek
169 % criterion)
170 OEW_torenbeek = 0.2*MTOW_Euler_torenbeek + 2*engine_weight+
171 % Delta_e+500;
172
173 % Relative deviation computation
174 OEW_torenbeek_deviation=abs(OEW_torenbeek-
175 OEW_tentative)/OEW_torenbeek;
176
177 % Data storage
178 data_storage_Euler_torenbeek(1,counter)=OEW_tentative; % Tentative result
179 data_storage_Euler_torenbeek(2,counter)=OEW_torenbeek; % Torenbeek result
180
181 error=false;

```

```

178 % If the convergence criterion is not fulfilled, the error is set back to
179 % true
180 if OEW_torenbeek_deviation>0.0005
181     error=true;
182
183     % Depending on the value, a different adjustment is made
184     if OEW_torenbeek>OEW_tentative
185         MTOW_Euler_torenbeek=MTOW_Euler_torenbeek+10;
186     else
187         MTOW_Euler_torenbeek=MTOW_Euler_torenbeek-10;
188     end
189
190 end % End of the conditional that checks the convergence
191
192 end % End of the loop
193
194 % Graphic plotting
195 fig1=figure(1);
196 set(fig1,'Renderer', 'painters', 'Position', [400 400 500 350]);
197 hold on
198
199 plot([1:1:size(data_storage_Euler_torenbeek,2)], data_storage_Euler_torenbeek(1,
200     :), 'b')
201 plot([1:1:size(data_storage_Euler_torenbeek,2)], data_storage_Euler_torenbeek(2,
202     :), 'r')
203
204 % Axis format
205 set(gca,'TickLabelInterpreter','latex','fontsize',13)
206 ylabel('$OEW\\left[\\mathrm{kg}\\right]$','interpreter','latex','FontSize',15)
207 xlabel('Number of iterations','interpreter','latex','FontSize',15)
208
209 % Grid format
210 grid on
211 ax = gca;
212 ax.GridColor = [0, 0, 0];

```

## Aircraft Design APPENDIX H. WEIGHT-COMPUTING MATLAB CODE (EULER)

```
212 ax.GridAlpha=0.2;
213 grid minor
214
215 legend('Tentative','Torenbeek','Location','northeast','interpreter','latex',
216      'fontsize',13)
217 %% SIMILARITIES CRITERION LOOP FOLLOWING ROSKAM'S
218 %<-- METHOD
219 % Initial error definition
220 error=true;
221 % Assigment of the estimated MTOW
222 MTOW_Euler_similarities=MTOW_estimated;
223 % Counter initialization
224 counter=0;
225 % Data storage matrix initialization
226 data_storage_Euler_similarities=[];
227
228 while error==true % Loop that is executed until convergence is achieved
229
230 counter=counter+1; % Counter addition
231
232 % Drag polar coefficients computation.
233 % It is only performed once, as it only depends on the MTOW
234 [C_D0,k] = Polar_parameters_function(MTOW_Euler_similarities,S,Wing_span);
235
236 % Mass at the beginning of the cruise stage
237 Mass_begin_cruise=fraction1*fraction2*fraction3*fraction4*MTOW_Euler_similarities;
238
239 % Fraction 5 initialization
240 fraction5_prod=1;
241
242 for stage=1:length(h_cruise_vector) % Loop that goes all over the phases of the
243      %<-- cruise
```

```

244 % Cruise height assignation
245 h_cruise=h_cruise_vector(stage);
246
247 % Euler resolution of this phase of the cruise
248 [~,~,fraction5(stage),Efficiency(stage,:)] = Euler_range_function(cj_cruise,
    M_cruise,C_D0,k,S,h_cruise,Mass_begin_cruise*9.81,R_stage,M);
249
250 % Mass at the end of the current stage =
251 % mass at the beginning of the next stage
252 Mass_begin_cruise=Mass_begin_cruise*fraction5(stage);
253
254 % Fraction 5 productory for phases
255 fraction5_prod=fraction5_prod*fraction5(stage);
256
257 end % End of the cruise loop
258
259 % The mass at the beginning of the loiter is the mass at the end of the
260 % cruise stage (i.e. the last cruise phase)
261 Mass_begin_loiter=Mass_begin_cruise;
262
263 % Euler resolution of the loiter
264 [~,~,fraction6] = Euler_autonomy_function(cj_loiter,M_loiter,C_D0,k,S,h_loiter,
    Mass_begin_loiter*9.81,Autonomy);
265
266 % Mass at the beginning of the reserve stage
267 Mass_begin_reserve=Mass_begin_loiter*fraction6;
268
269 % Euler resolution of the reserve stage
270 [~,~,fraction_reserve] = Euler_autonomy_function(cj_loiter,M_loiter,C_D0,k,S,
    h_reserve,Mass_begin_reserve*9.81,Autonomy);
271
272 % Mission fuel fraction
273 M_ff_Euler=fraction1*fraction2*fraction3*fraction4*fraction5_prod*fraction6*fraction_reserve*fraction_
274
275 % Total fuel weight computation
276 W_f_Euler = (1-M_ff_Euler)*MTOW_Euler_similarities;

```

```

277
278 % Operating empty weight computation (tentative)
279 OEW_tentative=MTOW_Euler_similarities-W_f_Euler-MPL;
280
281 % Allowable operating empty weight computation (according to similarities
282 % → criterion)
283 OEW_similarities=alpha*MTOW_Euler_similarities;
284
285 % Relative deviation computation
286 OEW_similarities_deviation=abs(OEW_similarities-
287 OEW_tentative)/OEW_similarities;
288
289 % Data storage
290 data_storage_Euler_similarities(1,counter)=OEW_tentative; % Tentative result
291 data_storage_Euler_similarities(2,counter)=OEW_similarities; % Similarities
292 % → result
293
294 error=false;
295
296 % If the convergence criterion is not fulfilled, the error is set back to
297 % true
298 if OEW_similarities_deviation>0.0005
299     error=true;
300
301     % Depending on the value, a different adjustment is made
302     if OEW_similarities>OEW_tentative
303         MTOW_Euler_similarities=MTOW_Euler_similarities+10;
304     else
305         MTOW_Euler_similarities=MTOW_Euler_similarities-10;
306     end
307
308 end % End of the conditional that checks the convergence
309
310 end % End of the loop

```

```

309 % Graphic plotting
310 fig2=figure(2);
311 set(fig2,'Renderer', 'painters', 'Position', [400 400 500 350]);
312 hold on
313
314 plot([1:1:size(data_storage_Euler_similarities,2)],
    ↪ data_storage_Euler_similarities(1,:),'b')
315 hold on
316 plot([1:1:size(data_storage_Euler_similarities,2)],
    ↪ data_storage_Euler_similarities(2,:),'r')
317
318 % Axis format
319 set(gca,'TickLabelInterpreter','latex','fontsize',13)
320 ylabel('$OEW\\left[\\mathrm{kg}\\right]$', 'interpreter','latex','FontSize',15)
321 xlabel('Number of iterations', 'interpreter','latex','FontSize',15)
322
323 % Grid format
324 grid on
325 ax = gca;
326 ax.GridColor = [0, 0, 0];
327 ax.GridAlpha=0.2;
328 grid minor
329
330 legend('Tentative','Similarities','Location','southeast','interpreter','latex',
    'fontsize',13)

```

### H.1.1 Range-solving function

This MATLAB function solves Breguet's differential equation for the cruise stage using a 1<sup>st</sup> order Euler numerical method.

```

1 % Function to solve the Breguet's differential equation in terms of range
2 % using a 4th order Runge-Kutta numerical method
3
4 % 2020, Aircraft Design

```

```

5 % Authors:
6 % Cristian Asensio García
7 % Juan Garrido Moreno
8 % Yi Qiang Ji Zhang
9 % Alexis Leon Delgado
10 % Alba Molina Cuadrado
11 % David Morante Torra
12 % Teresa Peña Mercadé
13 % Ferran Rubio Vallhonrat
14 % Iván Sermanoukian Molina
15 % Santiago Villarroya Calavia
16
17
18 function [X_sol,W_sol,frac,Efficiency] = RK4_range_function(c_t,M,C_D0,k,S,H,
   W_0,Range,N)
19
20 %% 1. Definition of Constants, Parameters and Variables
21
22 % 1.1. CONSTANTS
23 Ru = 8.31432; % Universal Constant for Ideal Gases [J/mole*K]
24 % Earth
25 g = 9.80665; % Acceleration at Earth's surface [m/s^2]
26 T0 = 288.15; % US Standard Sea Level Temperature [K]
27 P0 = 101325; % Pressure at Sea Level [Pa]
28 Mm = 28.9644*10^-3; % Molecular Mass [kg*mole^-1]
29 H_layer = 1e3*[0 11 20 32 47 52 61 69 79 90 100 110 117.776]; % Earth's
   ↪ atmospheric layers
30 lambda = 1e-3*[-6.5 0 1 2.8 0 -2 -4 -3 0 2 4.36 16.4596 0]; % Earth's
   ↪ atmospheric layers altitude thermal gradient [k/m]
31 gamma = 1.4; % Earth's air specific heats relation [adim]
32 R = Ru/Mm; % Gas constant for Earth's air
33
34 %% 2. PHYSICAL DATA
35
36 % Atmospherical properties

```

```

37 [T_h,rho]=ISA_atmosphere(H);
38
39 %% 3. RUNGE-KUTTA RK4
40
41 % 3.1 Numerical data
42
43 % Declaration of solution vectors
44 X_sol= linspace(0,Range,N);
45 DeltaX=X_sol(2)-X_sol(1);
46 W_sol = zeros(1, length(X_sol));
47 Efficiency = zeros(1, length(X_sol));
48
49 % 3.2 Initial conditions
50 W_sol(1) = W_0;
51
52 % 3.3 Runge-Kutta RK4
53 for i = 1:length(X_sol)-1
54
55     % Functions
56     F1 = @(X, W) -
57         c_t*g/(M*sqrt(gamma*R*T_h))*(0.5*C_D0*rho*(M^2*gamma*R*T_h)*S+k*(2*W^2)/(rho*S));
58     % Computation of coefficients sub 1
59     i1 = F1(X_sol(i), W_sol(i));
60     % Computation of coefficients sub 2
61     i2 = F1(X_sol(i)+ DeltaX/2, W_sol(i)+i1*DeltaX/2);
62     % Computation of coefficients sub 3
63     i3 = F1(X_sol(i)+ DeltaX/2, W_sol(i)+i2*DeltaX/2);
64     % Computation of coefficients sub 4
65     i4 = F1(X_sol(i)+ DeltaX, W_sol(i)+i3*DeltaX);
66     % Compute next step
67     W_sol(i+1) = W_sol(i) + (DeltaX/6)*(i1 + 2*i2 + 2*i3 + i4);
68
69     % Efficiency computation
70     C_L=(2*W_sol(i))/(rho*(M^2*gamma*R*T_h)*S);
    C_D=C_D0+k*C_L^2;

```

```

71 Efficiency(i)=C_L/C_D;
72
73 end % End of the Runge-Kutta loop
74
75 % Fraction between final and initial mass
76 frac = W_sol(end)/W_0;
77
78 end

```

### H.1.2 Autonomy-solving function

This MATLAB function solves Breguet's differential equation for the loiter stage using a 1<sup>st</sup> order Euler numerical method.

```

1 % Function to solve the Breguet's differential equation in terms of endurance
2 % using a 4th order Runge-Kutta numerical method
3
4 % 2020, Aircraft Design
5
6 % Authors:
7 % Cristian Asensio García
8 % Juan Garrido Moreno
9 % Yi Qiang Ji Zhang
10 % Alexis Leon Delgado
11 % Alba Molina Cuadrado
12 % David Morante Torra
13 % Teresa Peña Mercadé
14 % Ferran Rubio Vallhonrat
15 % Iván Sermanoukian Molina
16 % Santiago Villarroya Calavia
17
18 function [T_sol,W_sol,frac] = RK4_autonomy_function(c_t,M,C_D0,k,S,H,W_0,
19 %Autonomy)
20 %% 1. Definition of Constants, Parameters and Variables

```

```

21
22 % 1.1. CONSTANTS
23 Ru = 8.31432; % Universal Constant for Ideal Gases [J/mole*K]
24 % Earth
25 g = 9.80665; % Acceleration at Earth's surface [m/s^2]
26 T0 = 288.15; % US Standard Sea Level Temperature [K]
27 P0 = 101325; % Pressure at Sea Level [Pa]
28 Mm = 28.9644*10^-3; % Molecular Mass [kg*mole^-1]
29 H_layer = 1e3*[0 11 20 32 47 52 61 69 79 90 100 110 117.776]; % Earth's
   ↪ atmospheric layers
30 lambda = 1e-3*[-6.5 0 1 2.8 0 -2 -4 -3 0 2 4.36 16.4596 0]; % Earth's
   ↪ atmospheric layers altitude thermal gradient [k/m]
31 gamma = 1.4; % Earth's air specific heats relation [adim]
32 R = Ru/Mm; % Gas constant for Earth's air
33
34 %% 2. PHYSICAL DATA
35
36 % Atmospheric conditions
37 [T_h,rho]=ISA_atmosphere(H);
38
39 %% 3. RUNGE-KUTTA RK4
40
41 % 3.1 Numerical data
42 DeltaT = 10;
43
44 % Declaration of solution vectors
45 T_sol = 0:DeltaT:Autonomy;
46 W_sol = zeros(1, length(T_sol));
47
48 % 3.2 Initial conditions
49 W_sol(1) = W_0;
50 %[C_D0,k] = Polar_parameters_function(W_sol(1)/9.81,S,Wing_span);
51
52 % 3.3 Runge-Kutta RK4
53 for i = 1:length(T_sol)-1

```

## Aircraft Design APPENDIX H. WEIGHT-COMPUTING MATLAB CODE (EULER)

```
54 % Functions
55 F1 = @(T, W) -
56     c_t*(0.5*C_D0*rho*(M^2*gamma*R*T_h)*S+k*(2*W^2)/(rho*(M^2*gamma*R*T_h)*S))
57 % Computation of coefficients sub 1
58 i1 = F1(T_sol(i), W_sol(i));
59 % Computation of coefficients sub 2
60 i2 = F1(T_sol(i)+ DeltaT/2, W_sol(i)+i1*DeltaT/2);
61 % Computation of coefficients sub 3
62 i3 = F1(T_sol(i)+ DeltaT/2, W_sol(i)+i2*DeltaT/2);
63 % Computation of coefficients sub 4
64 i4 = F1(T_sol(i)+ DeltaT, W_sol(i)+i3*DeltaT);
65 % Compute next step
66 W_sol(i+1) = W_sol(i) + (DeltaT/6)*(i1 + 2*i2 + 2*i3 + i4);
67
68 end % End of the Runge-Kutta loop
69
70 % Fraction between final and initial mass
71 frac = W_sol(end)/W_0;
72
73 end
```

# Appendix I

## Parabolic polar

The following process for the drag polar determination is exclusively based on the methodology proposed by Roskam [8]. Assuming a parabolic drag polar, the drag coefficient of the airplane can be written as [8].:

$$C_D = C_{D0} + C_{Di}$$

where the parasite (or zero-lift) drag coefficient,  $C_{D0}$  can be expressed as:

$$C_{D0} = \frac{f}{S}$$

where  $f$  is equivalent to the parasite area and  $S$  is the wing area. The parasite area  $f$  is related to the wetted area  $S_{wet}$  through the following empirical equation:

$$\log_{10} f = a + b (\log_{10} S_{wet}) \quad (\text{I.1})$$

The correlation coefficients  $a$  and  $b$  are function of the equivalent skin friction coefficient of an airplane,  $c_f$ . This latter  $c_f$  is determined by the smoothness and streamlining designed into the airplane.

From analyzing Figure 3.21 in [8], it can be extracted a reasonable value of  $c_f = 0.003$  for the friction coefficient of business jets. In our case, the business jet we are developing have bigger dimensions than Roskam's business jet dimensions. Hence, the proper values are considering twin-engine propeller driven airplane. In this case, Table 3.4 in [8] gives the correlation coefficients for the parasite area

are:

$$a = -2.5229 \quad b = 1.0000 \quad (\text{I.2})$$

Additionally,  $S_{wet}$  correlates with  $W_{TO}$  for a wide range of airplanes.

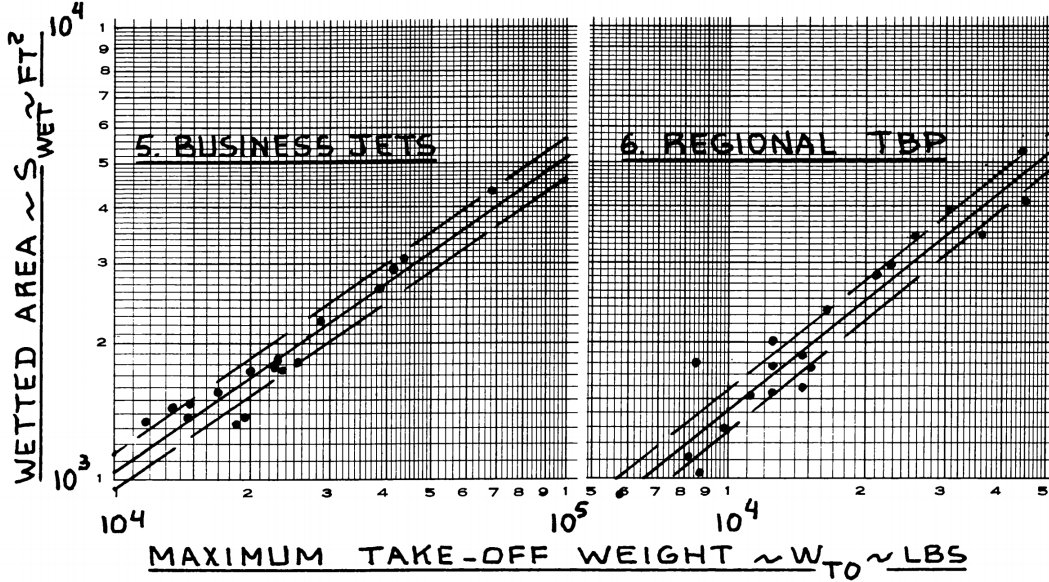


FIGURE I.1: Correlation between  $S_{wet}$  and Maximum Take-off Weight  $W_{TO}$

The scatter in Figure I.1 is mainly due to differences in wind loading, cabin sizes and nacelle design. Hence, it is possible to obtain an initial wetted area without knowing what the airplane actually looks like. This correlation can be translated into:

$$\log_{10} S_{wet} = c + d \log_{10} W_{TO} \quad (\text{I.3})$$

The constants  $c$  and  $d$  are regression line coefficients. In fact, values for  $c$  and  $d$  were obtained by correlating wetted area and take-off weight data. Next, regression line coefficients for Take-off weight are correlated with the wetted area as well, according to [8], for business jets:

$$c_1 = 0.8635 \quad d = 0.5632; \quad (\text{I.4})$$

Thus, the final equation may be obtained by combining (I.1) and (I.3):

$$\log_{10} f = a + b(c_1 + d \log_{10} W_{TO}) \quad (\text{I.5})$$

Rearranging the expressions above and particularizing to our problem:

$$\log_{10} f = -2.5229 + 1.0000 (0.8635 + 0.5632 \log_{10} W_{TO}) \quad (\text{I.6})$$

Since  $W_{TO}$  was already obtained, drag polar can now be determined. Note that Equation (I.6) weight must be in Imperial Units and so does the surface  $S_w$  in  $C_{Di}$ .

The  $C_{D0}$  obtained corresponds to clean configuration. For take-off and landing, it is need to take into consideration the effects of flaps and landing gear. The additional zero-lift coefficient is highly dependant with the size of the latter two gears ( $\Delta C_{D0}$  and  $e$  are mean values):

Configuration	$\Delta C_{D0}$	$e$	$C_{D0}$
Clean	0	0.85	0.020
Take-off flaps	0.015	0.77	0.035
Landing flaps	0.065	0.72	0.085
Landing gear	0.020	no effect	0.040

TABLE I.1:  $C_{D0}$  for different aircraft configurations.

Finally, with all these values it is possible to extract the parasite drag contribution  $C_{D0}$  as shown in the table I.1. Once parasite drag is calculated, the next contribution comes from the induced drag  $C_{Di}$ .

$$C_{Di} = \frac{C_L^2}{\pi A e}$$

Firstly, the Oswald's efficiency factor  $e$  can be identified. Recalling expression (2.2) for the induced drag, it can be seen that  $e$  is influenced by the taper ratio: more exactly,  $e$  lessens with increasing  $\delta$ , which can in turn be reduced through setting higher taper ratios. Secondly,  $A$  is the aspect ratio, already defined in section 2.2.3, and whose value can be found in Table I.1.

By means of the aircraft's parabolic polar approximation, it is now possible to estimate the design point taking into account that it shall comply with the limitations on take-off, second segment climb, cruise conditions and landing. Additionally, it must also meet the requirements for future versions of the aircraft requiring of greater capacity.

Finally, the following drag polars can be obtained:

Configuration	$\Delta C_D$
Clean	$C_D = 0.020 + 0.0438C_L^2$
Take-off flaps	$C_D = 0.035 + 0.0448C_L^2$
Landing flaps	$C_D = 0.085 + 0.0517C_L^2$
Landing gear	$C_D = 0.040 + 0.0438C_L^2$

TABLE I.2: Drag polars for different aircraft configurations.

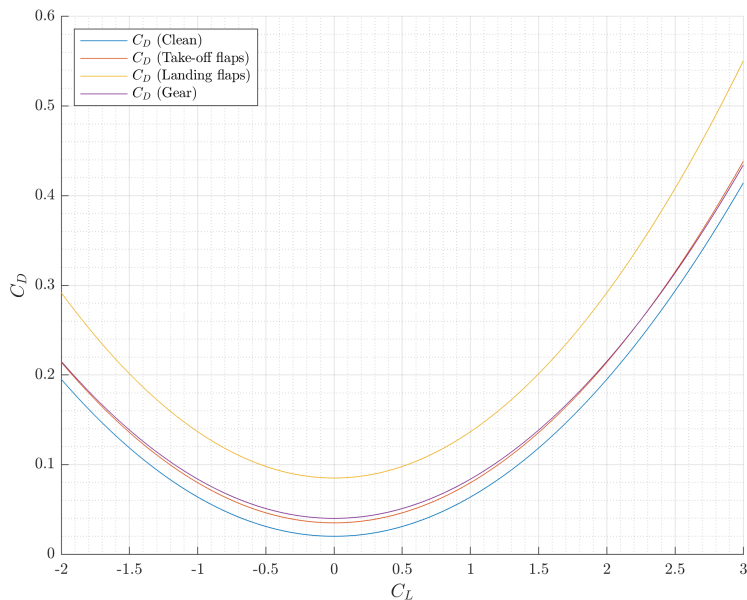


FIGURE I.2: Drag polar for different aircraft configurations.

### I.0.1 Parabolic Polar graph's representation

The following code encompasses the parabolic polar equations regarding different aircraft configurations as shown in Table I.2.

```

1
2 clc;
3 clear all;
4 close all;
5
6 C_L = [-2:0.01:3];

```

```

7 C_D_clean = 0.020+0.0438*C_L.^2;
8 C_D_to_flaps = 0.035+0.0448*C_L.^2;
9 C_D_l_flaps = 0.085+0.0517*C_L.^2;
10 C_D_l_gear = 0.040+0.0438*C_L.^2;
11
12
13 fig1=figure(1);
14 set(fig1,'Renderer', 'painters', 'Position', [400 400 500 350]);
15 hold on
16
17 grid on;
18 grid minor;
19 ax.GridColor = [0, 0, 0];
20 ax.GridAlpha=0.2;
21 plot(C_L,C_D_clean,'DisplayName','$C_D$ (Clean)');
22 plot(C_L,C_D_to_flaps,'DisplayName','$C_D$ (Take-off flaps)');
23 plot(C_L,C_D_l_flaps,'DisplayName','$C_D$ (Landing flaps)');
24 plot(C_L,C_D_l_gear,'DisplayName','$C_D$ (Gear)');
25 hold off;
26
27 % Axis format
28 set(gca,'TickLabelInterpreter','latex','fontsize',12)
29 xlabel('Lift coefficient $C_L$', 'interpreter','latex','FontSize',14)
30 ylabel('Drag coefficient $C_D$', 'interpreter','latex','FontSize',14)
31 legend('location','northwest','interpreter','latex');
32
33 print(gcf,'drag-polar.png','-dpng','-r800');

```



# Appendix J

## Parabolic polar MATLAB code

The following code encompasses the parabolic polar equations regarding different aircraft configurations as shown in Table I.2.

```
1 clc;
2 clear all;
3 close all;
4
5 C_L = [-2:0.01:3];
6
7 C_D_clean = 0.020+0.0438*C_L.^2;
8 C_D_to_flaps = 0.035+0.0448*C_L.^2;
9 C_D_l_flaps = 0.085+0.0517*C_L.^2;
10 C_D_l_gear = 0.040+0.0438*C_L.^2;
11
12 fig1=figure(1);
13 set(fig1,'Renderer', 'painters', 'Position', [400 400 500 350]);
14 hold on
15
16 grid on;
17 grid minor;
18 ax.GridColor = [0, 0, 0];
19 ax.GridAlpha=0.2;
```

```
21 plot(C_L,C_D_clean,'DisplayName','\$C_D\$ (Clean)');
22 plot(C_L,C_D_to_flaps,'DisplayName','\$C_D\$ (Take-off flaps)');
23 plot(C_L,C_D_l_flaps,'DisplayName','\$C_D\$ (Landing flaps)');
24 plot(C_L,C_D_l_gear,'DisplayName','\$C_D\$ (Gear)');
25 hold off;
26
27 % Axis format
28 set(gca,'TickLabelInterpreter','latex','fontsize',12)
29 xlabel('Lift coefficient \$C_L$', 'interpreter','latex','FontSize',14)
30 ylabel('Drag coefficient \$C_D$', 'interpreter','latex','FontSize',14)
31 legend('location','northwest','interpreter','latex');
32
33 print(gcf,'drag_polar.png','-dpng','-r800');
```

# Appendix K

## Design point MATLAB code

The following code computes and graphs the Design Point, including the 1st and 2nd iteration. The sizing data provided are: wing surface and thrust at take-off. It must be mentioned that this code needs the Parabolic Drag function included in Appendix I.

```
1 % Code for computing and graphing the Design Point (1st and 2nd iteration)
2 % The solutions provided are: required wing surface and needed thrust at take-
off
3
4 % 2020, Aircraft Design
5
6 % Authors:
7 % Cristian Asensio García
8 % Juan Garrido Moreno
9 % Yi Qiang Ji Zhang
10 % Alexis Leon Delgado
11 % Alba Molina Cuadrado
12 % David Morante Torra
13 % Teresa Peña Mercadé
14 % Ferran Rubio Vallhonrat
15 % Iván Sermanoukian Molina
16 % Santiago Villarroya Calavia
17
18 % PREAMBLE
```

```

19 clc
20 close all
21 clear all
22
23 % DATA INPUT
24 % S = 51.1; % Wing surface (1st iteration) [m^2]
25 S = 70.2; % Wing surface (2nd iteration) [m^2]
26
27 % Wing_span=20.9; % Wing span (1st iteration) [m]
28 Wing_span=23; % Wing span (2nd iteration) [m]
29
30 % MTOW=28643; % MTOW (1st iteration) [kg]
31 MTOW=26720; % MTOW (2nd iteration) [kg] computed by Multiple Height
   ↪ Methodology with Runge-Kuta
32
33 xlimsup=4500; % Upper limit of the x-axis
34 W_S_ratio=linspace(0,xlimsup,1000); % Wing loading vector
35
36 % 1. TAKE-OFF LIMITATION
37 T_W_ratio_to=8.37E-5*W_S_ratio;
38 figure
39 plot(W_S_ratio,T_W_ratio_to,'b','DisplayName','Take-off');
40 hold on
41
42 % 2. SECOND SEGMENT LIMITATION
43 Ne=2; % Number of engines
44 T_ratio=1;
45 W2_W_to_ratio=0.98;
46 DeltaCD_0=0.015;
47 % A = 8.57; % Aspect ratio (1st iteration)
48 A = 7.5; % Aspect ratio (2nd iteration)
49 phi = 0.85;
50 k=1/(pi*A*phi);
51 [CD_0_sec,k_sec] = Polar_parameters_function(MTOW,S,Wing_span);
52 CGR=0.024; % Climb gradient rate

```

```

53 CL_max_to=1.9;
54 CD=CD_0_sec+DeltaCD_0+k*CL_max_to^2;
55 T_W_ratio_second=Ne/(Ne-1)*T_ratio*W2_W_to_ratio*(CD/CL_max_to+CGR);
56 yline(T_W_ratio_second,'m','DisplayName','Second segment');
57 hold on
58
59 % 3. CRUISE LIMITATION
60 lambda = 4.3;
61 h = 12;
62 Tcr_Tto = (0.0013*lambda-0.0397)*h-0.0248*lambda+0.7125;
63 Tto_Tcr = Tcr_Tto^-1;
64 rho = 0.3108;
65 V_cr = 236.06;
66 Wcr_Wto = 0.9605; % Weight in cruise vs take-off ratio
67 W_cr=MTOW*Wcr_Wto;
68 [Cd0_cr,k_cr] = Polar_parameters_function(MTOW,S,Wing_span);
69 T_W_ratio_cruise =Tto_Tcr/2*rho*V_cr^2./W_S_ratio.*((Cd0_cr+
    ↳ (W_S_ratio*Wcr_Wto).^2/((0.5*rho*V_cr^2)^2*pi*A*phi));
70 plot(W_S_ratio,T_W_ratio_cruise,'g','DisplayName','Cruise');
71 hold on
72
73 % 4. LANDING LIMITATION
74 % s_l=1750; % Landing distance (1st iteration)
75 s_l=1670; % Landing distance (2nd iteration)
76 rho=1.225;
77 % CL_max_l=2.9; % (1st iteration)
78 CL_max_l=2.83; % (2nd iteration)
79 v_A=sqrt(s_l*3.2808/0.6/0.3)*0.51444; %[m/s]
80 v_sl=v_A/1.3;
81 Wl_S_ratio=v_sl^2*rho*CL_max_l/2;
82 Wto_Wl_ratio=0.456;
83 Wto_S_ratio=Wl_S_ratio*Wto_Wl_ratio;
84 xline(Wto_S_ratio,'r','DisplayName','Landing');
85 legend('location','northwest','interpreter','latex');
86

```

```

87 % 5. DESIGN POINT SELECTION
88 % Wto_S_ratio_design=4000; % (1st iteration)
89 Wto_S_ratio_design=3735; % (2nd iteration)
90 S_w=MTOW*9.81/Wto_S_ratio_design % Required wing surface [m^2]
91 % Tto_Wto_design=0.436; % (1st iteration)
92 Tto_Wto_design=0.4675; % (2nd iteration)
93 Tto=Tto_Wto_design*MTOW*9.81 % Required total thrust [N]
94
95 hold on
96 plot(Wto_S_ratio_design,Tto_Wto_design,'o','MarkerFaceColor','y',
      'DisplayName','Design point');
97
98 % Axis format
99 set(gca,'TickLabelInterpreter','latex','fontsize',10)
100 xlabel('$W_{to}/S_w$;\left[\mathrm{N}/\mathrm{m}^2\right]$','interpreter',
      'latex','FontSize',12)
101 ylabel('$T_{to}/W_{to}$','interpreter','latex','FontSize',12)
102 xlim([0 xlimsup])
103 ylim([0 1])
104
105 % Grid format
106 grid on
107 grid minor
108 ax = gca;
109 ax.GridColor = [0, 0, 0];
110 ax.GridAlpha=0.2;

```

# Appendix L

## Weight to Range Diagrams MATLAB code

### L.1 Main code

The following code is developed to analyse and study the Weight effect on the final range 5.2.

```
1 % Code for obtaining the weight design parameters
2
3 % 2020, Aircraft Design
4
5 % Authors:
6 % Cristian Asensio García
7 % Juan Garrido Moreno
8 % Yi Qiang Ji Zhang
9 % Alexis Leon Delgado
10 % Alba Molina Cuadrado
11 % David Morante Torra
12 % Teresa Peña Mercadé
13 % Ferran Rubio Vallhonrat
14 % Iván Sermanoukian Molina
15 % Santiago Villarroya Calavia
16
```

```

17 % PREAMBLE
18
19 clear
20 clc
21 close all
22 format long
23
24 %% DATA INPUT
25
26 % Fuselage dimensions
27 b_f_expected=2.02;
28 a_f_expected=1.819125;
29 l_f_expected=21.376375;
30
31 % Payload parameters
32 W_pax = 77 ; % Mass of a passenger [kg]
33 W_bagg = 20 ; % Mass of a passenger's baggage [kg]
34 rho_cargo = 160 ; % Cargo density [kg/m^3]
35 rho_bagg = 200 ; % Baggage density [kg/m^3]
36 kbd = 0.85 ; % Hold occupation efficiency
37
38 % Performance data
39 % Expected total range
40
41 M_cruise = 0.8; % Cruise Mach number
42 Efficiency = 15 ; % Aerodynamic efficiency during the cruise
43 h_cruise = 12000 ; % Cruise height [m]
44 cj_cruise = 2*1.8 * 10^(-5); % Cruise specific consumption [kg/N/s]
45 cj_loiter = 2*1.1 * 10^(-5); % Loiter specific consumption [kg/N/s]
46 E_loiter = 30 * 60 ; % Loiter time [s]
47 %E_reserve= 30 * 60 ; % Reserved time to reach alternate aerodrome [s]
48 MTOW_estimated = 30000 ; % MTOW estimation [kg]
49 engine_weight=634.225; % Average engine weight [kg]
50
51 % Termo-physical properties computation

```

```

52 [T_cruise,rho_cruise]=ISA_atmosphere(h_cruise);
53 R_g = 2.870528738362446e+02 ; % Constant for air
54 lambda = 1.4 ; % Heat relation for air
55 g = 9.81 ; % Gravity acceleration [m/s^2]
56
57 % Data regression loading
58 load('k_b_baggage.mat'); % Constant for the baggage volume
59 load('alpha.mat'); % Constant for the similarities criterion
60 load('Delta_W_e_regression.mat'); % Term for the Torenbeek criterion
61
62 %% WEIGHT FRACTIONS
63
64 N=100;
65 M=500;
66 TOW=zeros(N,1);
67 OEW=zeros(N,1);
68 PL=zeros(N,1);
69 W_f_reserve_analytical_vec=zeros(N,1);
70 %MTOW_SHA_torenbeek=32626;
71 Range_vec=linspace(4500,5500,N);
72 total_range=Range_vec*unitsratio('meter','nauticalmile'); % [m]
73 R_cruise = 0.8*total_range; % Cruise range [m]
74 PL_fullfuel=convmass(1700,'lbm','kg');
75
76
77 % pax=linspace(10,0,M);
78 pax=10;
79 % Baggage volume
80 V_bagg=k_b_baggage*b.f_expected^2*l.f_expected;
81 % Maximum payload calculation
82 MPL = pax * (W_pax+W_bagg) + (kbd*V_bagg -
     ((W_bagg*pax)/rho_bagg))*rho_cargo ; % Computation fo Payload Weight
83 PL_vec=linspace(MPL,0,M);
84
85 E_reserve=linspace(30,5,M)*60; %[s]

```

Aircraft ~~APPENDIX L.~~ WEIGHT TO RANGE DIAGRAMS MATLAB CODE

```

86
87 converge_final=true;
88 for r=1:N
89     if converge_final==false
90         break;
91     else
92         R_cruise_2=R_cruise(r);
93         for i=1:M
94             %converge_anterior=converge;
95             PL_2=PL_vec(i);
96             E_reserve_2=E_reserve(i);
97             [OEW_torenbeek,MTOW_SHA_torenbeek,W_f_analytical,W_f_trip,
98              W_f_reserve_analytical]=
99                 ↪ Weight_calculation_ANALYTICAL_roskam(PL_2,R_cruise_2,
100                E_reserve_2,b_f_expected,a_f_expected,l_f_expected,M_cruise,
101                Efficiency,cj_cruise,cj_loiter,E_loiter,MTOW_estimated,
102                engine_weight,T_cruise,R_g,lambda,g,Delta_W_e_regression);
103             %if (i<=M && converge==false)
104             if r==1
105                 OEW_bueno=OEW_torenbeek;
106                 OEW(r)=OEW_bueno;
107                 MTOW_MPL=MTOW_SHA_torenbeek;
108                 TOW(r)=MTOW_MPL;
109                 PL(r)=PL_2;
110                 W_f_reserve_analytical_vec(r)=W_f_reserve_analytical;
111                 break;
112             elseif ( (abs(MTOW_SHA_torenbeek-
113                 MTOW_MPL)/MTOW_MPL)<0.0005 &&
114                 ↪ (abs(OEW_torenbeek-OEW_bueno)/OEW_bueno)<0.0005
115                 && PL_2>=PL_fullfuel) % MTOW condition and
116                 ↪ maximum fuel weight payload condition
117                 TOW(r)=MTOW_SHA_torenbeek;
118                 OEW(r)=OEW_torenbeek;
119                 W_f_reserve_analytical_vec(r)=W_f_reserve_analytical;
120                 E_reserve_fullfuel=E_reserve_2;
121                 PL(r)=PL_2;
122                 converge=true;

```

```

114     r_MTOW=r;
115     i_Rmax=i;
116     R_MTOW=Range_vec(r);
117     W_f_analytical_max=W_f_analytical;
118     W_f_reserve_fullfuel=W_f_reserve_analytical;
119     break;
120   else
121     errorMTOW=abs(MTOW_SHA_torenbeek-
122                   MTOW_MPL)/MTOW_MPL;
123     errorOEW=abs(OEW_torenbeek-OEW_bueno)/OEW_bueno;
124     converge=false;
125
126   end
127   if (i==M && converge==false)
128     converge_final=false;
129     break;
130   end
131 end
132
133 end
134
135 TOW_final=OEW_bueno+W_f_analytical_max;
136 M_ff_analytical_final=1-W_f_analytical_max/TOW_final ;
137
138 fraction1 = 0.990 ; % Mass fuel fraction engine start phase
139 fraction2 = 0.995 ; % Mass fuel fraction taxi phase
140 fraction3 = 0.995 ; % Mass fuel fraction take off phase
141 fraction4 = 0.980 ; % Mass fuel fraction Climb phase
142 fraction6_analytical = exp(-E_loiter/(Efficiency/(g*cj_loiter))); % Mass fuel
143   ↪ fraction loiter phase analytical computation
144 fraction_reserve=exp(-E_reserve_fullfuel/(Efficiency/(g*cj_loiter))); % Mass fuel
145   ↪ fraction for reaching alternate aerodrome
146 fraction7 = 0.990 ; % Mass fuel fraction descend phase
147 fraction8 = 0.992; % Mass fuel fraction shutdown phase

```

## Aircraft ~~PERFORMANCE~~ APPENDIX L. WEIGHT TO RANGE DIAGRAMS MATLAB CODE

```
146
147 fraction5_analytical_final=M_ff_analytical_final/(fraction1*fraction2*fraction3*fraction4*fraction6*a);
148
149 ktf = Efficiency * M_cruise*sqrt(lambda*T_cruise*R_g)/(g*cj_cruise);
150
151 R_cruise_final=-log(fraction5_analytical_final)*ktf;
152 R_max=(R_cruise_final/0.8)*unitsratio('nauticalmile','meter');
153
154
155 Range_vec_1=[0 4500];
156 TOW_vec_1=[OEW_bueno+MPL+W_f_reserve_analytical_vec(1) MTOW_MPL];
157
158 Range_vec_2=[R_MTOW R_max];
159 TOW_vec_2=[TOW(r_MTOW) TOW_final];
160
161 PL_vec_1=[MPL MPL];
162 PL_vec_2=[PL(r_MTOW) 0];
163
164 W_f_reserve_analytical_vec_1=[W_f_reserve_analytical_vec(1)
165   ↪ W_f_reserve_analytical_vec(1)];
166 W_f_reserve_analytical_vec_2=[W_f_reserve_analytical_vec(r_MTOW)
167   ↪ W_f_reserve_analytical_vec(r_MTOW)];
168
169 %% DIAGRAMS
170 fig1=figure(1);
171 set(fig1,'Renderer', 'painters', 'Position', [400 400 800 450]);
172 hold on
173
174 plot(Range_vec_1,TOW_vec_1,'b','HandleVisibility','off');
175 hold on
176 plot(Range_vec(1:r_MTOW),TOW(1:r_MTOW),'b','DisplayName',
177   '$\mathit{TOW}$');
178 hold on
```

```

178 plot(Range_vec_2,TOW_vec_2,'b','HandleVisibility','off');
179 hold on
180
181 yline(OEW_bueno,'g','DisplayName','$\mathit{OEW}$');
182 hold on
183 xline(Range_vec(1),'-k','LineWidth',1.2,'HandleVisibility','off');
184 hold on
185 xline(Range_vec(r_MTOW),'-k','LineWidth',1.2,'HandleVisibility','off');
186 hold on
187 xline(Range_vec_2(2),'-k','LineWidth',1.2,'HandleVisibility','off');
188 hold on
189 plot(Range_vec_1,OEW_bueno+PL_vec_1,'m','HandleVisibility','off');
190 hold on
191 plot(Range_vec(1:r_MTOW),OEW_bueno+PL(1:r_MTOW),'m','DisplayName',
192     '$\mathit{OEW}+\mathit{PL}$');
193 hold on
194 plot(Range_vec_2,OEW_bueno+PL_vec_2,'m','HandleVisibility','off');
195 hold on
196 plot(Range_vec_1,OEW_bueno+PL_vec_1+W_f_reserve_analytical_vec_1,'r',
197     'HandleVisibility','off');
198 hold on
199 plot(Range_vec(1:r_MTOW),
200     OEW_bueno+PL(1:r_MTOW)+W_f_reserve_analytical_vec(1:r_MTOW),'r',
201     'DisplayName','$\mathit{OEW}+\mathit{PL}+\mathit{RF}$');
202 hold on
203 plot(Range_vec_2,OEW_bueno+PL_vec_2+W_f_reserve_analytical_vec_2,'r',
204     'HandleVisibility','off');
205 ylim([1E4 3.5e4])
206 xlim([3500 5000])
207
208 % Axis format
209 set(gca,'TickLabelInterpreter','latex','FontSize',15)
210 ylabel('Weight $\left[\mathrm{kg}\right]$', 'interpreter','latex','FontSize',16)
211 xlabel('Range $\left[\mathrm{NM}\right]$', 'interpreter','latex','FontSize',16)
212
213 % Grid format

```

## Aircraft Appendix L. WEIGHT TO RANGE DIAGRAMS MATLAB CODE

```
210 grid on
211 ax = gca;
212 ax.GridColor = [0, 0, 0];
213 ax.GridAlpha=0.2;
214 grid minor
215
216 text(4460,1.7E4,'$R_{\mathit{MPL}}$=4500$','Color','k','Rotation',90,
217     'interpreter','latex','Fontsize',16) ;
217 text(4740,1.7E4,'$R_{MTOW}=4783$','Color','k','Rotation',90,'interpreter',
218     'interpreter','Fontsize',16) ;
218 text(4950,1.7E4,'$R_{\max}=4989$','Color','k','Rotation',90,
219     'interpreter','latex','Fontsize',16) ;
220 legend('Location','Northeastoutside','Interpreter','latex');
221
222 xlim([3500 5000])
223
224 fig2=figure(2);
225 set(fig2,'Renderer', 'painters', 'Position', [400 400 800 450]);
226 hold on
227
228 plot(Range_vec_1,TOW_vec_1,'b','HandleVisibility','off');
229 hold on
230 plot(Range_vec(1:r_MTOW),TOW(1:r_MTOW),'b','DisplayName','$TOW$');
231 hold on
232 plot(Range_vec_2,TOW_vec_2,'b','HandleVisibility','off');
233 hold on
234 yline(OEW_bueno,'g','DisplayName','$\mathit{OEW}$');
235 hold on
236 xline(Range_vec(1),--k,'linewidth',1.2,'HandleVisibility','off');
237 hold on
238 xline(Range_vec(r_MTOW),--k,'linewidth',1.2,'HandleVisibility','off');
239 hold on
240 xline(Range_vec_2(2),--k,'linewidth',1.2,'HandleVisibility','off');
241
242 hold on
```

```

243 plot(Range_vec_1,OEW_bueno+PL_vec_1,'m','HandleVisibility','off');
244 hold on
245 plot(Range_vec(1:r_MTOW),OEW_bueno+PL(1:r_MTOW),'m','DisplayName',
246      '$\mathit{OEW}+\mathit{PL}$');
247 hold on
248 plot(Range_vec_2,OEW_bueno+PL_vec_2,'m','HandleVisibility','off');
249 hold on
250 plot(Range_vec_1,OEW_bueno+PL_vec_1+W_f_reserve_analytical_vec_1,'r',
251      'HandleVisibility','off');
252 hold on
253 plot(Range_vec(1:r_MTOW),
254       OEW_bueno+PL(1:r_MTOW)+W_f_reserve_analytical_vec(1:r_MTOW),'r',
255       'DisplayName' ,'$\mathit{OEW}+\mathit{PL}+\mathit{RF}$');
256 hold on
257
258 % Axis format
259 set(gca,'TickLabelInterpreter','latex','fontsize',15)
260 ylabel('Weight $\left[\mathrm{kg}\right]$','interpreter','latex','FontSize',16)
261 xlabel('Range $\left[\mathrm{NM}\right]$','interpreter','latex','FontSize',16)
262
263 % Grid format
264 grid on
265 ax = gca;
266 ax.GridColor = [0, 0, 0];
267 ax.GridAlpha=0.2;
268 grid minor
269
270 text(4420,1.8E4,'$R_{\mathrm{MPL}}=4500$', 'Color','k','Rotation',90,
271      'interpreter','latex','Fontsize',15) ;
272 text(4690,1.8E4,'$R_{\mathrm{MTOW}}=4783$', 'Color','k','Rotation',90,'interpreter',
273      'latex','Fontsize',15) ;
274 text(4905,1.8E4,'$R_{\mathrm{max}}=4989$', 'Color','k','Rotation',90,
275      'interpreter','latex','Fontsize',15) ;

```

```

273 legend('Location','Northwest','Interpreter','latex');
274
275 fig3=figure(3);
276 set(fig3,'Renderer', 'painters', 'Position', [400 400 800 500]);
277
278 hold on
279 xline(Range_vec(1), '--k','linewidth',1.2,'HandleVisibility','off');
280 hold on
281 xline(Range_vec(r_MTOW), '--k','linewidth',1.2,'HandleVisibility','off');
282 hold on
283 xline(Range_vec_2(2), '--k','linewidth',1.2,'HandleVisibility','off');
284
285 hold on
286 plot(Range_vec_1,PL_vec_1,'m','HandleVisibility','off');
287 hold on
288 plot(Range_vec(1:r_MTOW),PL(1:r_MTOW),'m','DisplayName','$PL$');
289 hold on
290 plot(Range_vec_2,PL_vec_2,'m','HandleVisibility','off');
291 hold on
292
293 ylim([0 1.4E3])
294 xlim([0 5000])
295
296 % Axis format
297 set(gca,'TickLabelInterpreter','latex','fontsize',14)
298 ylabel('Payload $\left[\mathrm{kg}\right]$', 'interpreter','latex','FontSize',15)
299 xlabel('Range $\left[\mathrm{NM}\right]$', 'interpreter','latex','FontSize',15)
300
301 % Grid format
302 grid on
303 ax = gca;
304 ax.GridColor = [0, 0, 0];
305 ax.GridAlpha=0.2;
306 grid minor
307

```

```

308 | text(4410,0.01E4,'$R_{\mathit{MPL}}$=4500$', 'Color', 'k', 'Rotation', 90,
      'interpreter', 'latex', 'Fontsize', 16) ;
309 | text(4690,0.01E4,'$R_{\mathrm{MTOW}}$=4783$', 'Color', 'k', 'Rotation', 90, 'interpreter',
      'latex', 'Fontsize', 16) ;
310 | text(4900,0.09E4,'$R_{\max}=\mathrm{4989}$', 'Color', 'k', 'Rotation', 90,
      'interpreter', 'latex', 'Fontsize', 16) ;
311 | legend('Location','Southwest','Interpreter','latex');
312 |
313 |
314 fig4=figure(4);
315 set(fig4,'Renderer', 'painters', 'Position', [400 400 800 500]);
316
317 hold on
318 xline(Range_vec(1), '--k', 'linewidth', 1.2, 'HandleVisibility', 'off');
319 hold on
320 xline(Range_vec(r_MTOW), '--k', 'linewidth', 1.2, 'HandleVisibility', 'off');
321 hold on
322 xline(Range_vec_2(2), '--k', 'linewidth', 1.2, 'HandleVisibility', 'off');
323
324 hold on
325 plot(Range_vec_1,PL_vec_1,'m','HandleVisibility','off');
326 hold on
327 plot(Range_vec(1:r_MTOW),PL(1:r_MTOW),'m','DisplayName','PL');
328 hold on
329 plot(Range_vec_2,PL_vec_2,'m','HandleVisibility','off');
330 hold on
331
332 ylim([0 1.4E3])
333 xlim([3500 5000])
334
335 % Axis format
336 set(gca,'TickLabelInterpreter','latex','fontsize',14)
337 ylabel('Payload $\left[\mathrm{kg}\right]$','interpreter','latex','FontSize',15)
338 xlabel('Range $\left[\mathrm{NM}\right]$','interpreter','latex','FontSize',15)
339
340 % Grid format

```

Aircraft Appendix L. WEIGHT TO RANGE DIAGRAMS MATLAB CODE

---

```
341 | grid on
342 | ax = gca;
343 | ax.GridColor = [0, 0, 0];
344 | ax.GridAlpha=0.2;
345 | grid minor
346 |
347 | text(4470,0.01E4,'$R_{\mathit{MPL}}$=4500$', 'Color', 'k', 'Rotation', 90,
      | 'interpreter', 'latex', 'Fontsize', 16) ;
348 | text(4750,0.01E4,'$R_{MTOW}$=4783$', 'Color', 'k', 'Rotation', 90, 'interpreter',
      | 'latex', 'Fontsize', 16) ;
349 | text(4955,0.07E4,'$R_{\mathrm{max}}$=4989$', 'Color', 'k', 'Rotation', 90,
      | 'interpreter', 'latex', 'Fontsize', 16) ;
```

---

# Bibliography

- [1] McCormick, B. W., *Aerodynamics, Aeronautics, and Flight Mechanics*. Wiley, 2 ed., 1994.
- [2] Kuethe, A. M., Chow, C. Y., *Foundation of aerodynamics. Bases of aerodynamics design*. John Wiley and Sons, 1998.
- [3] Schlichting, H. T. and Truckenbrodt, E. A., *Aerodynamics of the Airplane*. McGraw-Hill Companies, 1979.
- [4] NASA Glenn Research Center Office of Educational Programs in Cleveland, OH, and the NASA Aeronautics Research Mission Directorate, “A NASA Guide to Engines.” [https://er.jsc.nasa.gov/seh/ANASAGUIDETOENGINES\[1\].pdf](https://er.jsc.nasa.gov/seh/ANASAGUIDETOENGINES[1].pdf), Oct. 2020.
- [5] Torenbeek, E., *Synthesis of subsonic airplane design: an introduction to the preliminary design of subsonic general aviation and transport aircraft, with emphasis on layout, aerodynamic design, propulsion and performance*. Springer Science & Business Media, 1982.
- [6] Inouye, E. C., de Paula, A. A., Guedes, P. L., and Alves, W. M., “Twin-jet and trijet aircraft: a study for an optimal design of regional aircraft,” *Transportation Research Procedia*, vol. 29, pp. 169–180, 2018.
- [7] Gudmundsson, S., *General aviation aircraft design: applied methods and procedures*. Butterworth-Heinemann, 2014.
- [8] Roskam, J., *Airplane Design Part I : Preliminary Sizing of Airplanes*, vol. 1 of *Airplane Design*. DARcorporation, 1997.

- [9] EASA, “Type-certificate data sheet for cf34-8 series engines.” [https://www.easa.europa.eu/sites/default/files/dfu/EASA.IM\\_E.053%20issue%2003%20TCDS%20CF34-8\\_Issue%2003.pdf](https://www.easa.europa.eu/sites/default/files/dfu/EASA.IM_E.053%20issue%2003%20TCDS%20CF34-8_Issue%2003.pdf), 2020.
- [10] Brazilian Aircraft Evaluation Group, *Operational Evaluation Report Embraer 550 & 545*, December 2019.
- [11] Dassault Aviation, *Operating Limitations Dassault Falcon 2000EX*.
- [12] Federal Aviation Administration, *Operating Limitations Cessna Citation X*.
- [13] Federal Aviation Administration, *Operating Limitations Cessna Sovereign*.
- [14] Brunt, C., “Speech interference levels in aircraft interior noise measurement: Their use and interpretation.” <https://www.armchair.com/sci/brunt1.html>, 2000.
- [15] Robert Faye, R. L. and Winter, M., “Aerodynamics of winglets,” *Boeing Aero magazine*, no. 17.
- [16] Élodie Roux, *Turbofan and turbojet engines: database handbook*. Éditions Élodie Roux, 2007.
- [17] Coma Company, M., “Pesos y centrado del avión.” Escola Superior d’Enginyeries Industrial, Aeroespacial i Audiovisual de Terrassa. Grau en Enginyeria en Tecnologies Aeroespacials (Pla 2010). *Disseny d’Aeronaus*, 2017.
- [18] Organization, I. C. A., “Operation of aircraft, annex 6, part i.” [https://www.verifavia.com/bases/ressource\\_pdf/299/icao-annex-6-part-i.pdf](https://www.verifavia.com/bases/ressource_pdf/299/icao-annex-6-part-i.pdf), July 2010.
- [19] Kundu, Kumai, A., *Aircraft Design*. Cambridge University Press, 2010.
- [20] Hamburg Open Online University, “Aircraft Design — Chapter 5: Preliminary Sizing.” [https://www.fzt.haw-hamburg.de/pers/Scholz/HOOU/AircraftDesign\\_5\\_PreliminarySizing.pdf](https://www.fzt.haw-hamburg.de/pers/Scholz/HOOU/AircraftDesign_5_PreliminarySizing.pdf), Oct. 2016.
- [21] Coma Company, M., “Dimensionado inicial.” Escola Superior d’Enginyeries Industrial, Aeroespacial i Audiovisual de Terrassa. Grau en Enginyeria en Tecnologies Aeroespacials (Pla 2010). *Disseny d’Aeronaus*, 2017.

- [22] Carles Bonet Reves, Angel Jorba Monte, M. Teresa Martínez-Seara Alonso, Joaquím Masdemont Soler, Mercè Ollé Torner, Antoni Susin Sánchez, and Marta València Guitart, *Càlcul numèric*, ch. 9, pp. 229, 238–241. Edicions UPC, 2 ed., 2012.